DEVELOPING INTERPRETIVE TURBULENCE MODELS FROM A DATABASE WITH APPLICATIONS TO WIND FARMS AND SHIPBOARD OPERATIONS

by

Kyle A. Schau

A Thesis Submitted to the Faculty of

the College of Engineering and Computer Science

in Partial Fulfillment of the Requirements for the Degree of

Master of Science

Florida Atlantic University

Boca Raton, FL

December 2013

DEVELOPING INTERPRETIVE TURBULENCE MODELS FROM A DATABASE

WITH APPLICATIONS TO WIND FARMS AND SHIPBOARD OPERATIONS

by

Kyle A. Schau

This thesis was prepared under the direction of the candidate's thesis advisor, Dr. Gopal Gaonkar, Department of Ocean and Mechanical Engineering, and has been approved by the members of his supervisory committee. It was submitted to the faculty of the College of Engineering and Computer Science and was accepted in partial fulfillment of the requirements for the degree of Master of Science.

SUPERVISORY COMMITTEE:

Gopal Gaonkar, Ph.D.
Thesis Advisor

Davood Moslemian, Ph.D.

G.Q. Cai, Ph.D.

Javad Hashemi, Ph.D.
Chair, Department of Ocean and Mechanical Engineering

Mohammad Ilyas, Ph.D.
Dean, College of Engineering and Computer Science

Barry Rosson, Ph.D.
Dean, Graduate College

November 29, 2013
Date

ACKNOWLEDGMENTS

The completion of this work represents a collaborative effort by more people than I can remember, all of whom will get less credit than they deserve in this brief section. Professionally, I would like to thank Dr. Gaonkar, for seeing something in me and exposing me to the research presented here. Dr. Gaonkar, your attention to detail is second to none, and will be a standard I will strive towards for the rest of my scientific career. I will miss 'agreeing to disagree' with you very much. Second, thank you to Dr. Susan Polsky (NAVAIR, Patuxent River, MD) for providing the data that was used in the completion of this research. This data refers to CFD Airwake Data for a DDG-81 class ship with embedded H-60 Actuator Disk Model, and the permission of the Naval Air Warfare Center Aircraft Division (NAWCAD) to release this data is greatly appreciated. Lastly, the entire staff of the Department of Ocean and Mechanical Engineering at Florida Atlantic University (including my thesis committee of Dr. Moslemian and Dr. Cai) deserves credit for managing to turn a general lack of interest and apathy towards the field of mechanical engineering into a passion that has resulted in the most intellectually fulfilling years of my life, to date. I truly believe this place is a rare academic environment that has the patience to allow students to flounder for years until they are exposed to the topic that sparks an interest that grows into a passion that becomes a calling.

ABSTRACT

Author: Kyle A. Schau

Title: Developing Interpretive Turbulence Models from a Database with Applications to Wind Farms and Shipboard Operations

Institution: Florida Atlantic University

Thesis Advisor: Dr. Gopal Gaonkar

Degree: Master of Science

Year: 2013

This thesis presents a complete method of modeling the autospectra of turbulence in closed form via an expansion series using the von Kármán model as a basis function. It is capable of modeling turbulence in all three directions of fluid flow: longitudinal, lateral, and vertical, separately, thus eliminating the assumption of homogeneous, isotropic flow. A thorough investigation into the expansion series is presented, with the strengths and weaknesses highlighted. Furthermore, numerical aspects and theoretical derivations are provided. This method is then tested against three highly complex flow fields: wake turbulence inside wind farms, helicopter downwash, and helicopter downwash coupled with turbulence shed from a ship superstructure. These applications demonstrate that this method is remarkably robust, that the developed autospectral models are virtually tailored to the design of white noise driven shaping filters, and that

these models in closed form facilitate a greater understanding of complex flow fields in wind engineering.

DEDICATION

This thesis is dedicated to my friends and family. To the friends I have made, for providing the much needed distractions from my school work, even when I didn't even know I needed it. And especially to my parents, who deserve more credit than I can say for their handling of a moody child who has had eyes too big for his stomach his whole life. Thank you for letting me try to climb to so many heights I wasn't ready for and always being at the bottom to make sure it hurt just enough when I fell. Lastly, to my brother and sister for always giving me someone to try to impress.

DEVELOPING INTERPRETIVE TURBULENCE MODELS FROM A DATABASE WITH APPLICATIONS TO WIND FARMS AND SHIPBOARD OPERATIONS

LIST OF FIGURES

LIST OF TABLES

NOMENCLATURE

u, v, w	Longitudinal, lateral, and vertical turbulence, respectively
i	Arbitrary turbulence direction ($u, v,$ or w)
t	Time
τ	Lag time
$R_i(\tau)$	Normalized autocorrelation of the i^{th} direction wind velocity time history
$\xi_i(\tau)$	von Kármán autocorrelation model of the i^{th} wind direction
$\Gamma(z)$	Gamma function of argument z
$K_x(y)$	Modified Bessel function of the second kind of argument y, and power x
${}_pF_q(\{a_1 \dots a_p\}; \{b_1 \dots b_q\}; z)$	Generalized Hypergeometric function
α_i	Expansion series scaling parameter of the i^{th} velocity component
T_i	Time scale of turbulence of the i^{th} velocity component
σ_i^2	Variance of turbulence of the i^{th} velocity component
f	Frequency (Hz)
$f_{h.f.}$	High frequency limit
$S_i(f)$	One sided autospectrum of the i^{th} velocity component
$S_i(f_{h.f.})$	High-frequency or asymptotic limit of the autospectrum of the i^{th} velocity component

$\widetilde{\mathrm{R}}_i(\tau)$	Expansion series of $\xi_i(\tau)$
$\chi_{ni}(f)$	Result of the Fourier cosine transform $\mathcal{F}\left(\xi_i^n(\tau)\right)$
$\tilde{S}_i(f)$	Resulting spectra of the Fourier cosine transform $\mathcal{F}\left(\widetilde{\mathrm{R}}_i(\tau)\right)$
β_n	Expansion coefficient where $n = 1,2, \ldots, \infty$
A_i	Scaling parameter to fit the model for the i^{th} velocity component to Kolmogorov's -5/3 law (when used generically, the subscript is suppressed)
A_{model}	Level of expansion series at high frequencies
$A_{measured}$	Level of calculated autospectrum at high frequencies, determined by least squares fit
A_{error}	Error between A_{model} and $A_{measured}$
i_{raw}	Measured wind velocities of the i^{th} wind component, equation (2.1)
$\bar{\imath}$	Mean wind velocity of the i^{th} wind component, equation (2.1)
f_k	Indexed frequencies for calculation of the discrete PSD
ε	Error used for fitting expansion series to calculated data
j	Imaginary number $\sqrt{-1}$
n	Dimensionless frequency $n = fz/\overline{U}$
z	Height of wind velocity measurements taken (Equal to 30 feet in all cases it appears in this thesis)

CHAPTER 1: INTRODUCTION

In 1948, Theodore von Kármán introduced the longitudinal (u direction), lateral (v direction), and vertical (w direction) autocorrelation functions (von Kármán, 1948) based on G.I. Taylor's theory of homogeneous, isotropic, turbulent flow (Taylor, 1935), seen in Equations (1.1)-(1.3) and plotted in Figure 1.1.

Longitudinal Autocorrelation

$$\xi_u(\tau) = \frac{2^{2/3}}{\Gamma\left(\frac{1}{3}\right)}\left(\frac{\tau}{a_u T_u}\right)^{1/3} \times \left[K_{1/3}\left(\frac{\tau}{a_u\, T_u}\right)\right] \tag{1.1}$$

Lateral Autocorrelation

$$\xi_v(\tau) = \frac{2^{2/3}}{\Gamma\left(\frac{1}{3}\right)}\left(\frac{\tau}{a_v\, T_u}\right)^{1/3} \times \left[K_{1/3}\left(\frac{\tau}{a_v T_v}\right) - \frac{1}{2}\left(\frac{\tau}{a_v T_v}\right) K_{2/3}\left(\frac{\tau}{a_v T_v}\right)\right] \tag{1.2}$$

Vertical Autocorrelation

$$\xi_w(\tau) = \frac{2^{2/3}}{\Gamma\left(\frac{1}{3}\right)}\left(\frac{\tau}{a_w T_w}\right)^{1/3} \times \left[K_{1/3}\left(\frac{\tau}{a_w T_w}\right) - \frac{1}{2}\left(\frac{\tau}{a_w T_w}\right) K_{2/3}\left(\frac{\tau}{a_w T_w}\right)\right] \tag{1.3}$$

where $a_u = \frac{\Gamma\left(\frac{1}{3}\right)}{\sqrt{\pi}\,\Gamma\left(\frac{5}{6}\right)} = 1.338985$ and $a_v = a_w = \frac{2\Gamma\left(\frac{1}{3}\right)}{\sqrt{\pi}\,\Gamma\left(\frac{5}{6}\right)} = 2.677971$. These estimates in and of themselves are of little practical use, however, their respective Fourier transforms, given in Equations (1.4)-(1.6) and plotted in Figure 1.2, provide models of the frequency domain (autospectrum) for longitudinal, lateral, and vertical turbulence that

have been adopted by many practical applications, wind engineering being a major subscriber.

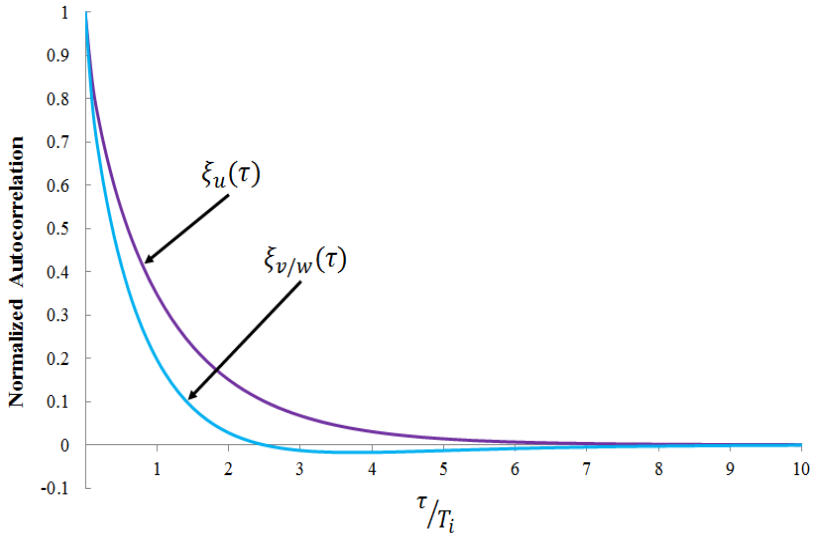

Figure 1.1: Longitudinal and Lateral/Vertical von Kármán Autocorrelation Models

Longitudinal Autospectrum

$$\frac{fS_u(f)}{\sigma_u^2} = \frac{4T_u f}{[1 + 70.8(T_u f)^2]^{5/6}} \tag{1.4}$$

Lateral Autospectrum

$$\frac{fS_v(f)}{\sigma_v^2} = \frac{4T_v(1 + 755.2\,(T_v f)^2)}{(1 + 283.2\,(T_v f)^2)^{11/6}} \tag{1.5}$$

Vertical Autospectrum

$$\frac{fS_w(f)}{\sigma_w^2} = \frac{4T_w(1 + 755.2\,(T_w f)^2)}{(1 + 283.2\,(T_w f)^2)^{11/6}} \tag{1.6}$$

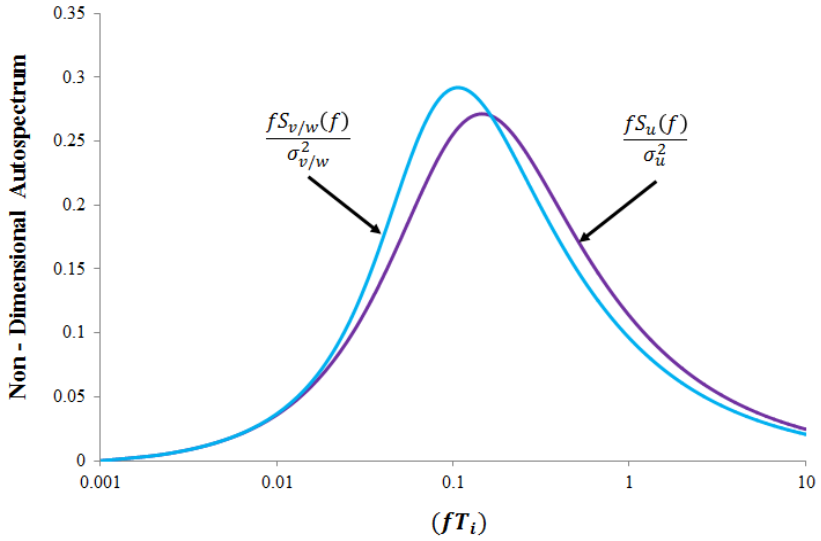

Figure 1.2: Longitudinal and Lateral/Vertical von Kármán Autospectrum Models

These estimations of autospectrum provide a remarkable approximation for a wide range of turbulence, despite their seemingly restrictive nature. However, these estimations, as with all empirical expressions, have limitations. The most glaring of these limitations, is the assumption of homogeneous, isotopic, turbulence. This assumption is almost never valid outside of laboratory settings. Throughout the decades, several alternatives to the von Kármán spectrum have been proposed as both fitting and predictive tools, however, none attain the same level of mathematical rigor as the von Kármán models (to be discussed in a later section).

In 1990, R.I. Harris suggested a method of modifying the von Kármán spectral model in order to achieve a better fit via a perturbation-type series expansion, in which the von Kármán model serves as the basis function, or the first term of the series (Harris, 1990). This method of modification provides a number of variations (unlike the original model) while maintaining all the mathematical properties of the original model. This report will detail the formulation of this modification, as presented by Harris, as well as

provide a more in-depth investigation into this scheme than is currently available. Also provided in this report is an advancement of the original work by Harris, that will yield a complete methodology for spectral modeling of turbulence. Furthermore, this report will demonstrate two significant areas within wind engineering that may benefit from the application of this modification of the von Kármán model: wake turbulence inside wind farms, and on ship decks with and without helicopter downwash coupling.

1.1 Literature Review

1.1.1 Practical Application of the von Kármán Model

Simulation of turbulence is the predominant modern use of the von Kármán spectral model. If the time scale parameter in (1.4)-(1.6) is known, and the data is represented well, filters can be designed to process random data, such that the filter output has the same autospectral characteristics as the modeled data. The U.S. Military has developed two standards concerning this procedure (MIL-HDBK-1797, 1997 and MIL-F-8785C, 1980). The frequency domain is being modeled; therefore dynamic analysis is best served by these models of autospectra.

1.1.2 Limitations of the von Kármán Model

The von Kármán model has only one varying parameter, T_i (where $i = u, v, or\ w$), that determines the turbulence time scale. Given this fact, it is amazing this formula can model turbulence as well as it does. This model has been used in wind engineering applications for decades, with modest success. However, as more experimental results have been subjected to the fit, several deficiencies have become apparent (Harris, 1990). For example:

(1) For the measured values of the atmospheric boundary layer (ABL) close to the surface, the peak of the power spectrum generally becomes broader and lower than the von Kármán model;

(2) If the model is used to fit this peak value at these elevations, the model over approximates the high frequency range;

(3) Using the Kolmogorov -5/3 decay rate at higher frequencies as a fit to estimate the parameters of the von Kármán model, generally leads to an under approximation of the low-frequency range;

(4) Mathematically, the formulation of the von Kármán model allows no way of fitting the model to represent the position of the power spectrum peak, the height of this peak, or the magnitude of the decay range at high frequencies.

These criticisms are fairly specific to applications. Table 1.1 outlines the three major concerns that this thesis will provide a means to rectify.

Table 1.1: Three major shortcomings of the von Kármán model

(i)	Upon selecting T_i in (1.1)-(1.3), the height of the spectrum seen in Figure 1.2 is fixed;
(ii)	Upon selecting T_i, the location of the peak in Figure 1.2 is fixed; and
(iii)	Upon selecting T_i, the elevation of the high

frequency decay range in Figure 1.2 is fixed.

Generally speaking, a user can vary T_i until one of the three characteristics in Table 1.1 is met, and the other two are left to chance. The fact that the von Kármán model is so limited in its parameters, and was developed to fit homogeneous, isotropic turbulence, suggests that for any nonlinearly transformed turbulence, the model will be deficient. Therefore, if this model is a valid fit of any complicated flow data found in engineering, 'good fortune' is as important as the model itself. Evidence of this fact was seen in a study comparing the von Kármán model with the measured spectra of wind over a complex terrain and through wind turbine wakes (Morfiadakis, Glinou, & Koulouvari, 1996). It was found that free stream conditions were modeled well by the von Kármán model, however, the introduction of complex terrain or wake effects rendered the model unable to represent the data set. Figure 1.3 shows a comparison of the model for (a) free stream conditions and (b) complex terrain of a Greek island.

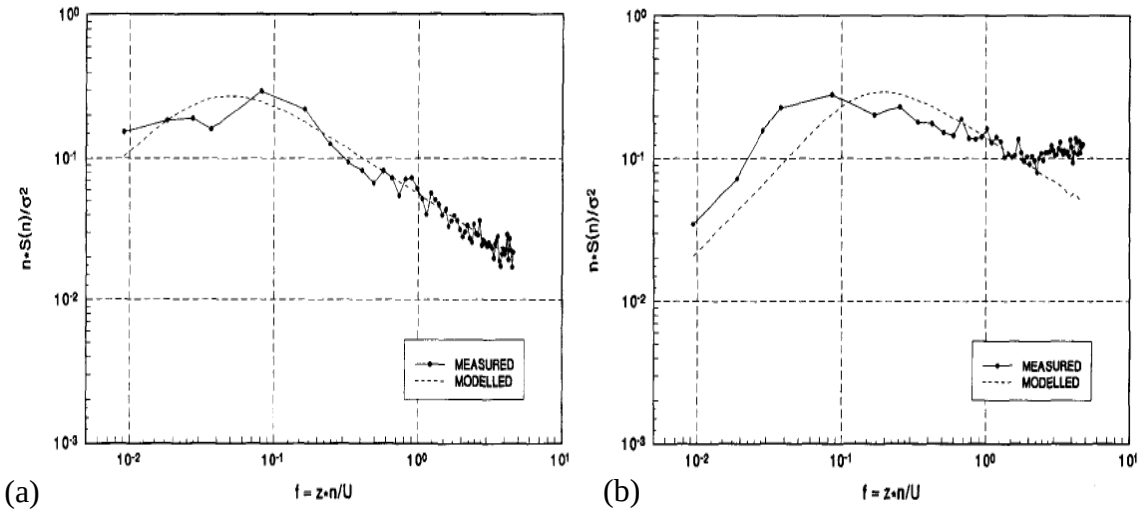

Figure 1.3: Comparison of von Kármán model for (a) free stream ABL conditions and (b) complex terrain on the Greek Island

As more complex flows became important in various wind engineering industries, several different empirical models have been developed, and applied on an *ad hoc* basis to suit the user's needs. The most popular of these modifications were developed by Kaímal, Davenport, and Harris. These models are given by Equations (1.7)-(1.10):

(von Kármán) $$\frac{fS_u(f)}{\sigma_u^2} = \frac{4T_u f}{[1 + 70.8(T_u f)^2]^{\frac{5}{6}}} \quad (1.7)$$

(Kaímal) $$\frac{fS_u(f)}{\sigma_u^2} = \frac{a_1 T_u f}{[1 + a_2 T_u f]^{\frac{5}{3}}} \quad (1.8)$$

(Davenport) $$\frac{fS_u(f)}{\sigma_u^2} = \frac{0.67(T_u f)^2}{[1 + T_u f]^{\frac{4}{3}}} \quad (1.9)$$

(Harris) $$\frac{fS_u(f)}{\sigma_u^2} = \frac{0.6(T_u f)^2}{[2 + T_u f]^{\frac{5}{6}}} \quad (1.10)$$

These models have proven reliable enough to become used in many recent and current wind engineering codes and standards. Table 1.2 shows the application of these spectra in various countries (Tamura, 2003).

Table 1.2: Spectral model used in various standards and codes concerning wind turbine development

Code/Standard	Model Used
AIJ-RLB, Japan	von Kármán
AS1170.2, Australia	Harris
AS/NZS1170.2. Australia / New Zealand	von Kármán
ASCE7-98, United States	Modified Kaimal

1.1.3 Qualifications of a Spectral Model

When creating any model of an autospectrum, three criteria have been determined to be desirable, if not essential, in the validation of any empirical spectral model used to characterize turbulence (Tamura, 2003). These criteria are:

$$\text{(i)} \quad \frac{1}{\sigma_i^2}\int_0^\infty S_i(f)df = 1$$

$$\text{(ii)} \quad S_i(0) = 4\sigma_i^2 T_i \tag{1.11}$$

$$\text{(iii)} \quad \frac{fS_i(f_{h.f.})}{\sigma_i^2} \propto A(fT_i)^{-2/3}$$

where $S_i(f_{h.f.})$ is the high frequency or asymptotic case of the spectrum. Conditions (i) and (ii) are statistical necessities based solely on the definition of the autospectrum. Condition (ii) is valid only when the time scale T_i is taken to be the integration of the autocorrelation function from zero to infinity (to be discussed later). Condition (iii) is to satisfy Kolmogorov's equilibrium condition of energy decay. Of the above criteria, only the von Kármán model is capable of ensuring that all three are satisfied. For this reason, it was chosen as the model to modify, in order to provide a wider range of fitting forms, while still maintaining the mathematical rigor of the original model.

1.2 Significance to Wind Farms

The flow field within a wind farm is extremely complex, and difficult to analyze. The passing of the ABL through the rotor of a wind turbine is considered a highly non-

linear transformation. Therefore, an extremely wide range of turbulence flows can be present. More understanding and modeling of these flows are needed to further the development of large scale wind farms. Turbulence inside wind farms (land-based as well as offshore) reduces the energy generated by downstream machines by up to 40% (Barthelmie et al., 2009) and increases their fatigue loading up to 80% (Vemeer et al., 2003). A greater ability to study, model, and simulate this complex turbulence will lead to significant improvements of current wind farm energy production.

A complete treatment of rotor wakes, on a theoretical level, is beyond the scope of this thesis. Interested readers are encouraged to see Fay (1994) for a more complete treatment of rotor wakes on a theoretical level.

1.3 Significance to Shipboard Operations

Similar to wind farm turbulence, airwake shed from the ship superstructure coupled with the downwash from a helicopter, is highly complicated. The transformation of ABL turbulence by the ship superstructure, coupled with the downwash of a helicopter, is again, a highly nonlinear transform of the ABL. Turbulence on ship decks with and without downwash coupling severely impacts the safety of helicopter landing and take-off operations (Wilkinson et al, 1998). The current understanding of this turbulence with respect to shipboard operations merits significant improvements as well.

1.4 Past Applications

This series expansion approach has been applied by Gaonkar and Mohan (2012) to model ship airwake from a database of spectral points from experimental and CFD-based studies. Harris (1990) was the first to propose the series expansion approach for the

treatment of turbulence. However, Harris's treatment does not include any applications and addresses only the longitudinal (u component) autospectrum, and the lateral and vertical (v and w components) are treated by invoking the continuity requirement of homogeneous, isotropic turbulence ($\sigma_u = \sigma_v = \sigma_w \; and \; S_v(f) = S_w(f)$. Built on the work of Harris, Gaonkar and Mohan (2012) developed a perturbation scheme for wake turbulence on a ship deck with emphasis on spectral models for the low frequency bandwidth ($0 < f\ (Hz) < 1.6$) as required for flight dynamics applications. In their investigation, each of the three velocity components has its own time scale and rms value, and each is treated independently of the other. Given the emphasis on the low-frequency bandwidth, the Kolmogorov -5/3 law, criterion (iii) of (1.11) on page 8 was not addressed. Figure 1.4 shows one of the demanding cases of a database from a CFD-based simulation. While the sharp peaks are not captured, the three term series does meet the roll-off trend of the data.

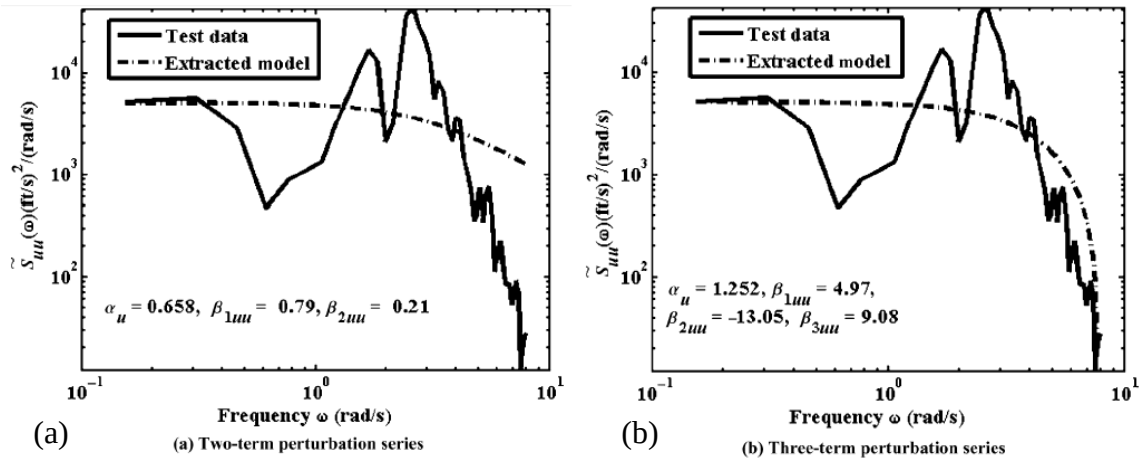

Figure 1.4: Two term (a) and three term (b) series expansion of longitudinal von Kármán spectrum

1.5 A Summary of the State of the Art

- Harris (1990) was the first to propose the series expansion approach to the treatment of longitudinal turbulence, but provided no applications;
- Gaonkar and Mohan (2012) developed a perturbation scheme for wake turbulence on a ship deck, emphasizing the low frequency bandwidth ($0 \leq f\ (Hz) \leq 1.6$); thus, the asymptotic decay of the autospectra according to the Kolmogorov -5/3 law was not addressed;
- Moreover, in their perturbation scheme, all results were calculated numerically, no closed form expressions were provided, and the strengths and weaknesses of the scheme were identified as one of the future areas of research.

1.6 Overview of Thesis

Given the above background, this thesis is noteworthy in the following respects:

i. The treatment of Harris is extended by including the asymptotic decay of the vertical and lateral autospectra according to the Kolmogorov minus-five-thirds-law. (Although this law is theoretically applicable to isotropic flows, it is supported by experiments for a wide range of nonhomogeneous, anisotropic flows (Mathieu and Julian, 2000);

ii. With this extension, the framework is tested against a comprehensive database of turbulence inside a wind farm and over a ship deck. The database is demanding: The wind farm topography refers to a complex terrain, and the ship-deck database includes helicopter rotor downwash coupling with airwake turbulence shed from the ship superstructure. Moreover, the database includes

cases where the Kolmogorov law is not observed. A discussion of these cases is included as well;

iii. On the basis of this testing, the strengths and weaknesses of the series expansion approach are addressed for developing interpretive models from a database;

iv. This work also demonstrates that the design of white-noise-driven shaping filters for these models is as routine as the widely used scheme for the von Kármán spectra.

CHAPTER 2: MATHEMATICAL BACKGROUND

The key of the model presented in this thesis is the fitting of the model to data from the frequency domain description of turbulence, specifically, the autospectrum/power spectral density functions (PSD) of 'random data'. It is therefore imperative that the calculation of the PSD is done properly, and with caution, not only to accurately capture the qualities of the raw data, but also to allow the presented model the best chance of representing the spectrum over a sufficiently wide bandwidth. Although there are mathematical definitions that are rigorous in their form, there exist significant variations available to a user when calculating these functions discretely. This section will detail the most accurate and effective way to calculate the PSD from raw turbulence data. All the continuous and discrete versions of the formulations and related definitions follow Bendat and Piersol (2010).

2.1 Treatment of Raw Data

The calculation of any PSD begins with raw data. In the case of this thesis, raw data, collected at a point in space, refers to gathering time histories of wind velocities in three components, or mutually orthogonal directions: u to represent the downwind, or longitudinal directions, v for a direction perpendiculat to u, termed the lateral direction, and w for a direction perpendicular to both u and v, termed the vertical direction. The treatment of each of these components are the same, therefore, all definitions and prescriptions throughout this chapter will be the same for all three models. Before

beginning, in this chapter it is assumed that $u(t)$ is an array (when discussing discrete calculations) that consists of N total samples, sampled Δt seconds apart, for a total time of $T = N \cdot \Delta t$, and are indexed by $n = 1, 2, 3 \ldots N$. The sampling frequency is therefore $f = 1/\Delta t$. The quantity $u[n]$ refers to the n^{th} sampled data point within the $u(t)$ array.

When gathering discrete data from turbulence, the major question to be answered is: *What should be the sample rate?* The sample rate will determine two things: 1) the highest frequency at which accurate data will be available in the PSD, and 2) the stability of the PSD near zero frequency range (to be discussed), especially if fast Fourier transform algorithms are to be utilized. For reasons that will be made apparent in subsequent chapters, the sample frequency should be, at a minimum, 20 Hz. At this frequency, PSD data will be available at 10 Hz, and typically, turbulent energy will have decayed to a sufficiently low level to be neglected above this frequency. However, this sampling frequency should be determined on a case by case basis. Specific applications with important bandwidths should gather data fast enough to contain those frequencies within the PSD.

A second concern regarding discrete sampling of turbulence is the duration of sampling. In subsequent sections, it will be shown that averaging is a major aid in the calculation of a stable, accurate, discrete PSD. Therefore, having data sets in the range of 10,000 + samples is highly desirable. Assuming the turbulence to be analyzed is free of trends and can be considered ergodic, this should not be an issue.

Lastly, it is imperative to remember that the entire analysis being performed represents turbulence along with the mean flow field. Therefore, for a particular time series of wind velocities, the mean value must be calculated, and subtracted from the data set, as shown in (2.1).

$$u(t) = u_{raw}(t) - \bar{U} \tag{2.1}$$

where $\bar{U}$ is the mean wind speed of the wind data set, u_{raw}.

2.2 Calculation of PSD

A PSD can be calculated via two methods: 1) from raw turbulence data, and 2) from the autocorrelation of raw data. This section will detail both methods.

2.2.1 PSD from the Autocorrelation

The autocorrelation of a function can be viewed as a test of how related a function is with itself, in other words, how random is a series of data. The mathematical definition of the autocorrelation of a continuous function $u(t)$ can be seen in (2.2):

$$R_u(\tau) = \frac{1}{\sigma_u^2} \lim_{T\to\infty} \frac{1}{2T} \int_{-T}^{T} u(t)u(t+\tau)d\tau \tag{2.2}$$

where σ_u^2 is the variance of the random process $u(t)$.

A periodic function will have distinct patterns in its corresponding autocorrelation, however, a random process will not. Furthermore, a random process that fluctuates at higher frequencies will decay much faster than a process that fluctuates at slower frequencies. The properties of this function (for any time history, not just turbulence) are the following:

(i) $R_u(\tau)$ is a real valued function if $u(t)$ is real

(ii) $R_u(\tau)$ is an even function (2.3)

(iii) $R_u(0) = 1 = R_u(\tau)_{maximum}$

The autocorrelation function from (2.2) is the function that the von Kármán model in (1.1) attempts to represent. The discrete calculation of this function is not a trivial task. As seen in (2.2), a true autocorrelation requires an infinite and continuous set of data. Numerically, this represents a challenge in that all values outside the range of a particular data set must be considered zero. There are two separate methods of calculating the autocorrelation of a data set discretely:

1.) Unbiased Autocorrelation

The unbiased autocorrelation is a discrete version of the calculation of the autocorrelation that is as close to (2.2) as possible. It is defined as:

$$R_u[m]_{unbiased} = \frac{1}{N - |m|} \sum_{n=0}^{N-m-1} u[n]u[n+m] \tag{2.4}$$

where N is the total number of samples and n is an index within the data set and m is a lag index that can be related to the time domain as, $\tau = m\Delta t$. This definition creates a problem when the end of the data set is reached and $m \to N$. The continuous decay of the autocorrelation at greater lags begins to become unstable as shown in Figure 2.1.

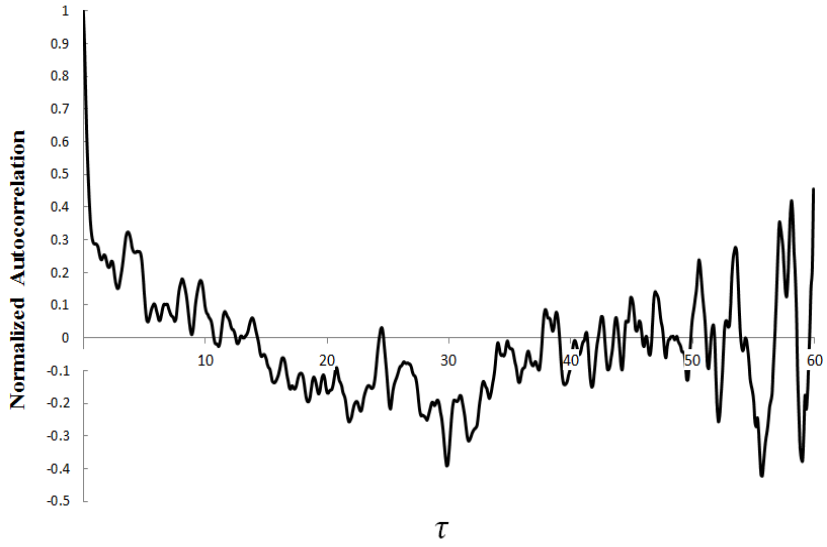

Figure 2.1: Unbiased autocorrelation estimate. Note the unstable range towards the end of the data set

2.) Biased Autocorrelation

An alternate, but less exact discretization is the biased autocorrelation defined in (2.5).

$$R_u[m]_{biased} = \frac{1}{N} \sum_{n=0}^{N-m-1} u[n]u[n+m] \tag{2.5}$$

It can be seen in this definition that as $m \to N$ the autocorrelation will not become unstable, and the decay will continue. The biased autocorrelation of the data from Figure 2.1 is shown in Figure 2.2.

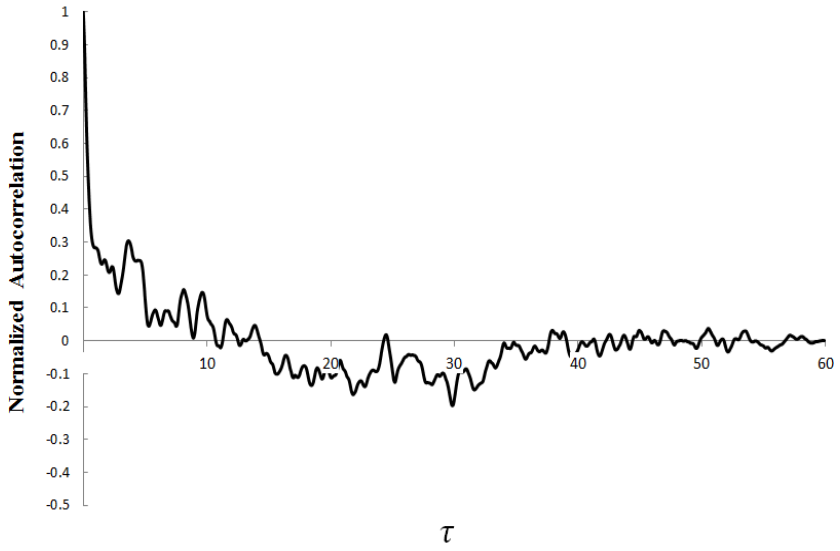

Figure 2.2: Biased autocorrelation estimate in which the decay continues to the end of the data set

With a stable computation of an autocorrelation, the Weiner-Khintchine relation (Weiner, 1949) can be used to determine the PSD of the raw data, $u(t)$. The Weiner-Khintchine relation states that the autocorrelation and PSD of a function are Fourier Transform pairs, shown in (2.6).

$$S_u(f) = \mathcal{F}\big(R_u(\tau)\big)$$

$$S_u(f) = \int_{-\infty}^{\infty} R_u(\tau) e^{-2\pi i f \tau} d\tau \tag{2.6}$$

Due to the properties of the autocorrelation, detailed in (2.3), the Fourier Transform in (2.6) can be reduced to a one sided PSD via a Fourier Cosine transform, which, due to symmetry, is multiplied by four, as in (2.7).

$$S_u(f) = 4\int_0^{\infty} R_u(\tau)\cos(2\pi f\tau)d\tau \tag{2.7}$$

A variety of discrete methods of calculating this set of data have been proposed, the fast Fourier Transform (FFT) being the most popular. However, in the case of the present research, the FFT has been found to be computationally excessive, as well as limiting in its ability to develop stable, consistent PSDs from a dataset. Therefore, a direct computation of the Fourier Transform of $R_u(\tau)$ has been accomplished by the following:

Begin by creating a suitable array of frequencies to calculate the PSD, equally spaced between zero and the Nyquist frequency.

$$f_k = \frac{k}{N\Delta t} \quad k = 0, 1, 2 \ldots N/2 - 1 \tag{2.8}$$

where Δt is the time between samples. Therefore:

$$S_u(f_k) \; = 4\Delta t \sum_{n=0}^{N/2-1} R_u[n] * \cos(2\pi f_k n\Delta t) \tag{2.9}$$

The result of this operation is a PSD array with values corresponding to the frequency array in (2.8).

Despite the validity of the presented operations, the model presented in this thesis is an attempt to interpret and characterize turbulence on a more general level, not for one span of time. The presented method in this section, does not utilize averaging in the arrival of the PSD in (2.9), and cannot take advantage of long, ergodic datasets, and the results are prone to erroneous variations within the frequency spectrum. Another method,

called ensemble averaging, has been found to produce highly stable, and accurate PSD functions.

2.2.2 Calculation of PSD via Ensemble Averaging

The PSD of raw data is generally calculated directly from the raw data, through a process to be detailed shortly, without ever calculating the autocorrelation. The reason for including the previous section is to show the justification for the models in (1.1)-(1.3). These models represent the autocorrelation of turbulence data, and through the same procedure as depicted in the previous section, one can arrive at the PSD models in (1.4)-(1.6). However, the use of the model detailed in this thesis, does not require the autocorrelation of raw turbulence data, that is, it is based entirely from the PSD of raw data. In order to avoid numerical error by calculating the autocorrelation of raw turbulence data, and *then* the discrete Fourier transform, it is more effective to do the following, more direct, procedure to calculate the PSD. The infinite-range Fourier transform of a function $u(t)$ is defined as

$$\mathcal{F}\big(u(t)\big) = U(f) = \int_{-\infty}^{\infty} u(t)e^{-2\pi i f t}dt \tag{2.10}$$

The one sided PSD is defined as the Fourier transform of $u(t)$ multiplied by its complex conjugate, and is shown in (2.11):

$$S_u(f) = 2\big(U(f)U^*(f)\big) = 2|U(f)|^2 \tag{2.11}$$

where $U^*(f)$ is the complex conjugate of $U(f)$. The result of this operation is a real valued function. Discretely, this is done beginning in the same manner as before. Again begin with a discrete array of sampled data, $u(t)$ sampled at Δt seconds apart. The idea

of ensemble averaging is to divide $u(t)$ into n_d segments of N samples, represented by u_{in}, where $n = 1, 2, 3, \ldots N$, and $i = 1, 2, \ldots n_d$. Then calculate the PSD of each segment separately, and average them together. The first step is once again to select equally spaced frequencies to evaluate the PSD. Repeated here as

$$f_k = \frac{k}{N\Delta t} \quad k = 0, 1, 2 \ldots N/2 - 1 \tag{2.12}$$

As shown in (2.12), the length of the segments will determine the resolution of the PSD, i.e. longer segments result in higher resolution of the PSD, but fewer averaged segments. Calculating the discrete Fourier transform by

$$U_i(f_k) = \Delta t \sum_{n=1}^{N/2} u_{in} \exp[-2\pi i f_k n \Delta t] \tag{2.13}$$

And performing this operation for all n_d segments, the final PSD of $u(t)$ can be found by averaging each $|U_i(f_k)|^2$ for all i. That is,

$$S_u(f_k) = \frac{2}{n_d N \Delta t} \sum_{i=1}^{n_d} |U_i(f_k)|^2 \tag{2.14}$$

The resulting PSD will have the benefit of averaging over long data sets that will compensate for erroneous errors that may arise in the numerical calculation of the PSD.

One final aid in calculating the PSD of discrete data that is especially important for ensemble averaging is the concept of windowing. When dealing with discrete, finite data sets, the ends of the sets can sometimes lead to what is called strobe leakage. This is essentially an attribution of erroneous magnitude due to the sudden discontinuity at the ends of data sets. This can be mitigated by using a very effective method called,

windowing. The idea is to taper the ends of the data set, in order to gradually merge the ends of the set with the lack of data on either side. The most popular method of windowing, is the Hanning Window defined as

$$h(t) = \begin{cases} 1 - \cos^2\left(\frac{\pi t}{T}\right) & 0 \le t \le T \\ 0 & otherwise \end{cases} \tag{2.15}$$

This window is introduced discretely into (2.13), yielding

$$U_i(f_k) = \sqrt{\frac{8}{3}}\,\Delta t \sum_{n=1}^{N/2} \left(1 - \cos^2\left(\frac{2\pi n}{N}\right)\right) u_{in} \exp[-2\pi i f_k n \Delta t] \tag{2.16}$$

The $\sqrt{\frac{8}{3}}$ is a scaling factor that is included to compensate for the loss of magnitude within the sum of (2.16). The derivation of this factor is available in Bendat and Piersol (2010). The combination of (2.16) and (2.14) represent the most accurate, and reliable means of calculating a PSD from raw data when utilizing the model to be presented later. The results have been averaged over a sufficiently long time period, and have significantly eliminated some of the numerical errors that can be accumulated. This will provide a quality PSD that is robust and can be modeled with reliability.

CHAPTER 3: LONGITUDINAL EXPANSION

As mentioned in the introduction, the model to be presented has three components: longitudinal, lateral, and vertical. Harris (1990) has provided the derivation of the longitudinal scheme. In this chapter, a summary of Harris's treatment of the longitudinal von Kármán model will be presented along with some additional figures and details not provided in the original presentation (Harris 1990).

3.1 Justification of the Scheme

Begin with a time history $u(t)$ of longitudinal wind velocities at a location of interest. The normalized autocorrelation of this data series from Chapter 2 is:

$$R_u(\tau) = \frac{1}{\sigma_u^2} \lim_{T\to\infty} \frac{1}{2T} \int_{-T}^{T} u(t)u(t+\tau)d\tau \tag{3.1}$$

The one sided, non-dimensional, autospectrum of the time series $u(t)$ can be calculated by a Fourier cosine transform of the autocorrelation, namely:

$$\frac{fS_u(f)}{\sigma_u^2} = 4f \int_0^{\infty} R_u(\tau)\cos(2\pi f\tau)\,d\tau \tag{3.2}$$

where $R_u(\tau)$ can be realized by

$$R_u(\tau) = \frac{1}{\sigma_u^2} \int_0^{\infty} S_u(f)\cos(2\pi f\tau)\,df \tag{3.3}$$

Due to the fact that $R_u(\tau)$ is an even, real valued function, $fS_u(f)/\sigma_u^2$ will be a positive, real valued function. From Chapter 1 in equation (1.1), $\xi_u(\tau)$, is the von Kármán autocorrelation model of $R_u(\tau)$ from (3.3). The von Kármán form calls for a parameter T_u with the dimensions of time. One option would be to use the time scale of the time history $u(t)$ defined as:

$$T_u = \int_0^\infty R_u(\tau)d\tau \tag{3.4}$$

By setting $\tau = 0$ in (3.3), and $f = 0$ in (3.2), it follows that

$$\frac{1}{\sigma_u^2}\int_0^\infty S_u(f)df = 1 \tag{3.5}$$

And

$$S_u(0) = 4\sigma_u^2\int_0^\infty \xi_u(\tau)d\tau = 4\sigma_u^2 T_u \tag{3.6}$$

With these definitions in place, a series expansion can be applied. It is a well-known feature of stochastic process theory that for a random process with a normalized autocorrelation $\xi_u(\tau)$, that undergoes a non-linear transform, for many nonlinearities, the resulting output process will have an autocorrelation that can be represented by a perturbation series of the form (Harris, 1990)

$$\tilde{R}_u(\tau) = \beta_{1u}\xi_u(\tau) + \beta_{2u}\xi_u^2(\tau) + \beta_{3u}\xi_u^3(\tau) + \cdots + \beta_{nu}\xi_u^n(\tau) \tag{3.7}$$

where the parameters $\beta_{nu}, n = 1,2,3 \ldots \infty$ are unknown constants. Figure 3.1 shows the first three terms of the expanded series with $\beta_{nu} = 1$.

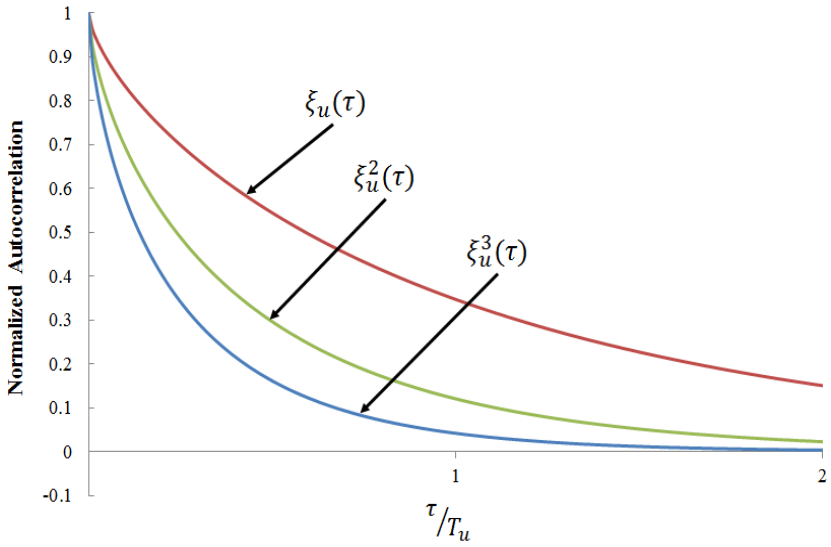

Figure 3.1: First three terms of the longitudinal expansion series

The resulting spectrum from the Fourier transform of (3.7) will then be:

$$\tilde{S}_u(f) = \beta_{1u}\,\chi_{1u}(f) + \beta_{2u}\,\chi_{2u}(f) + \beta_{3u}\,\chi_{3u}(f) + \cdots + \beta_{nu}\,\chi_{nu}(f) \qquad (3.8)$$

where

$$\chi_{nu}(f) = 4\int_0^{\infty} \xi_u^n(\tau)\cos(2\pi f\tau)\,d\tau \qquad n = 1,2,3,\ldots,\infty \qquad (3.9)$$

Since this expansion is applied to the von Kármán model, the basis autocorrelation function would be:

$$\xi_u(\tau) = \frac{2^{2/3}}{\Gamma\left(\frac{1}{3}\right)}\left(\frac{\alpha_u\tau}{T_u}\right)^{1/3} \times \left[K_{1/3}\left(\frac{\alpha_u\tau}{T_u}\right)\right] \qquad (3.10)$$

The α_u parameter presented in (3.10) merits some comments. This is a scaling parameter that must be introduced into the model, to further ensure that the expanded autocorrelation in (3.7) maintains the property in (3.4). The following is a treatment of the first three terms in the expansion shown in (3.8).

3.2 First Term $\xi_u(\tau)$

$$\xi_u(\tau) = \frac{2^{2/3}}{\Gamma\left(\frac{1}{3}\right)}\left(\frac{\alpha_u \tau}{T_u}\right)^{1/3} \times \left[K_{1/3}\left(\frac{\alpha_u \tau}{T_u}\right)\right]$$

$$\chi_{1u}(f) = 4\int_0^\infty \xi_u(\tau)\cos(2\pi f\tau)\, d\tau \tag{3.11}$$

$$= 4T_u \frac{\sqrt{\pi}\,\Gamma\left(\frac{5}{6}\right)}{\Gamma\left(\frac{1}{3}\right)}\, \alpha_u^{2/3}\, \frac{1}{(\alpha^2 + 4\pi^2 f^2 T_u^2)^{5/6}} \tag{3.12}$$

At high frequencies

$$f\chi_{1u}(f_{h.f.}) \approx \frac{\sqrt{\pi}\Gamma\left(\frac{5}{6}\right)}{\Gamma\left(\frac{1}{3}\right)}\, \frac{4}{(2\pi)^{5/3}}\, \alpha_u^{2/3}(f_{h.f.}T_u)^{-2/3} \tag{3.13}$$

$$= 0.139632\, \alpha_u^{2/3}(fT_u)^{-2/3} \tag{3.14}$$

Moreover, for $f = 0$, (3.12) simplifies to

$$\chi_{1u}(0) = 4\int_0^\infty \xi_u(\tau)d\tau \tag{3.15}$$

$$= \frac{4T_u}{\alpha_u}\frac{\sqrt{\pi}\Gamma\left(\frac{5}{6}\right)}{\Gamma\left(\frac{1}{3}\right)} \tag{3.16}$$

$$= 4T_u\left(\frac{0.746834}{\alpha_u}\right) \tag{3.17}$$

Plotted in Figure 3.2 is the dimensionless autospectrum of the first term of the series, along with the limiting case in (3.14).

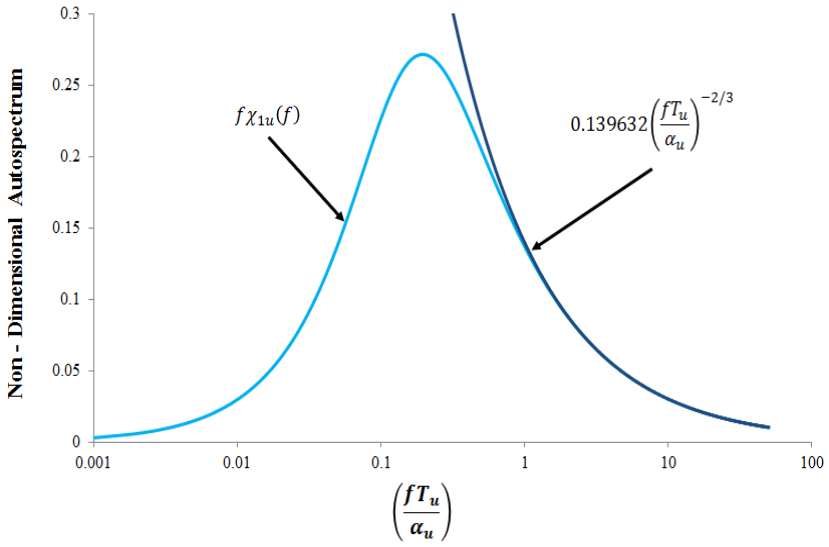

Figure 3.2: First term of the longitudinal series along with its high frequency limit

As expected, Figure 3.2 is identical to the original von Kármán model in (1.4). After all, the von Kármán model can be seen as a special case of the presented series expansion for $\beta_{1u} = 1$ and $\beta_{nu} = 0, n \geq 2$. It is instructive to notice that the model approaches the -2/3 decay rate at approximately $\left(\frac{fT_u}{\alpha_u}\right) = 1$. Experience shows that, in general, T_u is of the order from 0-10, while α_u is between zero and one. Thus, an order of magnitude estimate of when the dimensional von Kármán longitudinal spectrum begins to manifest its high frequency limit is 1 Hz. (Note: the plot in Figure 3.2 is non-dimensional in both axes.)

3.3 Second Term $\xi_u^2(\tau)$

$$\xi_u^2(\tau) = \frac{2^{4/3}}{\Gamma\left(\frac{1}{3}\right)^2}\left(\frac{\alpha_u \tau}{T_u}\right)^{2/3} \times \left[K_{1/3}\left(\frac{\alpha_u \tau}{T_u}\right)\right]^2 \tag{3.18}$$

$$\chi_{2u}(f) = 4\int_0^\infty \xi_u^2(\tau)\cos(2\pi f\tau)\, d\tau \tag{3.19}$$

$$= 4T_u \frac{\sqrt{\pi}\,\Gamma\left(\frac{5}{6}\right)}{\Gamma\left(\frac{1}{3}\right)}\,\alpha_u^{2/3}\,\frac{1}{(\alpha_u^2+\pi^2 f^2 T_u^2)^{5/6}}\left[{}_2F_1\left(\frac{5}{6},\frac{1}{6};\frac{4}{3};\frac{\pi^2 f^2 T_u^2}{\alpha_u^2+\pi^2 f^2 T_u^2}\right)\right] \quad (3.20)$$

where ${}_2F_1$ is a hypergeometric function, with many useful properties that are well documented. At high frequencies

$$f\chi_{2u}(f_{h.f.}) \approx \frac{\sqrt{\pi}\Gamma\left(\frac{5}{6}\right)}{\Gamma\left(\frac{1}{3}\right)}\,\frac{8}{(2\pi)^{5/3}}\,\alpha_u^{2/3}(f_{h.f.}T_u)^{-2/3} \quad (3.21)$$

$$= 0.279264\,\alpha_u^{2/3}(fT_u)^{-2/3} \quad (3.22)$$

which is exactly twice (3.14). Moreover, as seen from (3.19),

$$\chi_{2u}(0) = 4\int_0^\infty \xi_u^2(\tau)d\tau \quad (3.23)$$

$$= \frac{4T_u}{\alpha_u}\frac{\sqrt{\pi}\Gamma\left(\frac{5}{6}\right)}{\Gamma\left(\frac{1}{3}\right)}\frac{\sqrt{3}}{4} \quad (3.24)$$

$$= 4T_u\left(\frac{0.323389}{\alpha_u}\right) \quad (3.25)$$

Plotted in Figure 3.3 is the dimensionless autospectrum of the second term of the series, along with the limiting case in (3.22).

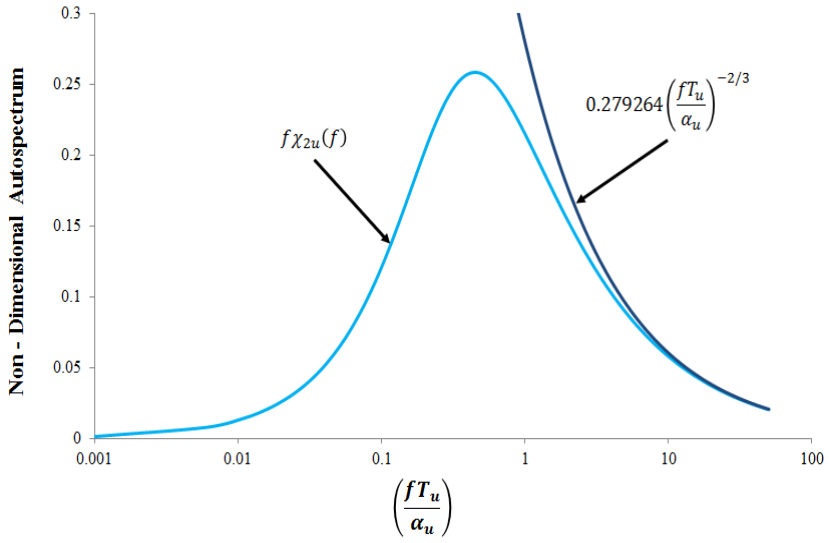

Figure 3.3: Second term of the longitudinal series along with its high frequency limit

Similar to Figure 3.2, it can be seen in Figure 3.3 that an order of magnitude estimate of when the dimensional second term of the expansion series reaches its high frequency limit is 10 Hz.

3.4 Third Term $\xi_u^3(\tau)$

$$\xi_u^3(\tau) = \frac{4}{\Gamma\left(\frac{1}{3}\right)^3}\left(\frac{\alpha_u\tau}{T_u}\right) \times \left[K_{1/3}\left(\frac{\alpha_u\tau}{T_u}\right)\right]^3 \tag{3.26}$$

$$\chi_{3u}(f) = 4\int_0^\infty \xi_u^3(\tau)\cos(2\pi f\tau)\,d\tau \tag{3.27}$$

This integral is not found in an analytical form; however, the following results were calculated numerically. At high frequencies

$$f\chi_{3u}(f_{h.f.}) \approx \frac{\sqrt{\pi}\Gamma\left(\frac{5}{6}\right)}{\Gamma\left(\frac{1}{3}\right)}\frac{12}{(2\pi)^{5/3}}\,\alpha_u^{2/3}\left(f_{h.f.}T_u\right)^{-2/3} \tag{3.28}$$

$$= 0.418895\ \alpha_u^{2/3}(fT_u)^{-2/3} \tag{3.29}$$

which is exactly three times (3.14). Similarly, (3.27) for $f = 0$ gives,

$$\chi_{3u}(0) = 4\int_0^\infty \xi_u^3(\tau)d\tau \tag{3.30}$$

$$= \frac{4T_u}{\alpha_u}\frac{\sqrt{\pi}\Gamma\left(\frac{5}{6}\right)}{\Gamma\left(\frac{1}{3}\right)} \times D \tag{3.31}$$

$$= T_u\left(\frac{0.194116}{\alpha_u}\right) \tag{3.32}$$

From numerical integration, it can be shown that $D = 0.259919$ to six decimal places. Plotted in Figure 3.4 is the dimensionless autospectrum of the third term of the series, along with the limiting case in (3.29).

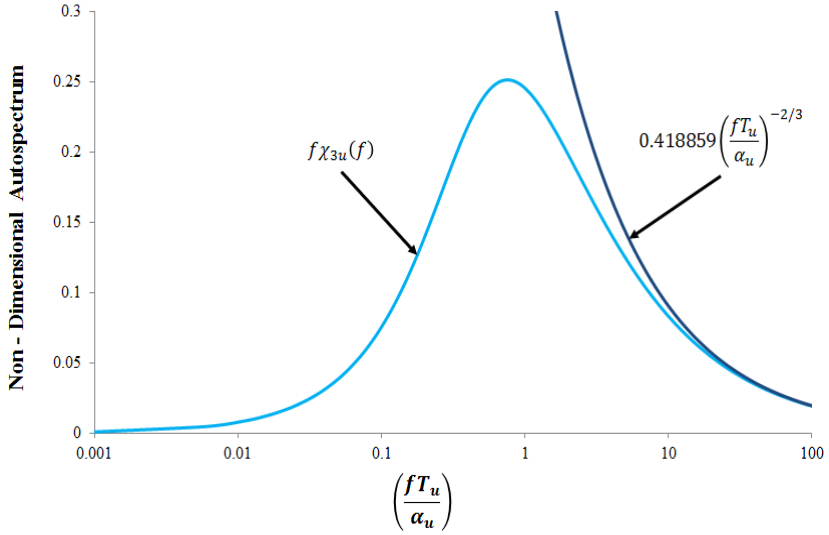

Figure 3.4: Third term of the longitudinal series along with its high frequency limit

Similar to Figure 3.2, it can be seen in Figure 3.4 that an order of magnitude estimate of when the dimensional second term of the expansion series reaches its high frequency limit is 50 Hz.

3.5 Implications of Terms

Given a data set, three conditions can be established regarding $\alpha_u, \beta_{1u}, \beta_{2u}$ ... etc. The β_{nu} coefficients are subject to only one constraint

$$\sum_{n=1}^{\infty} \beta_{nu} = 1 \tag{3.33}$$

This constraint is necessary to ensure that the resulting autocorrelation $\widetilde{\mathrm{R}}_u(\tau)$ from (3.7) maintains the foremost property of a normalized autocorrelation, i.e. $\widetilde{\mathrm{R}}_u(0) = 1$. The value of α_u is not arbitrary, unlike the β coefficients. The α_u parameter is fixed in that it is based on the selection of the β coefficients. The derivation for this scaling parameter is as follows.

Begin with the expanded series:

$$\tilde{R}_u(\tau) = \beta_{1\mathrm{u}}\xi_u(\tau) + \beta_{2\mathrm{u}}\xi_u^2(\tau) + \beta_{3\mathrm{u}}\xi_u^3(\tau) + \cdots + \beta_{nu}\xi_u^n(\tau)$$

With the properties:

$$\tilde{R}_u(0) = 1$$

$$\int_0^{\infty} \tilde{R}_u(\tau)d\tau = T_u$$

expansion of (3.7) yields

$$\int_0^\infty \tilde{R}_u(\tau)d\tau = \beta_{1u}\int_0^\infty \xi_u(\tau)d\tau + \beta_{2u}\int_0^\infty \xi_u^2(\tau)d\tau + \cdots + \beta_{nu}\int_0^\infty \xi_u^n(\tau)d\tau = T_u \qquad (3.34)$$

Let

$$\bar{\tau} = \frac{\alpha_u \tau}{T_u}$$

Therefore,

$$d\bar{\tau} = \frac{\alpha_u}{T_u}d\tau \quad \Longrightarrow \quad d\tau = \frac{T_u}{\alpha_u}d\bar{\tau} \qquad (3.35)$$

Substituting (3.35) into the right hand side equivalencies of (3.34) results in,

$$\frac{T_u}{\alpha_u}\left[\beta_{1u}\int_0^\infty \xi_u(\bar{\tau})d\bar{\tau} + \beta_{2u}\int_0^\infty \xi_u^2(\bar{\tau})d\bar{\tau} + \cdots + \beta_{nu}\int_0^\infty \xi_u^n(\bar{\tau})d\bar{\tau}\right] = T_u$$

Equivalently,

$$\alpha_u = \beta_{1u}\int_0^\infty \xi_u(\bar{\tau})d\bar{\tau} + \beta_{2u}\int_0^\infty \xi_u^2(\bar{\tau})d\bar{\tau} + \cdots + \beta_{nu}\int_0^\infty \xi_u^n(\bar{\tau})d\bar{\tau} \qquad (3.36)$$

In light of (3.17), (3.25), (3.32), and (3.36) it can be shown that

$$\alpha_u = 0.746834\beta_{1u} + 0.323389\beta_{2u} + 0.194116\beta_{3u} + \cdots \qquad (3.37)$$

An examination of condition (iii) of (1.11), in conjunction with (3.14), (3.22), and (3.29) will yield

$$\frac{A_u}{\alpha_u^{2/3}} = \frac{4\sqrt{\pi}\,\Gamma\left(\frac{5}{6}\right)}{\Gamma\left(\frac{1}{3}\right)}\frac{1}{(2\pi)^{5/3}}[\beta_{1u} + 2\beta_{2u} + 3\beta_{3u} + \cdots] \qquad (3.38)$$

$$= 0.139632\beta_{1u} + 0.279264\beta_{2u} + 0.418895\beta_{3u} + \cdots \qquad (3.39)$$

The preceding perturbation scheme, or series expansion approach is typified by (3.7) and (3.8), and by the three constraints typified by (3.33), (3.38), and (3.39). Descriptively stated, the developed model involves selecting a series of spectral points from a database, and extracting a least squares fit subject to these three constraint equations. In doing so, a representation of the longitudinal spectrum of turbulence with a closed form expression can be created, and maintain the properties of a valid spectral model detailed in (1.11) on page 8. Although this scheme does not guarantee that $(\beta_1 \gg \beta_2)$ and that $(\beta_2 \gg \beta_3)$, it does provide a practical means of developing interpretive models of formidably complex flow fields. The developed models, by design, have a simple analytical structure that facilitates delineation and simulations. Moreover, they satisfy all three mathematical qualifiers that are required of a spectral model. As it turns out, no more than a second order correction (a three term series) is required.

Figure 3.5 shows the first three terms of (3.8) plotted independently of each other. Three trends can be identified from this figure:

(i) The height of the spectrum decreases with increasing terms;

(ii) The location at the peak of the spectrum shifts towards the higher frequency range; and

(iii) The elevation of the high frequency limiting case of the spectrum increases with increasing terms.

These qualities aside, the fact that there is variation amongst the three characteristics listed above is of importance. These three characteristics coincide perfectly with the criticisms in Table 1.1; that is, for most spectra that are not well represented by the von Kármán model, there exists a combination of β_{nu} coefficients in (3.7), subject to the constraints of (3.33), (3.38), and (3.39), that will represent a better fit of the power spectrum of turbulence than the von Kármán model, by itself.

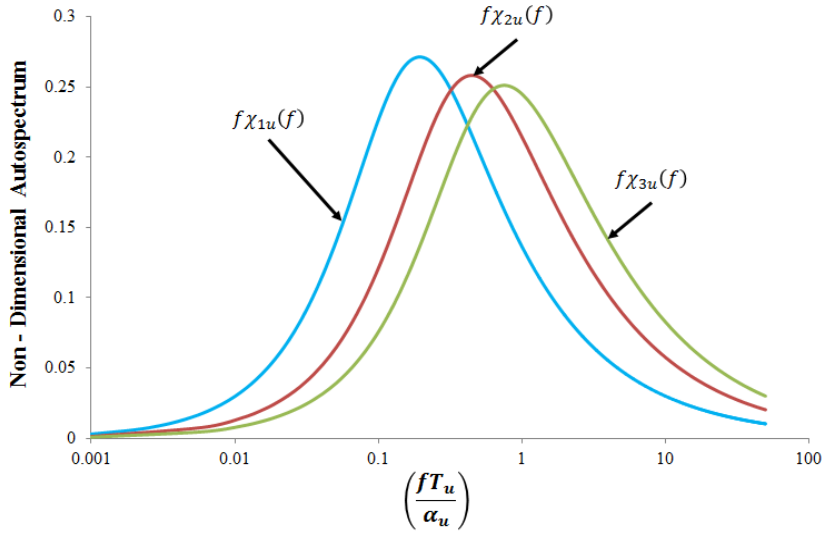

Figure 3.5: First three terms of expansion series in the frequency domain

For reference, provided in Table 3.1 are the constants from equation (3.37) and equation (3.39) up to seven terms with high accuracy precision.

Table 3.1: Constants from Equations (3.37) and (3.39) for first seven terms

TERM	Equation (3.37)	Equation (3.39)
1	0.7476834201056597	0.1396318231
2	0.323388695258742	0.2792636462
3	0.194117929829485	0.4188954693
4	0.133860978362717	0.5585272923
5	0.099798309222461	0.6981591154
6	0.078244974866071	0.8377909385
7	0.063551213297927	0.9774227616

CHAPTER 4: LATERAL EXPANSION

Presented in the previous chapter was Harris's treatment of the von Kármán model of longitudinal turbulence. In Harris's original treatment of the lateral component of turbulence, continuity and an assumption of isotropic turbulence are invoked, and the resulting model is composed of ambiguously defined parameters. The current chapter is a separate derivation of an expansion series, similar to, but completely separate from the longitudinal series. With the addition of this series expansion, users have the ability to model longitudinal and lateral turbulence using the same scheme while avoiding the assumption of isotropic turbulence. As mentioned in the introduction, this assumption is, at best, a theoretical artifact and it is hardly applicable to flow fields of engineering interest. It should be noted that this entire chapter will refer to 'lateral' turbulence; however, as seen in (1.2) and (1.3), 'lateral' and 'vertical' are equivalent in their treatment. Therefore, the entirety of this chapter's content is valid for vertical turbulence, except for the adjustments of component specific parameters such as time scale and variance.

4.1 Justification of the Scheme

The justification for the lateral expansion is identical to what was presented in the previous chapter. In order to avoid confusion and to facilitate continuity of presentation, the justification is repeated here with proper notation. Begin with a time history $v(t)$ of

lateral turbulence velocities at a location of interest. The normalized autocorrelation of this data series from Chapter 2 is:

$$R_v(\tau) = \frac{1}{\sigma_v^2} \lim_{T\to\infty} \frac{1}{2T} \int_{-T}^{T} v(t)v(t+\tau)d\tau \tag{4.1}$$

The one sided, non-dimensional, autospectrum of the time series $v(t)$ can be calculated by a Fourier cosine transform of the autocorrelation, namely:

$$\frac{fS_v(f)}{\sigma_v^2} = 4f \int_0^{\infty} R_v(\tau)\cos(2\pi f\tau)\, d\tau \tag{4.2}$$

where the autocorrelation $R_v(\tau)$ is realized via the inverse Fourier transform:

$$R_v(\tau) = \frac{1}{\sigma_v^2} \int_0^{\infty} S_v(f)\cos(2\pi f\tau)\, df \tag{4.3}$$

Due to the fact that $R_v(\tau)$ is an even, real valued function, $fS_v(f)/\sigma_v^2$ will be a positive, real valued function. From Chapter 1 equation (1.2) (or (1.3) for the vertical), $\xi_v(\tau)$, is the von Kármán autocorrelation model of $R_v(\tau)$ in (4.3). The von Kármán form calls for a parameter T_v with the dimensions of time. One option would be to use the time scale of the time history $v(t)$ defined as:

$$T_v = \int_0^{\infty} R_v(\tau)d\tau \tag{4.4}$$

By setting $\tau = 0$ in (4.3), and $f = 0$ in (4.2), it is seen that

$$\frac{1}{\sigma_v^2}\int_0^\infty S_v(f)df = 1 \tag{4.5}$$

And

$$S_v(0) = 4\sigma_v^2\int_0^\infty \xi_v(\tau)d\tau = 4\sigma_v^2 T_v \tag{4.6}$$

With these definitions in place, a perturbation scheme can be applied. It is a well-known feature of stochastic processed theory that for a random process with a normalized autocorrelation $\xi_v(\tau)$, that undergoes a non-linear transform, for many nonlinearities, the resulting output process will have an autocorrelation that can be represented by a perturbation series of the form

$$\tilde{R}_v(\tau) = \beta_{1v}\xi_v(\tau) + \beta_{2v}\xi_v^2(\tau) + \beta_{3v}\xi_v^3(\tau) + \cdots + \beta_{nv}\xi_v^n(\tau) \tag{4.7}$$

where the parameters $\beta_{nv}, n = 1,2,3 \ldots \infty$ are unknown constants. Figure 4.1 shows the first three terms of the expanded series with $\beta_{nv} = 1$.

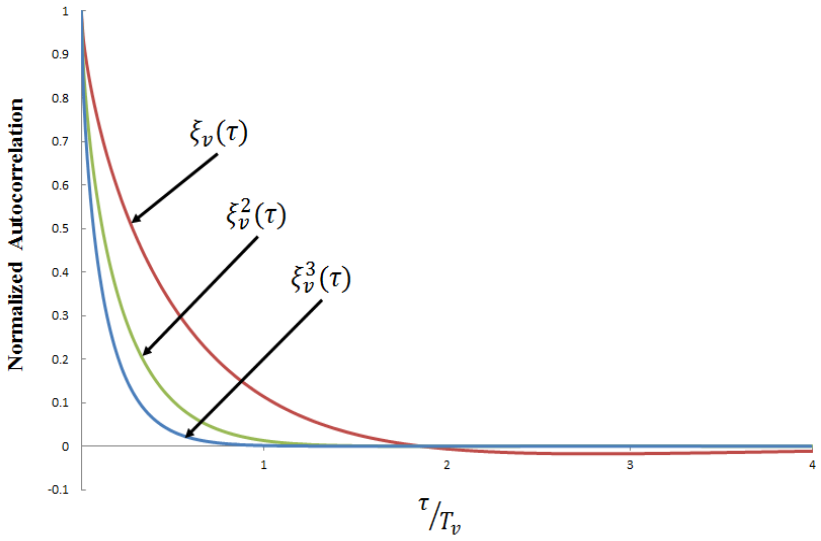

Figure 4.1: First three terms of the lateral expansion series

The resulting spectrum from the Fourier transform of (4.7) will then be:

$$\tilde{S}_v(f) = \beta_{1v}\,\chi_{1v}(f) + \beta_{2v}\,\chi_{2v}(f) + \beta_{3v}\,\chi_{3v}(f) + \cdots + \beta_{nv}\,\chi_{nv}(f) \qquad (4.8)$$

where

$$\chi_{nv}(f) = 4\int_0^{\infty} \xi_v^n(\tau)\cos(2\pi f\tau)\,d\tau \qquad n = 1,2,3,\ldots,\infty \qquad (4.9)$$

Since this expansion is applied to the lateral von Kármán model, the basis autocorrelation function would be:

$$\xi_v(\tau) = \frac{2^{2/3}}{\Gamma\left(\frac{1}{3}\right)}\left(\frac{\alpha_v\tau}{T_v}\right)^{1/3} \times \left[K_{1/3}\left(\frac{\alpha_v\tau}{T_v}\right) - \frac{1}{2}\left(\frac{\alpha_v\tau}{T_v}\right)K_{2/3}\left(\frac{\alpha_v\tau}{T_v}\right)\right] \qquad (4.10)$$

The α_v parameter presented in (4.10) merits explanation. This is a scaling parameter that must be introduced into the model, to further ensure that the expanded autocorrelation in

(4.7) maintains the property in (4.4). The following is a treatment of the first three terms in the expansion shown in (4.8).

4.2 First Term $\xi_v(\tau)$

$$\xi_v(\tau) = \frac{2^{2/3}}{\Gamma\left(\frac{1}{3}\right)}\left(\frac{\alpha_v\tau}{T_v}\right)^{1/3} \times \left[K_{1/3}\left(\frac{\alpha_v\tau}{T_v}\right) - \frac{1}{2}\left(\frac{\alpha_v\tau}{T_v}\right)K_{2/3}\left(\frac{\alpha_v\tau}{T_v}\right)\right]$$

$$\chi_{1v}(f) = 4\int_0^\infty \xi_v(\tau)\cos(2\pi f\tau)\,d\tau \tag{4.11}$$

$$= 4T_v\frac{\sqrt{\pi}\,\Gamma\left(\frac{5}{6}\right)}{6\,\Gamma\left(\frac{1}{3}\right)}\,\alpha_v^{2/3}\left[\frac{3\alpha_v^2 + 32f^2T_v^2\pi^2}{(\alpha_v^2 + 4f^2T_v^2\pi^2)^{11/6}}\right] \tag{4.12}$$

At very high frequencies

$$f\chi_{1v}(f_{h.f.}) \approx \frac{16}{3(2\pi)^{5/3}}\,\frac{\sqrt{\pi}\,\Gamma\left(\frac{5}{6}\right)}{\Gamma\left(\frac{1}{3}\right)}\,\alpha_v^{2/3}(T_vf)^{-2/3} \tag{4.13}$$

$$= 0.186176\,\alpha_v^{2/3}(T_vf)^{-2/3} \tag{4.14}$$

$$\chi_{1v}(0) = 4\int_0^\infty \xi_v(\tau)d\tau \tag{4.15}$$

$$\chi_{1v}(0) = \frac{4T_v}{\alpha_v}\,\frac{\sqrt{\pi}\,\Gamma\left(\frac{5}{6}\right)}{2\,\Gamma\left(\frac{1}{3}\right)} \tag{4.16}$$

$$= 4T_v\left(\frac{0.373417}{\alpha_v}\right) \tag{4.17}$$

Plotted in Figure 4.2 is the dimensionless autospectrum of the first term of the series, along with the limiting case in (4.14).

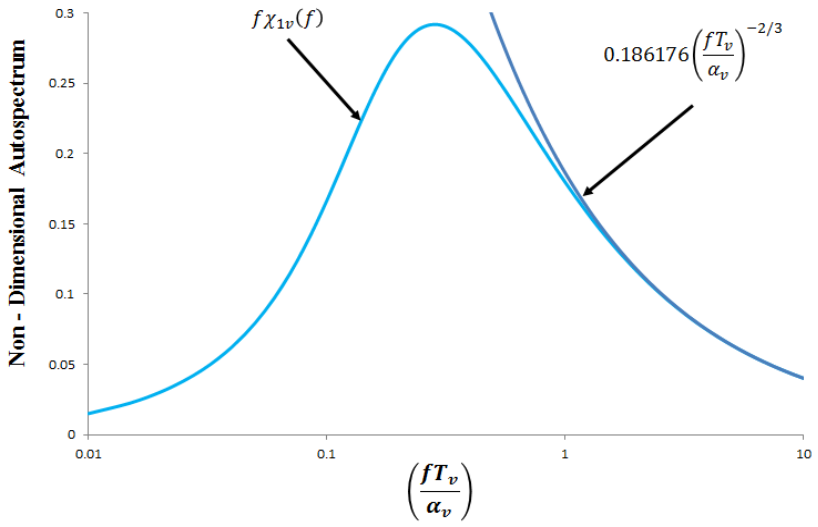

Figure 4.2: First term of the lateral series along with its high frequency limit

Observe that Figure 4.2 is identical to the original von Kármán model in (1.5) and (1.6). This is expected, for a von Kármán model is a special case of the presented series expansion for $\beta_{1v} = 1$ and $\beta_{nv} = 0, n \geq 2$. Also note that the model approaches the -2/3 decay rate at approximately $\left(\frac{fT_v}{\alpha_v}\right) = 1$. Experience shows that, in general, T_v is of the order from 0-10, while α_v is between zero and one. Thus, an order of magnitude estimate of when the dimensional von Kármán model reaches its high frequency limit is 1 Hz.

4.3 Second Term $\xi_v^2(\tau)$

$$\xi_v^2(\tau) = \frac{2^{4/3}}{\Gamma\left(\frac{1}{3}\right)^2}\left(\frac{\alpha_v\tau}{T_v}\right)^{2/3} \times \left[K_{1/3}\left(\frac{\alpha_v\tau}{T_v}\right) - \frac{1}{2}\left(\frac{\alpha_v\tau}{T_v}\right)K_{2/3}\left(\frac{\alpha_v\tau}{T_v}\right)\right]^2 \tag{4.18}$$

$$\chi_{2v}(f) = 4\int_0^\infty \xi_v^2(\tau)\cos(2\pi f\tau)\,d\tau \tag{4.19}$$

$$\begin{aligned}
&= \left(4T_v \frac{\sqrt{\pi}\,\Gamma\left(\frac{5}{6}\right)}{6\,\Gamma\left(\frac{1}{3}\right)}\alpha^{-1}\right) \\
&\times \left[\frac{3\sqrt{3}}{4}\frac{\alpha_v^{5/3}}{(\alpha_v^2 + f^2T_v^2\pi^2)^{5/6}}\ {}_2F_1\left(\frac{5}{6},\frac{1}{6};\frac{4}{3};\frac{\pi^2f^2T_v^2}{\alpha_v^2 + f^2T_v^2\pi^2}\right)\right. \\
&+ \frac{35\sqrt{3}}{32}\left(\frac{\pi^2f^2T_v^2}{\alpha_v^2 + f^2T_v^2\pi^2}\right)\frac{\alpha_v^{5/3}}{(\alpha_v^2 + f^2T_v^2\pi^2)^{5/6}}\ {}_2F_1\left(\frac{11}{6},\frac{1}{6};\frac{7}{3};\frac{\pi^2f^2T_v^2}{\alpha_v^2 + f^2T_v^2\pi^2}\right) \\
&+ \frac{45\sqrt{3}}{256}\,{}_2F_1\left(\frac{11}{6},\frac{7}{6};\frac{7}{3};-\frac{\pi^2f^2T_v^2}{\alpha_v^2}\right) \\
&- \frac{165\sqrt{3}}{256}\left(\frac{\pi^2f^2T_v^2}{\alpha_v^2}\right){}_2F_1\left(\frac{13}{6},\frac{17}{6};\frac{10}{3};-\frac{\pi^2f^2T_v^2}{\alpha_v^2}\right) \\
&\left.+ \frac{2431\sqrt{3}}{6144}\left(\frac{\pi^2f^2T_v^2}{\alpha_v^2}\right)^2{}_2F_1\left(\frac{19}{6},\frac{23}{6};\frac{13}{3};-\frac{\pi^2f^2T_v^2}{\alpha_v^2}\right)\right]
\end{aligned} \tag{4.20}$$

At very high frequencies

$$f\chi_{2v}(f_{h.f.}) \approx \frac{32}{3(2\pi)^{5/3}}\,\frac{\sqrt{\pi}\Gamma\left(\frac{5}{6}\right)}{\Gamma\left(\frac{1}{3}\right)}\,\alpha_v^{2/3}(T_vf)^{-2/3} \tag{4.21}$$

$$= 0.372352\,\alpha_v^{2/3}(T_vf)^{-2/3} \tag{4.22}$$

which is exactly twice (4.14). Moreover,

$$\chi_{2v}(0) = 4\int_0^\infty \xi_v^2(\tau)d\tau \tag{4.23}$$

The above integral lends itself to the closed form solution:

$$\chi_{2v}(0) = \frac{4T_v}{\alpha_u} \frac{\sqrt{\pi}\Gamma\left(\frac{5}{6}\right)}{2\,\Gamma\left(\frac{1}{3}\right)} \left(\frac{79\sqrt{3}}{256}\right) \tag{4.24}$$

$$= 4T_v \left(\frac{0.199591}{\alpha_v}\right) \tag{4.25}$$

Plotted in Figure 4.3 is the dimensionless autospectrum of the first term of the series, along with the limiting case in (4.22).

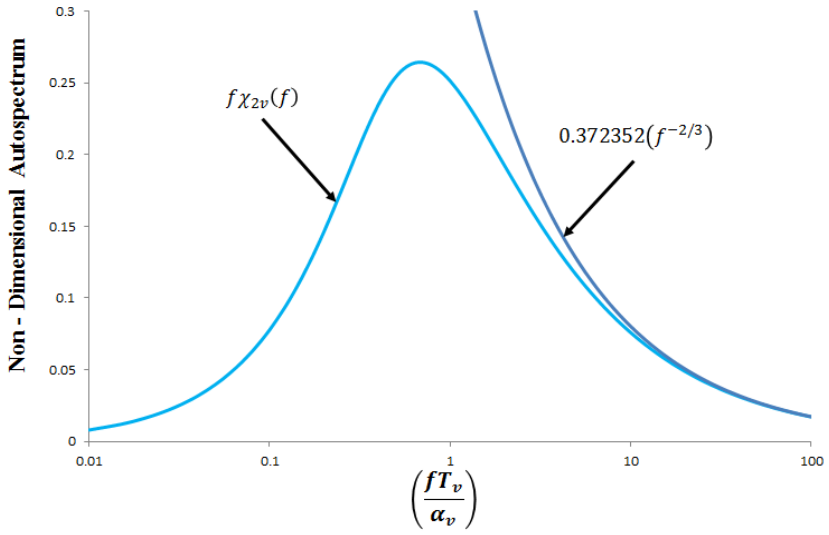

Figure 4.3: Second term of the lateral expansion spectrum with its high frequency limit

Similar to Figure 4.2, it can be seen in Figure 4.3 that an order of magnitude estimate of when the dimensional second term of the expansion series reaches its high frequency limit is 10 Hz.

4.4 Third Term $\xi_v^3(\tau)$

$$\xi_v^3(\tau) = \frac{4}{\Gamma\left(\frac{1}{3}\right)}\left(\frac{\alpha_v\tau}{T_v}\right) \times \left[K_{1/3}\left(\frac{\alpha_v\tau}{T_v}\right) - \frac{1}{2}\left(\frac{\alpha_v\tau}{T_v}\right)K_{2/3}\left(\frac{\alpha_v\tau}{T_v}\right)\right]^3 \tag{4.26}$$

$$\chi_{3v}(f) = 4\int_0^\infty \xi_v^3(\tau)\cos(2\pi f\tau)\,d\tau \tag{4.27}$$

This integral is not found in an analytical form; however, the following results can be calculated numerically, and by identifying the pattern in (4.13) and (4.21). At high frequencies

$$f\chi_{3v}(f_{h.f.}) \approx \frac{48}{3(2\pi)^{5/3}}\,\frac{\sqrt{\pi}\Gamma\left(\frac{5}{6}\right)}{\Gamma\left(\frac{1}{3}\right)}\,\alpha_v^{2/3}(T_v f)^{-2/3} \tag{4.28}$$

$$= 0.558527\,\alpha^{2/3}(T_v f)^{-2/3} \tag{4.29}$$

which is exactly three times (4.14). Moreover,

$$\chi_{3u}(0) = 4\int_0^\infty \xi_u^3(\tau)d\tau \tag{4.30}$$

$$= \frac{4T_u}{\alpha_u}\frac{\sqrt{\pi}\Gamma\left(\frac{5}{6}\right)}{2\,\Gamma\left(\frac{1}{3}\right)} \times D \tag{4.31}$$

$$= 4T_v\left(\frac{0.122360}{\alpha_v}\right) \tag{4.32}$$

From numerical integration, it can be shown that $D = 0.327676$ to six decimal places. Plotted in Figure 4.4 is the dimensionless autospectrum of the third term of the series, along with the limiting case in (4.29).

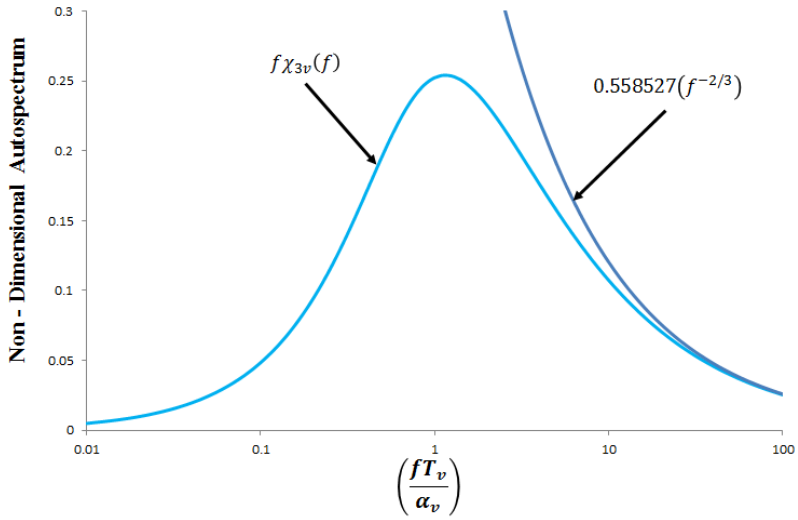

Figure 4.4: Third term of lateral expansion series spectrum with its high frequency limit

Similar to Figure 4.2, it can be seen in Figure 4.4 that an order of magnitude estimate of when the dimensional second term of the expansion series reaches its high frequency limit is 50 Hz.

4.5 Implications of Terms

The results of the lateral expansion series are remarkably close to the longitudinal. Therefore, three similar constraints can be determined, first:

$$\sum_{n=1}^{\infty} \beta_{nv} = 1 \tag{4.33}$$

which is required to ensure that the resulting autocorrelation $\widetilde{\mathrm{R}}_v(\tau)$ maintains the foremost property of a normalized autocorrelation, i.e. $\widetilde{\mathrm{R}}_v(0) = 1$. The value of α_v is again dependent upon the β coefficients. The α_u parameter can be derived from (4.17), (4.25), (4.32), and integrating (4.7). This results in

$$\alpha_v = \frac{\sqrt{\pi}\Gamma\left(\frac{5}{6}\right)}{2\,\Gamma\left(\frac{1}{3}\right)}\left[\beta_{1v} + \beta_{2v}\frac{79\sqrt{3}}{256} + \beta_{3v} \times D\right] \tag{4.34}$$

$$\alpha_v = 0.373417\beta_{1v} + 0.199591\beta_{2v} + 0.122360\beta_{3v} \tag{4.35}$$

Furthermore, from condition (iii) of (1.11), in conjunction with (4.14), (4.22), and (4.29) the Kolmogorov asymptotic law or the 'A' constraint yields

$$\frac{A_v}{\alpha_v^{2/3}} = \frac{16}{3(2\pi)^{5/3}}\,\frac{\sqrt{\pi}\,\Gamma\left(\frac{5}{6}\right)}{\Gamma\left(\frac{1}{3}\right)}\,[\beta_{1v} + 2\beta_{2v} + 3\beta_{3v} + \cdots] \tag{4.36}$$

$$\frac{A_v}{\alpha_v^{2/3}} = 0.186176\beta_{1v} + 0.372352\beta_{2v} + 0.558527\beta_{3v} \tag{4.37}$$

Similar to the longitudinal expansion of the previous chapter, the lateral expansion results in autocorrelation and autospectrum models of the form in (4.7) and (4.8), and is subject to the constraints of (4.33), (4.35), and (4.37). Figure 4.5 shows the first three terms of the expanded spectrum, with the same patterns apparent as the longitudinal expansion on page 34.

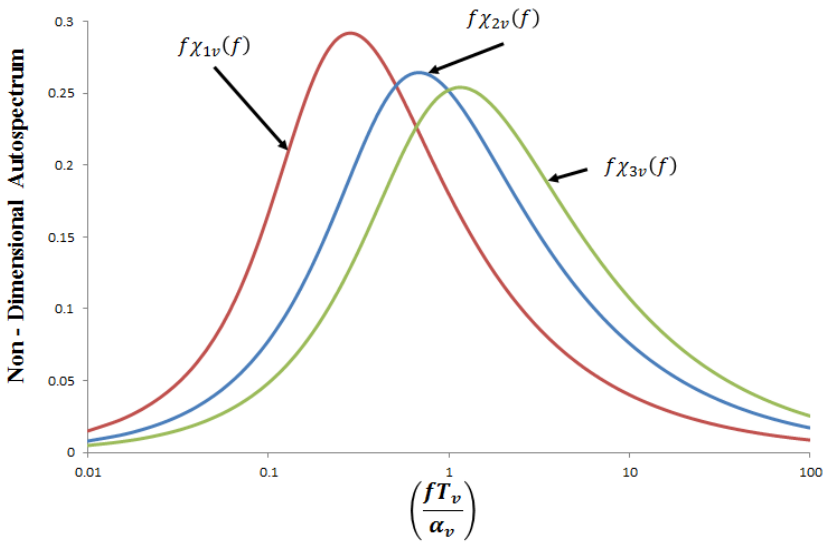

Figure 4.5: First three terms of the lateral spectrum expansion series

For reference, Table 4.1 shows high accuracy resolution for the first seven constants of (4.35) and (4.37).

Table 4.1: Constants from Equations (4.35) and (4.37) for first seven terms

TERM	Equation (4.35)	Equation (4.37)
1	0.373417100215128	0.1861757641
2	0.199591460470270	0.3723515282
3	0.122359610949040	0.5585272923
4	0.085254426617168	0.7447030565
5	0.063913059182907	0.9308788206
6	0.050279901221780	1.117054585
7	0.040929782158207	1.303230349

CHAPTER 5: SERIES CHARACTERISTICS

The formulation of the series expansion equations and the constants in the respective constraint equations are strikingly similar for all three velocity components. In fact, these constraints are identical for the lateral and vertical. Thankfully, this allows an investigation into one formulation, lateral or longitudinal, to be applied to the other. This chapter will discuss each of the three constraints that were derived in the previous chapters, to provide insight into the consequences of each constraint. Table 5.1 below, summarizes these three constraints, in general terms. Due to the similarity of these two models, throughout this chapter, all results and prescriptions are applicable to all three velocity components, and for notational simplicity, the subscripts are omitted.

Table 5.1: Three constraints in general terms

(a) $$\beta_1 + \beta_2 + \beta_3 + \cdots = 1$$

(b) $$\alpha = C_1\beta_2 + C_2\beta_2 + C_3\beta_3 + \cdots + C_n\beta_n$$

(c) $$\frac{A}{\alpha^{2/3}} = Y_1\beta_2 + Y_2\beta_2 + Y_3\beta_3 + \cdots + Y_n\beta_n$$

where Y_n and C_n are the constants detailed in the Chapters 3 and 4.

5.1 Beta Constraint (a)

$$\beta_1 + \beta_2 + \beta_3 + \cdots = 1$$

The purpose of this constraint is to maintain the identity:

$$\frac{1}{\sigma^2}\int_0^\infty S(f)df = 1$$

As well as

$$R(0) = 1$$

Explicitly stated, this constraint ensures that the expansion series model with the von Kármán autocorrelation model as the basis function will be one at lag time of zero, and that the area under the corresponding normalized spectrum will be one. This constraint is highly flexible, and is met with ease. The possible combinations of β coefficients that will satisfy this constraint are infinite. Even with a truncated series of two or three terms, there is no problem identifying β coefficients that improve the fit, and sum to one. Table 5.2 shows several combinations of β coefficients that sum to one. As a visual aid, the graphs of the lateral expansion models with the corresponding α and A values from constraints (b) and (c) of Table 5.1 are shown in Figure 5.1-Figure 5.8.

Table 5.2: An example of β coefficients with corresponding α_v and $'A_v'$ values for the lateral expansion series

Figure	$\boldsymbol{\beta_{1v}}$	$\boldsymbol{\beta_{2v}}$	$\boldsymbol{\beta_{3v}}$	$\boldsymbol{\alpha_v}$	$\boldsymbol{A}$
Figure 5.1	1.500	-0.500	0.000	0.460323	0.055497
Figure 5.2	1.250	-0.250	0.000	0.416874	0.077921
Figure 5.3	1.000	0.000	0.000	0.373417	0.096543
Figure 5.4	0.750	0.250	0.000	0.329961	0.111124
Figure 5.5	0.500	0.500	0.000	0.286504	0.121367
Figure 5.6	0.333	0.333	0.333	0.231558	0.140268
Figure 5.7	0.250	0.500	0.250	0.223740	0.137230
Figure 5.8	0.000	0.500	0.500	0.160976	0.137732

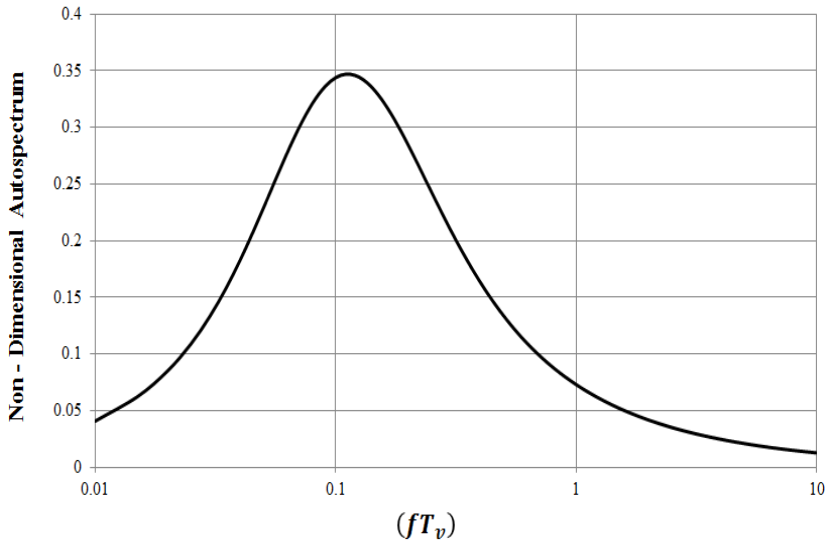

Figure 5.1: Lateral expansion series with $\beta_1 = 1.500,\ \beta_2 = -0.500$, and $\beta_3 = 0.000$

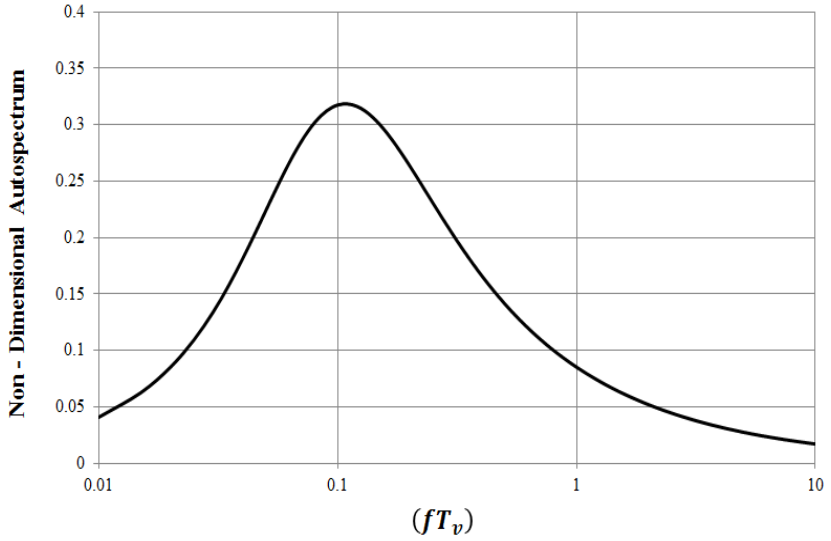

Figure 5.2: Lateral expansion series with $\beta_1 = 1.250,\ \beta_2 = -0.250$, and $\beta_3 = 0.000$

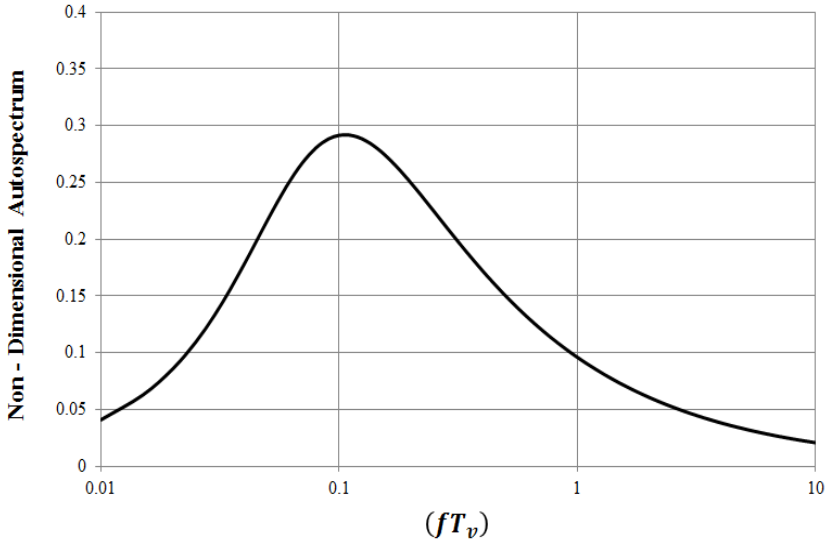

Figure 5.3: Lateral expansion series with $\beta_1 = 1.000,\ \beta_2 = 0.000$, and $\beta_3 = 0.000$

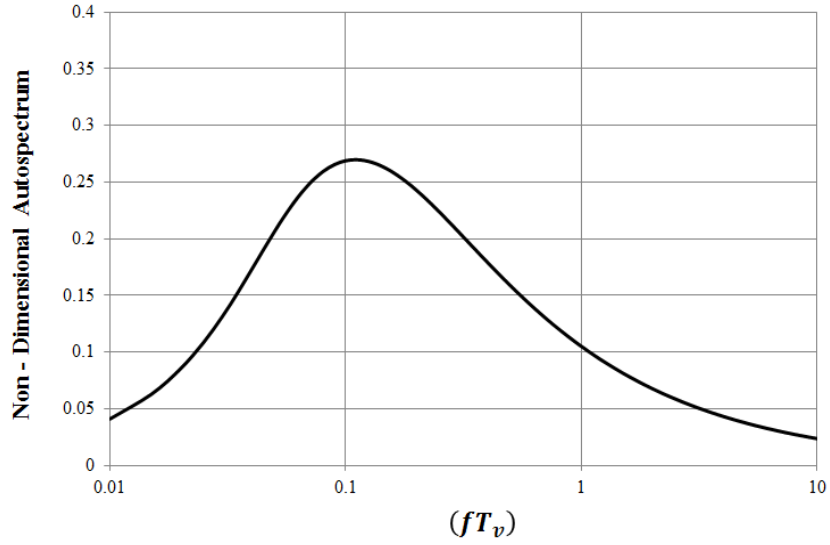

Figure 5.4: Lateral expansion series with $\beta_1 = 0.750,\ \beta_2 = 0.250$, and $\beta_3 = 0.000$

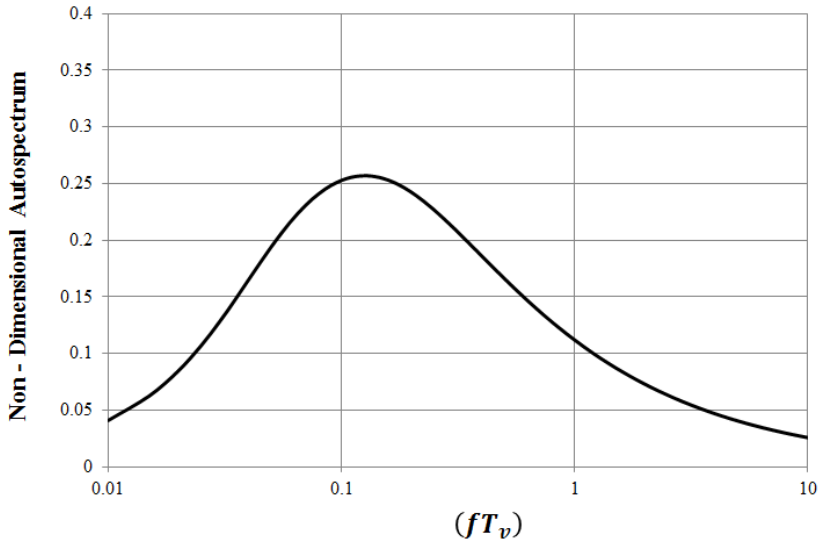

Figure 5.5: Lateral expansion series with $\beta_1 = 0.500,\ \beta_2 = 0.500$, and $\beta_3 = 0.000$

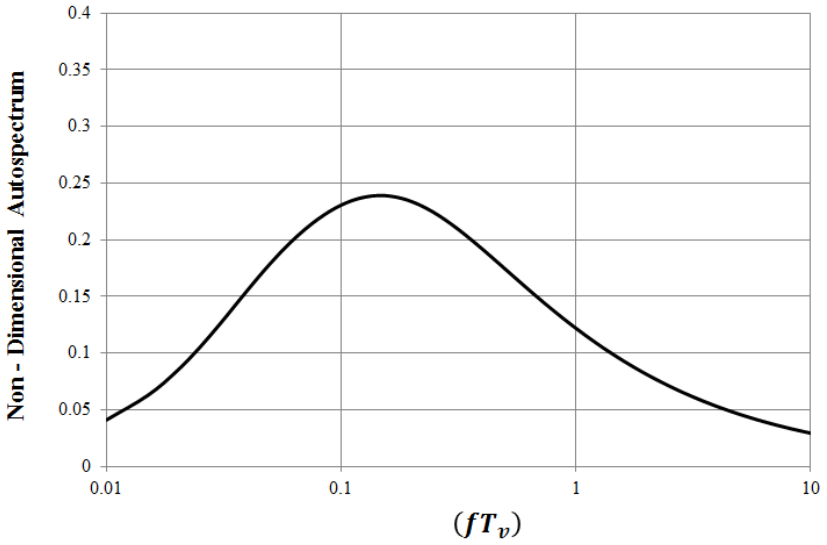

Figure 5.6: Lateral expansion series with $\beta_1 = 0.333,\ \beta_2 = 0.333$, and $\beta_3 = 0.333$

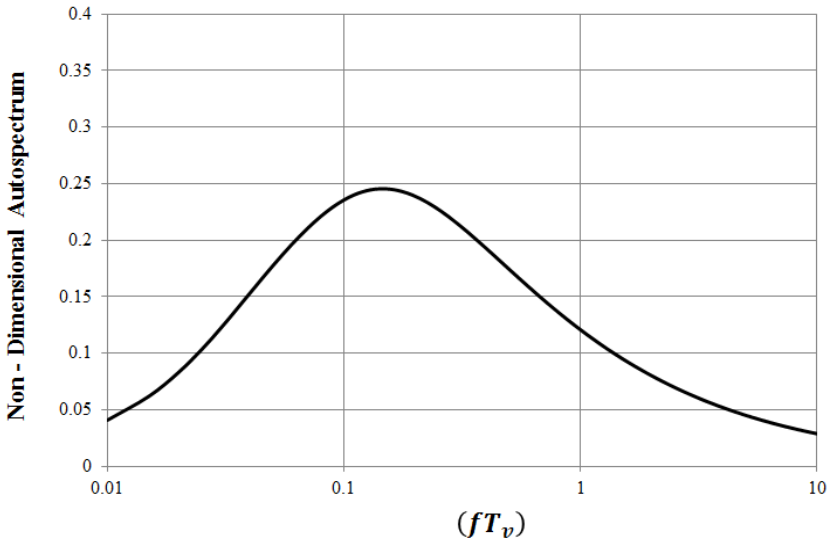

Figure 5.7: Lateral expansion series with $\beta_1 = 0.250,\ \beta_2 = 0.500$, and $\beta_3 = 0.250$

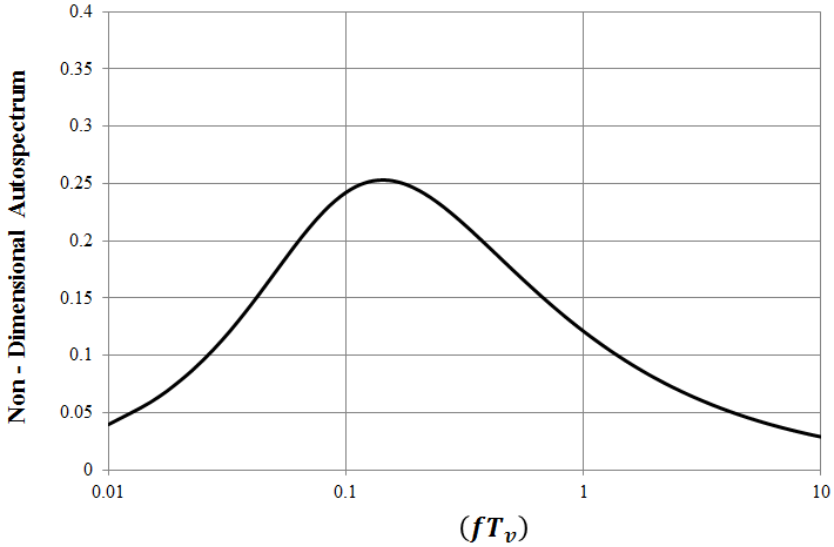

Figure 5.8: Lateral expansion series with $\beta_1 = 0.000,\ \beta_2 = 0.500$, and $\beta_3 = 0.500$

It is apparent from Figure 5.1-Figure 5.8 that the variation of β coefficients exhibits tremendous shape modification of the expansion series. Specifically, the variation in three key characteristics can be seen: 1) the height of the peak can be varied significantly, 2) the location of the peak can be moved towards both a higher and lower frequency, and 3) the width of the peak can also be modified significantly as well.

5.2 Alpha Constraint (b)

$$\alpha = C_1\beta_2 + C_2\beta_2 + C_3\beta_3 + \cdots + C_n\beta_n$$

Up until this point, the function above has been termed a 'constraint' as though it is a separate function from the other two in Table 5.1. This gives the incorrect idea of the problem: "three equations, and n unknowns." However, this is not the case. It should be noted that α is a scaling parameter that is dependent on the β coefficients, not the other way around. When selecting 'n' β's, this 'constraint' is not limiting in anyway, because α remains undetermined. Despite this fact, there are very significant implications that the α parameter has on the variation of the expansion series model.

As mentioned in Chapters Three and Four, the purpose of the α parameter is to ensure that $\int_0^\infty R_i(\tau) = T_i$ and that this property holds even for the expansion series. In the frequency domain, this parameter ensures that the value of $S_i(0) = 4\sigma_i^2 T_i$, which is one of the criteria deemed necessary from (1.11) on page 8. In other words, if one calculates the value of $S_i(0)$ from raw data, so long as the α parameter is calculated properly, the expansion series will match with $S_i(0) = \tilde{S}_i(0)$. It is noteworthy, that this quantity is not represented on a log-log plot of the autospectrum as seen in the sample plot in Figure 5.9.

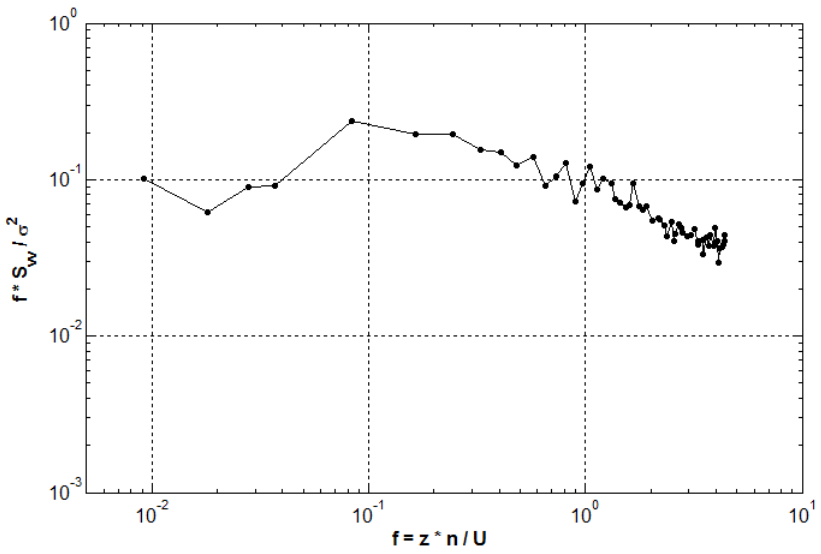

Figure 5.9: A sample of non-dimensional autospectrum of lateral turbulence. Note the lack of data below f=0.01

As seen in the figure above, the spectrum data in the log-log plot above does not concern the spectrum at zero frequency. Figure 5.9 is a representative sample of autospectrum that wind engineers are concerned with, and is the type of spectrum that modeling in this thesis is concerned with. Due to this fact, it is recommended that the time scale of turbulence be calculated from the first value of that spectrum that is to be modeled. Therefore, if:

$$S_i(0) = 4\sigma_i^2 T_i$$

Then

$$T_i = \frac{S_i(0)}{4\sigma_i^2} \tag{5.1}$$

In (5.1), $S_i(0)$ is the point on the calculated autospectrum at the lowest frequency that is to be modeled. In Figure 5.9, this would be the far left point. The reason for this indirect calculation of T_i is twofold:

1) It avoids the complication detailed in the discrete calculation of the autocorrelation function detailed in Chapter 2; and
2) It provides a fitting aid in ensuring that the expansion series will be equivalent to the calculated spectrum at the first point of the data

To illustrate the importance of the α parameter, Figure 5.10 shows the case of $\beta_{1v} = 1$ and $\beta_{nv} = 0,\ n \geq 2$ (the original lateral von Kármán model) with T_v set in accordance with (5.1).

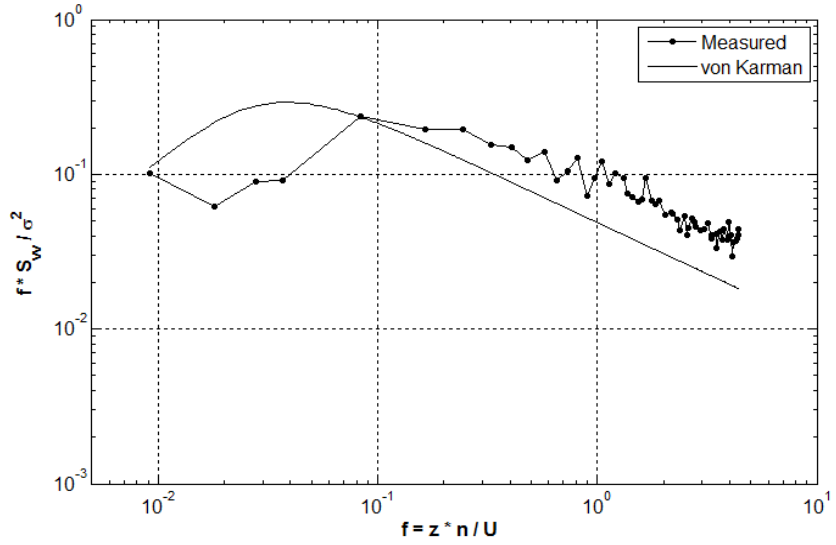

Figure 5.10: Lateral von Kármán fit of a measured spectrum where the time scale is calculated in accordance with (5.1)

Figure 5.10 shows an important consequence of prescribing T_i in such a manner. It can be seen that the von Kármán lateral model and the measured spectrum agree at the first

point on the spectrum. The trade-off of using the definition of T_i from (5.1), is that all other features of the von Kármán model are retained, and the general shape of the model following the lowest frequency data point, may disagree with the measured spectra. Plotted in Figure 5.11 is an attempt to utilize the lateral expansion series to more accurately model the spectrum.

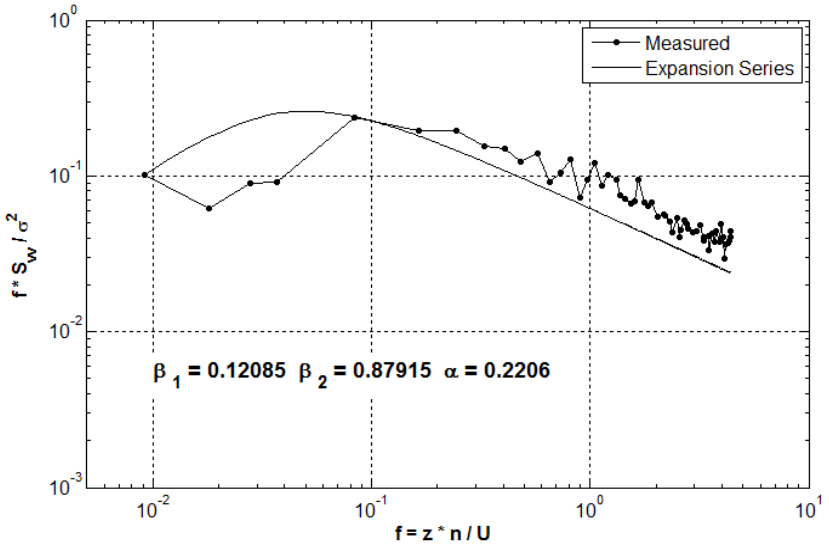

Figure 5.11: Lateral Expansion series fit

From Figure 5.11, it can be seen that a slightly better fit is achieved than the original von Kármán model from Figure 5.10, and that the first points of both the expansion series and the measured data are identical, due to the α parameter. Apart from this, the series struggles to find the level of the rest of the data. This fact brings up an issue that was stressed in Chapter 2, in the calculation of the autospectrum: the importance of stable, reliable power spectrum data near the zero frequency region. Examination of Figure 5.9 will show a trend as the spectrum nears the zero frequency mark, and an outlier, as displayed in Figure 5.12.

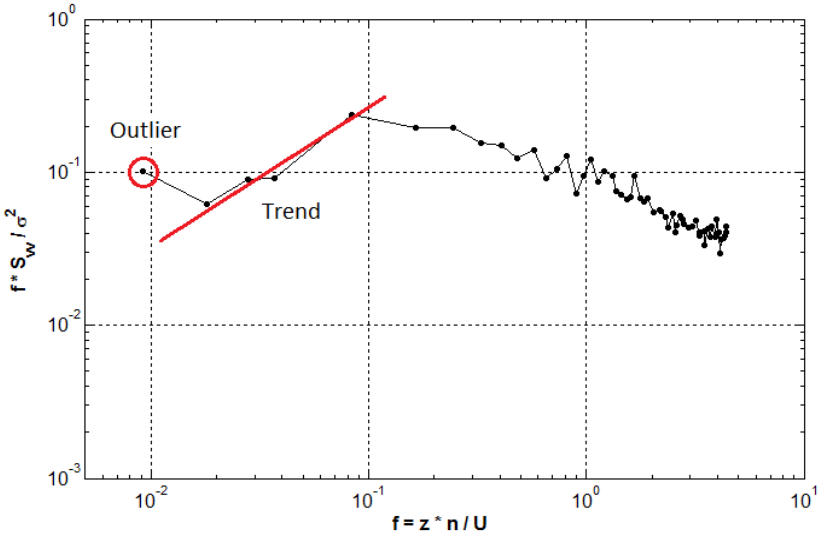

Figure 5.12: Identification of trend and outlier in sample data

The sudden change in the trend in Figure 5.12 may or may not be significant, and data at lower frequencies would be necessary to determine this. Assuming it is an outlier, notice the consequences of this outlier in Figure 5.11. Due to the α parameter setting the first spectral data point, even the great variability detailed in the previous section, there is not enough to fit the rest of the spectrum. Figure 5.13 shows the result if this outlier is ignored, and the trend was to continue.

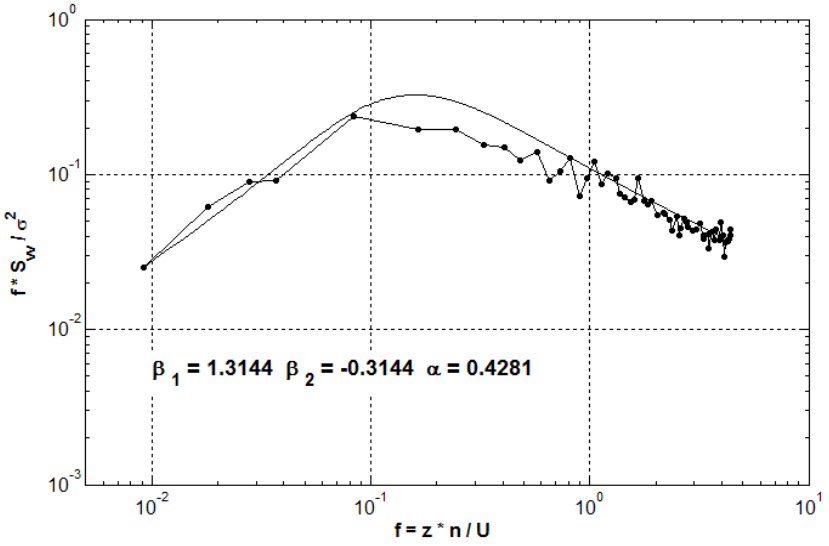

Figure 5.13: Result of expansion series if the outlier from Figure 5.12 is replaced by a data point that follows the rest of the trend.

Comparison between Figure 5.11 and Figure 5.13 shows the importance of two facets of the expansion series: 1) the necessity of a proper calculation of the autospectrum from raw data, and 2) the impact the α parameter has on the ability of the expansion series to provide an adequate fit of the data.

5.3 'A' Constraint (c)

$$\frac{A}{\alpha^{2/3}} = Y_1\beta_2 + Y_2\beta_2 + Y_3\beta_3 + \cdots + Y_n\beta_n$$

This constraint, unlike the α 'constraint' from the previous section, is a "true" constraint on the β coefficient selection; this is due to the fact that 'A' is a fixed value, that is determined from the autospectrum of raw data. Manipulation of the 'A' constraint and the definition of the α parameter yield (5.2):

$$A = (Y_1\beta_2 + Y_2\beta_2 + \cdots + Y_n\beta_n)(C_1\beta_2 + C_2\beta_2 + \cdots + C_n\beta_n)^{2/3} \qquad (5.2)$$

5.3.1 'A' Constraint and a Two Term Series

The 'A' constraint in (5.2), coupled with the β constraint from Section 5.1, provides two equations, one highly non-linear, that can be used to solve for all possible values of β_1 and β_2, assuming the series is truncated at $n = 2$. Generally, the possible combinations of β coefficients that will satisfy these two equations will be limited, and a least squares fitting will be unnecessary. One will simply choose between the limited options, which models the spectrum best. The addition of the 'A' constraint, makes this model highly restrictive, and possibly unattainable, for a two term approach. Figure 5.14 shows a case in which two terms could be found that satisfy the constraints, and an accurate fit is produced.

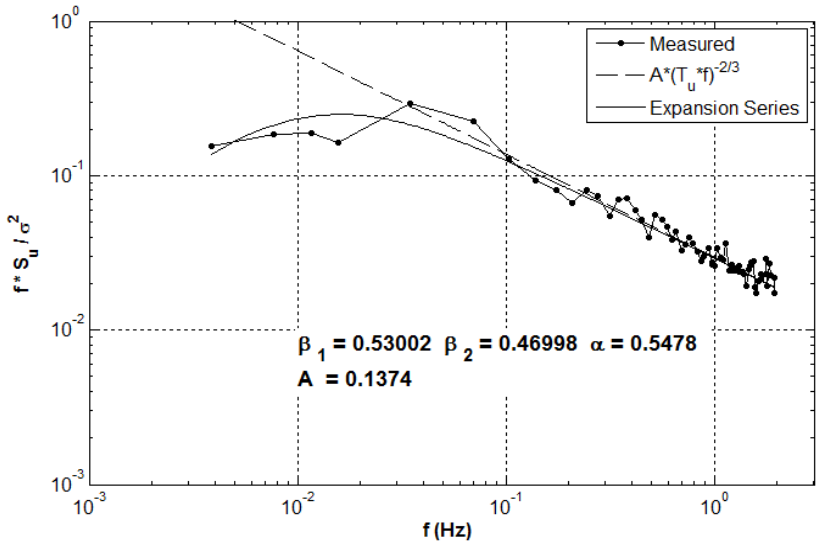

Figure 5.14: A case in which all conditions are satisfied, and an accurate fit is produced

Also shown in Figure 5.14 is the high-frequency decay rate $A(T_i f)^{-2/3}$. It can be seen, that the measured data begins this decay at a frequency of approximately 0.03 Hz, which coincides with the peak of the spectrum. It should be noted that this is a rare instance, and

that most data does not achieve this rate of decay until much higher frequencies. Figure 5.15 is an example of the measured data that does not achieve this decay rate within the available spectrum.

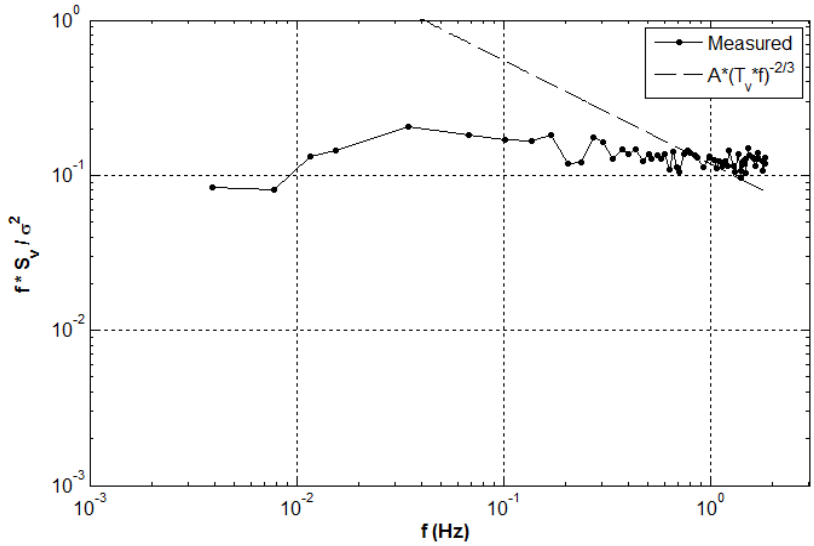

Figure 5.15: Measured data that does not comply with the Kolmogorov decay rate criterion

Specifically, Figure 5.15 is an example of a type of spectrum that does not satisfy the Kolmogorov equilibrium condition. The constraint that at high frequencies, $\frac{fS_i(f_{h.f.})}{\sigma_i^2} \propto A(fT_i)^{-2/3}$ can only be valid if it is true for the measured data that is to be modeled. It is obvious that this criterion should not be enforced if the actual data does not comply, as typified by Figure 5.15. The value of 'A' in Figure 5.15 is virtually meaningless. It is emphasized that the Kolmogorov equilibrium condition is generally observed for fully developed turbulence at "large-enough" Reynolds numbers. This fact was emphasized in Section 2.1 when discussing the collection of raw data. If the high frequency decay rate is

important to a specific wind engineering problem, raw data at sufficiently high frequencies must be available in the calculation of the power spectrum.

In light of these situations, the user generally has three options if the 'A' constraint cannot be satisfied, or the 'A' constraint can be satisfied but the resulting fit is not adequate:

1) If the 'A' condition is desirable for the user's purpose and the measured spectrum does decay at the correct rate, but explicit solutions are not possible with a two terms series, statistical leeway can be afforded. If the value of 'A' is calculated, and a range within a tolerable error is computed, the possibilities of solutions that yield the modeled 'A' within this tolerable range are possible. Due to the fact that 'A' is a subjectively calculated parameter from the data, tolerable ranges can be quite large.
2) Another solution to the problem detailed in number (1) is to no longer consider the 'A' constraint as a constraint, but instead as another parameter to consider in the least squares fitting. In other words, instead of minimizing the least squares error with respect to β's alone, minimize:

$$\epsilon = LS_{Error} + A_{Error} \tag{5.3}$$

where LS_{Error} is the error of the model in a least squares sense, and A_{Error} is the error between A_{model} and $A_{measured}$. This method was utilized for the calculation of all the results of this thesis (unless stated otherwise).

3) Lastly, it should be noted that the Kolmogorov equilibrium decay rate, or minus-five-thirds-law, is strictly applicable to homogeneous, isotropic flow. As it turns

out, measured spectra of a wide range of nonhomogeneous, anisotropic turbulence display the minus-five-thirds decay rate. There are also cases where this law is not displayed. This being the case, there is no reason why condition (iii) of (1.11) on page 8 has any bearing on these types of spectra. Eliminating this condition leaves the model with only one constraint and infinite fitting possibilities to choose from, and can be found using an appropriate minimization technique.

Seemingly, the addition of the 'A' constraint can be limiting; experience, however, shows that this constraint, acts as a stabilizing agent and prevents the outputs of the minimization algorithms used from resulting in unacceptable results.

5.3.2 'A' Constraint and a Three Term Series

The addition of a third term to the series expansion significantly simplifies the constraints, in that there are an arbitrary number of possible solutions to the two constraint equations and the three unknown β coefficients. It should be noted that if a fit is not satisfactory, the same measures detailed at the end of Section 5.3.1 can be taken, namely to exclude the 'A' constraint.

CHAPTER 6: APPLICATIONS TO WAKES

This chapter will present a set of representative samples of the results of the longitudinal, lateral, and vertical expansion series. That is, some results will be improvements on the von Kármán models, others will be improvements, but still not adequate to capture the database spectrum accurately. Three types of flow will be analyzed as mentioned in the Introduction: 1) wake turbulence inside a wind farm, 2) helicopter downwash, and 3) helicopter downwash with ship airwake. It is worth reiterating, that for all three types, the current understanding of their autospectra and such fundamental statistics merits significant improvement. For the results in this chapter, as well as all others in this thesis, MATLAB's minimization function *fmincon* was utilized; specifically, the minimization technique '*spq'* was used (MATLAB, 2013), with the initial guessed value of the original von Kármán model (i.e. $\beta_1 = 1$).

6.1 Wind Farm Application (Morfiadakis et. al., 1996)

Figure 6.1 shows the longitudinal expansion series compared to the von Kármán model when fitted to wake affected, longitudinal turbulence found within a wind farm. This figure shows the determined β coefficients, based on a least squares fit, the resulting value of α_u, as well as the A_{error}: the percent error of A_{model} from $A_{measured}$ (see (5.3)). In this case, the fitting was performed as detailed in "option 2)" on page 61. The figure shows that the model is able to match $A_{measured}$, of the data's high frequency value. Furthermore, just by inspection, as well as the fact that $\beta_1 \neq 1$ (see APPENDIX D:

NUMERICAL ASPECTS) the expansion series better captures the spectrum than the von Kármán model.

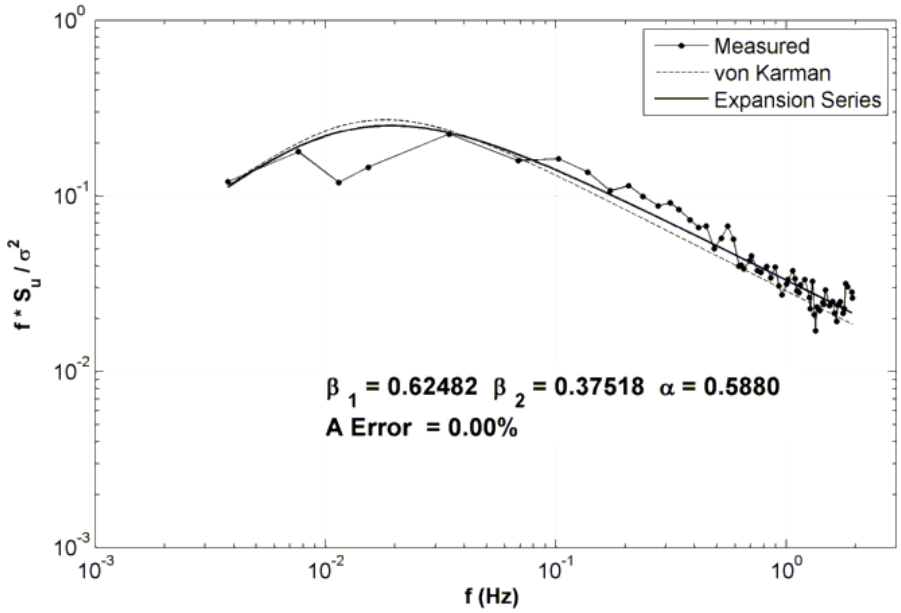

Figure 6.1: Spectrum of longitudinal turbulence within a wind farm, along with von Kármán and expansion model

Figure 6.2 shows the lateral turbulence from the same point as in Figure 6.1. In this case the fit is objectively better than the lateral von Kármán model, however, the coefficient 'A' is not matched exactly. The model is within 3.03% of $A_{measured}$, which is considered acceptable. As mentioned in Section 5.3, there is some measure of subjectivity in the value of $A_{measured}$, and this value may be poorly defined if high frequency data is not available.

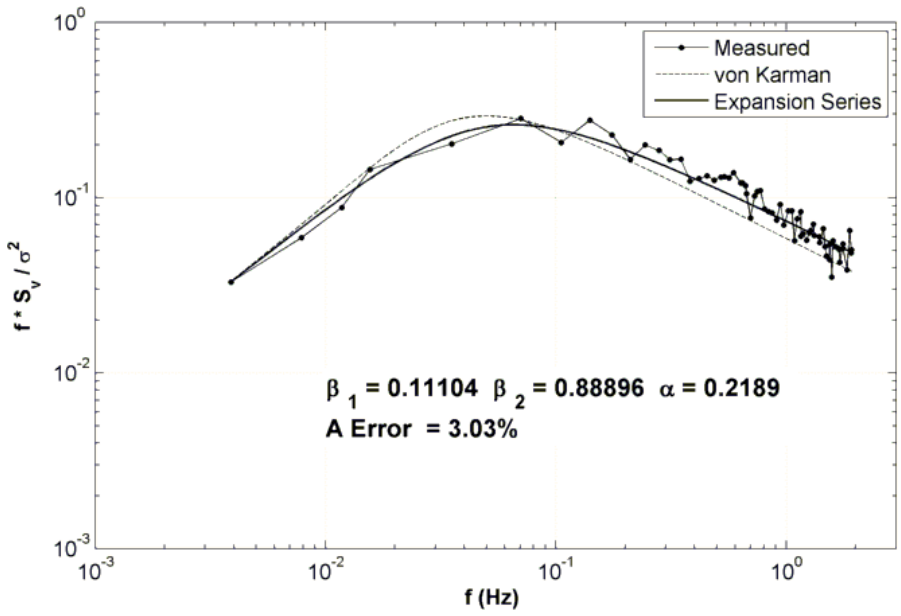

Figure 6.2: Spectrum of lateral turbulence within a wind farm, along with von Kármán and expansion model

Figure 6.3 shows the vertical component of turbulence for the same point treated in the previous two figures. This figure shows a spectrum that both the von Kármán and the expansion series "struggle" to fit.

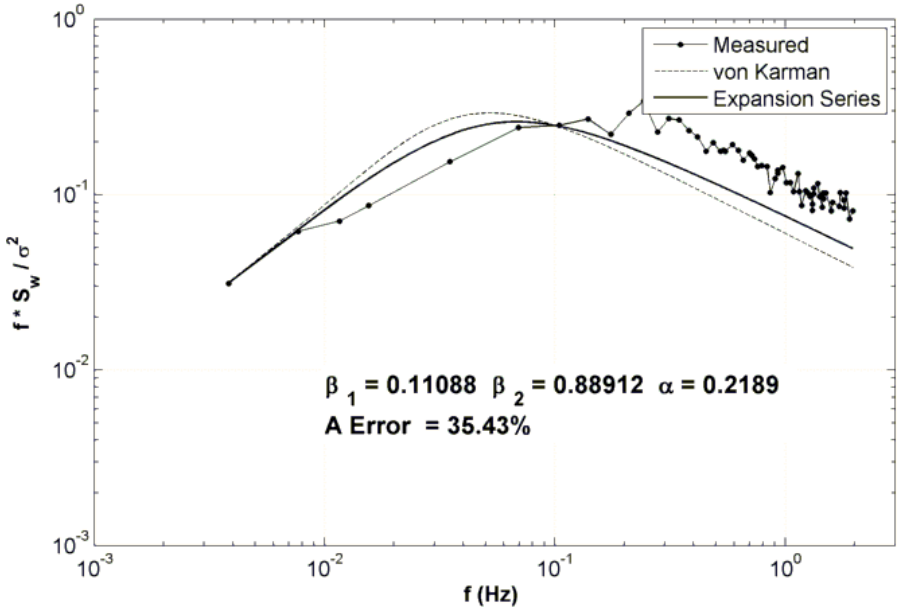

Figure 6.3: Spectrum of vertical turbulence within a wind farm, along with von Kármán and expansion model

While the expansion series is a better fit than the von Kármán, the high frequency data is not reached to an acceptable level. The model can only be within 35.43% of the determined 'A' coefficient from the data. A possible solution to this issue is to add a third term to the series; as seen in Chapter 3 on page 34, addition of higher terms brings A_{model} to higher elevation at high frequencies. This is shown in Figure 6.4.

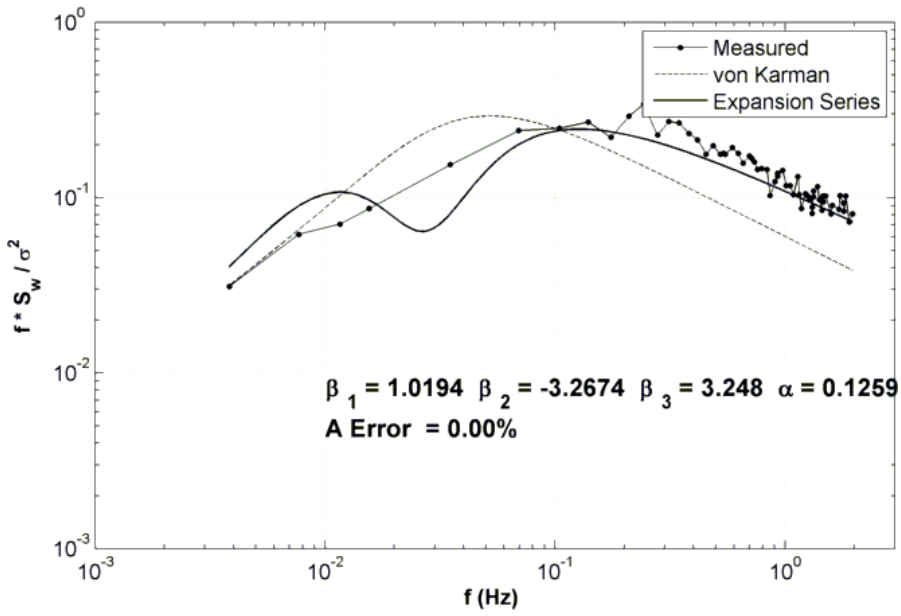

Figure 6.4: Three term series expansion model of vertical turbulence in a wind farm

Unfortunately, this spectrum appears to be so elevated at high frequencies, that meeting the '$A_{measured}$' value with the expansion series results in instability in the lower frequency region of the model. The third term is forced to be so significant, that the second term must subtract from its peak region. Another option is to continue to further refine this model by adding β_4; this refinement is addressed next.

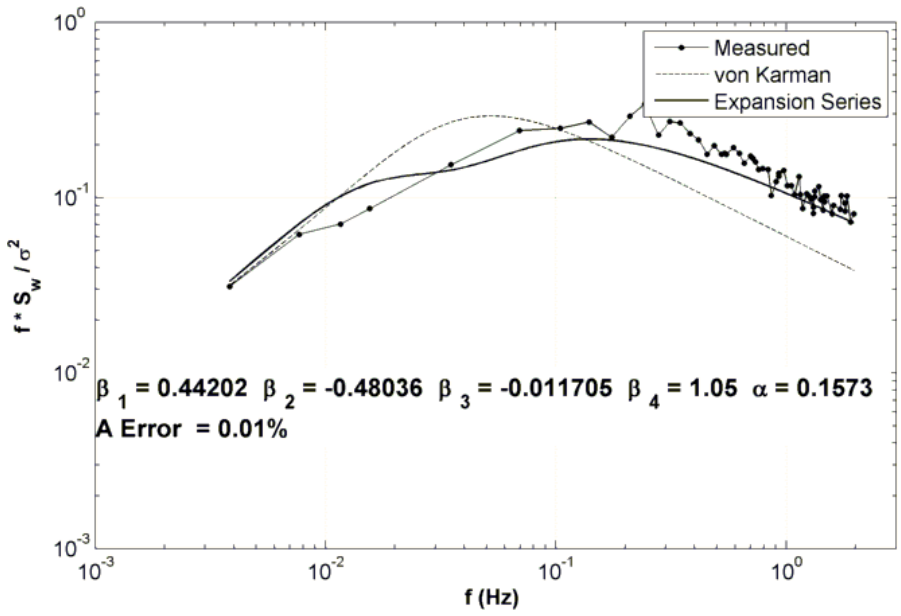

Figure 6.5: Four term series expansion model of vertical turbulence in a wind farm

Figure 6.5 shows an instructive possibility of how a three-term model could be further refined by adding the fourth term. While it is true that a four term series is a better fit, it may be approaching a point of diminishing return in that the algebraic simplicity of this refined model gets diminished as well. Also notice that the third term in Figure 6.5 (β_3) is nearly zero. Therefore, is this four term series expansion truly a four term series? The possibility of neglecting intermediate terms en route to further refinement is one that should be addressed if research on this topic is furthered. As shown in Figure 6.5, the 'A' condition is met, and the data is captured fairly well. Some additional figures are included in Appendix E.

6.2 Helicopter Downwash

This section will address spectra of helicopter downwash from CFD data. As with the previous section, the emphasis will be on the quality of the fit, as opposed to the

characteristics of the spectra. Figure 6.6 shows a two term series expansion of the longitudinal turbulence located 10 feet below the rotor of a hovering helicopter. The calculated spectra does follow Kolmogorov's -5/3 law, and the expansion series is able to match the high frequency limit. The series expansion is objectively better than the von Kármán model.

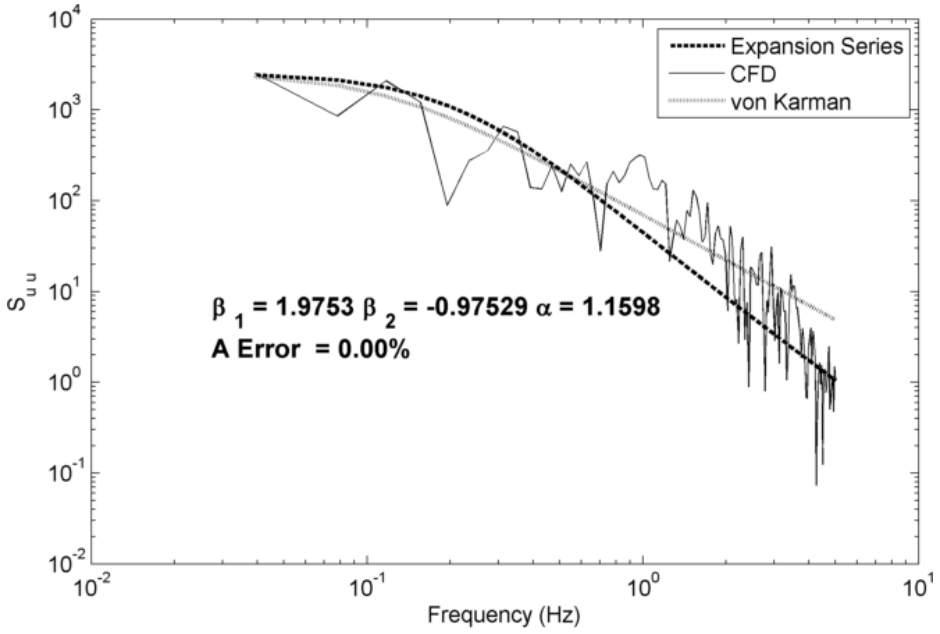

Figure 6.6: Two term longitudinal turbulence model of helicopter downwash from CFD data with the 'A' constraint enforced

Figure 6.7 shows the lateral turbulence of the helicopter downwash with a two term series from the same point as in Figure 6.6. Both the von Kármán and two term series somewhat over predict within the high-energy bandwidth of $0.04 \leq f \leq 0.8$ and thereafter follow the roll off trend of the calculated spectrum from the data. Overall, while the von Kármán appears to intersect with most of the CFD spectrum, the expansion series clearly captures the major features of this spectrum, including the 'A' constraint.

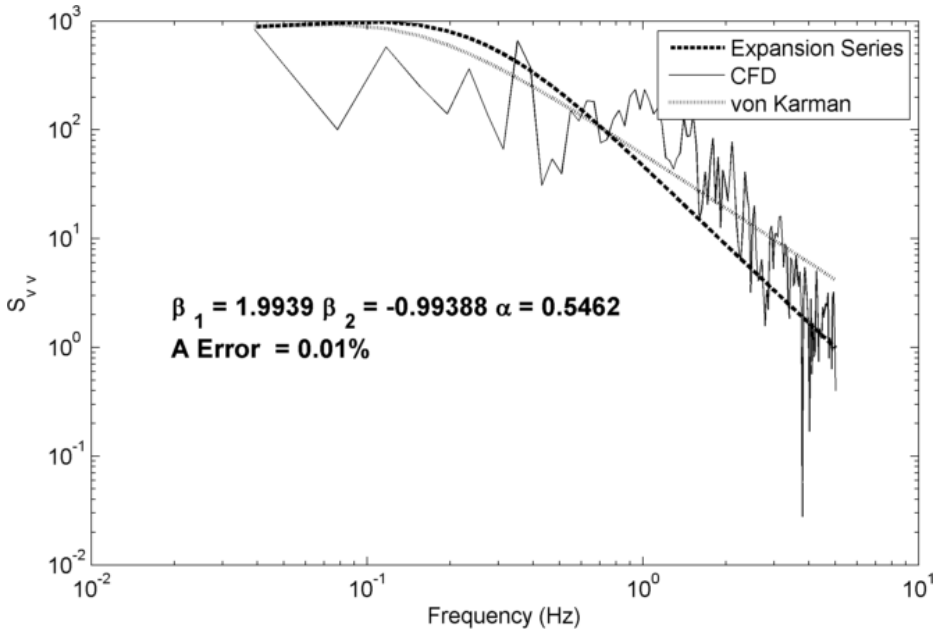

Figure 6.7: Two term lateral turbulence model of helicopter downwash from CFD data with the 'A' constraint enforced

Figure 6.8 shows a two term expansion series of vertical turbulence 10 feet below the helicopter rotor. As for fitting the calculated CFD spectrum, the performances of this two term expansion model and the von Kármán are strikingly similar to that in Figure 6.6 for the longitudinal component. That is, the two term expansion model provides an excellent approximation to the calculated spectrum for the entire bandwidth of the database; this includes matching the $A_{measured}$ value. Furthermore, it is a significant improvement over the von Kármán.

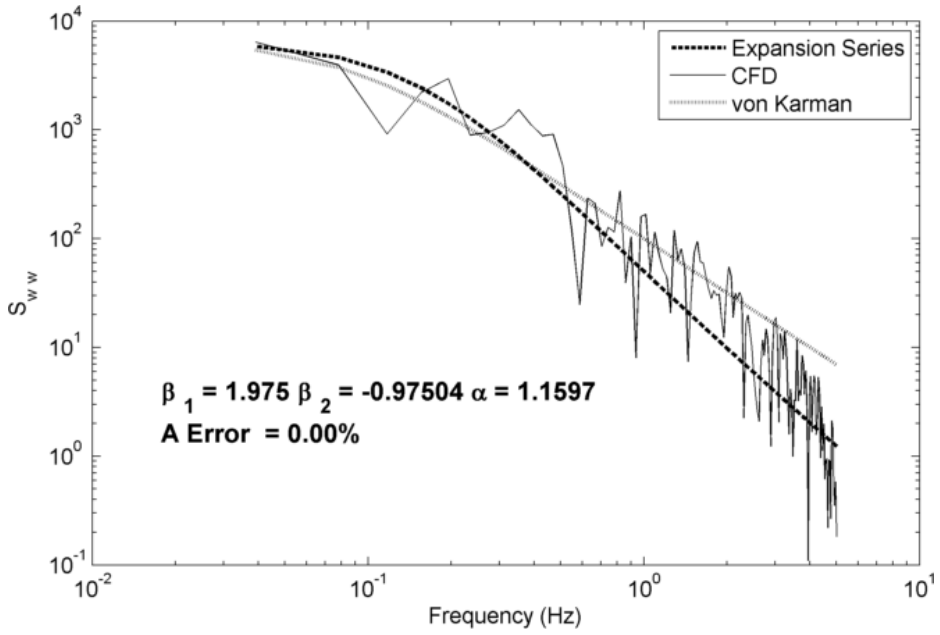

Figure 6.8: Two term vertical turbulence model of helicopter downwash from CFD data

Further figures are included in Appendix F.

6.3 Helicopter Downwash with Ship Airwake

The following figures show the spectra from the same point behind the ship superstructure as in Section 6.2; now the downwash is coupled with airwake turbulence shed from the ship superstructure. Figure 6.9 shows the longitudinal turbulence at this point along with a two term expansion series model. Observe that the determined '*A*' constraint is met by the model. It should be noted that this calculated spectrum, unlike the wind farm spectra, is a dimensional, non-normalized spectrum. Therefore, the Kolmogorov -2/3's Law is now the -5/3 Law. This turbulence spectrum, in fact, does decay at the proper rate towards the very high end of the spectrum. The expansion series clearly captures the data better than the von Kármán model.

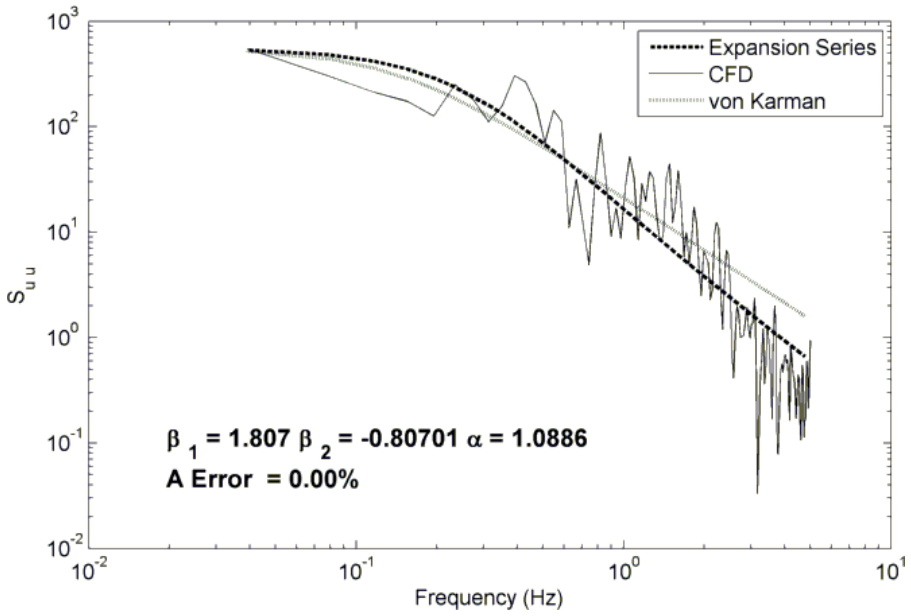

Figure 6.9: Longitudinal turbulence from ship airwake coupled with helicopter downwash with a two term expansion series

Figure 6.10 shows the lateral spectrum at the same point as in Figure 6.9. These results are very similar to those in the previous one.

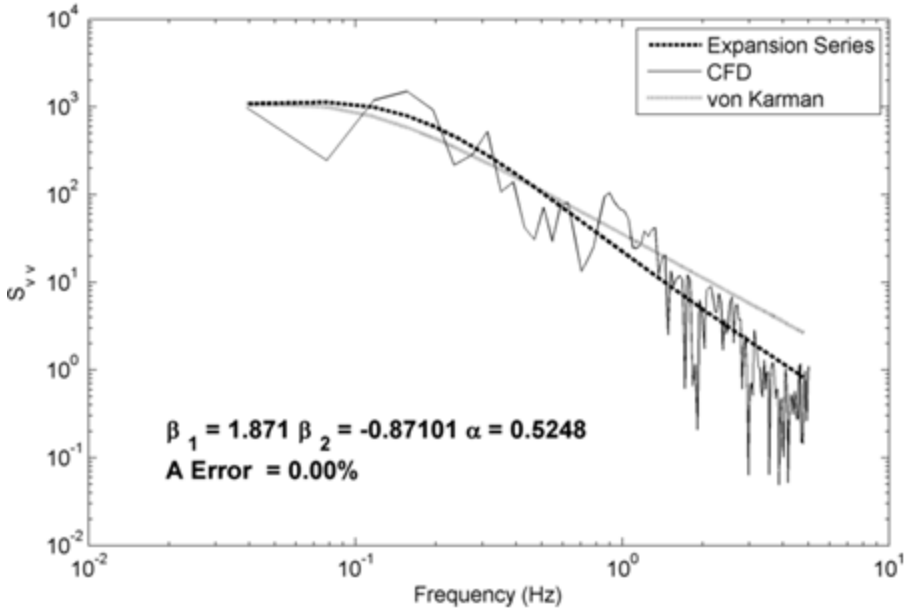

Figure 6.10: Lateral turbulence from ship airwake coupled with helicopter downwash with a two term expansion series

Figure 6.11 shows vertical turbulence from the same point as in the previous two figures. This figure is instructive in that the 'A' constraint is met by the model. This zero percent A_{error}, however, should be tempered by the fact that the high frequency range of the data either does not, or has not yet, approached a high frequency limit that agrees with Kolmogorov's Law.

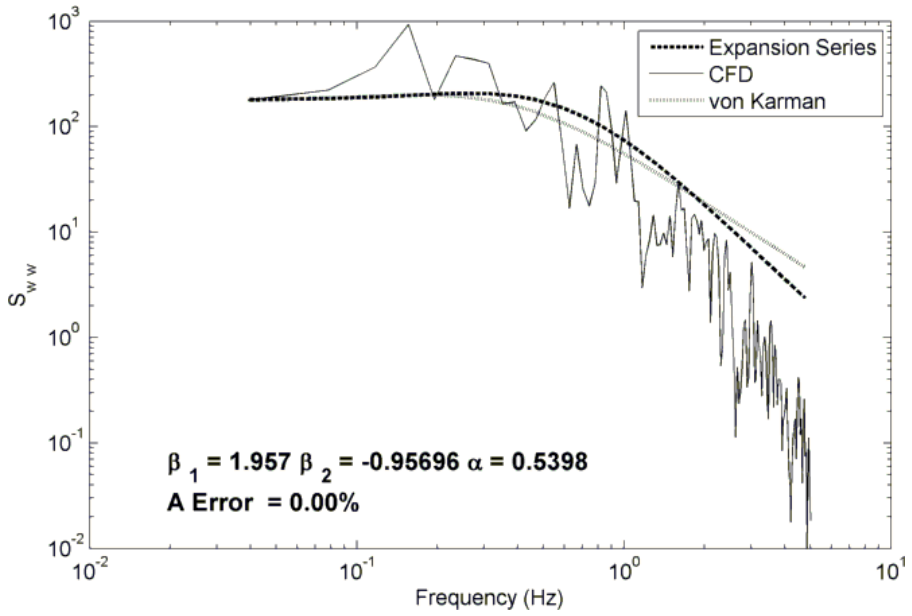

Figure 6.11: Vertical turbulence from ship airwake coupled with helicopter downwash with a two term expansion series utilizing the 'A' constraint.

As suggested earlier, one method of achieving a better fit if the high frequency data does not achieve Kolmogorov's decay rate is to ignore that constraint in the development of the expansion series. This can result in a higher quality model, for representing the data range available. Ignoring this 'A' constraint, opens up many possible fitting ranges, but the numerical scheme is susceptible to undesirable results. Figure 6.12 shows one of the possibilities that can result if only a least squares fit is considered. On face value, this seems to be a suitable fit of the data; however, a closer examination of the very high end region of the expansion series model shows a sharp downward trend. This is one of the consequences of not considering the 'A' constraint in determining the β coefficients.

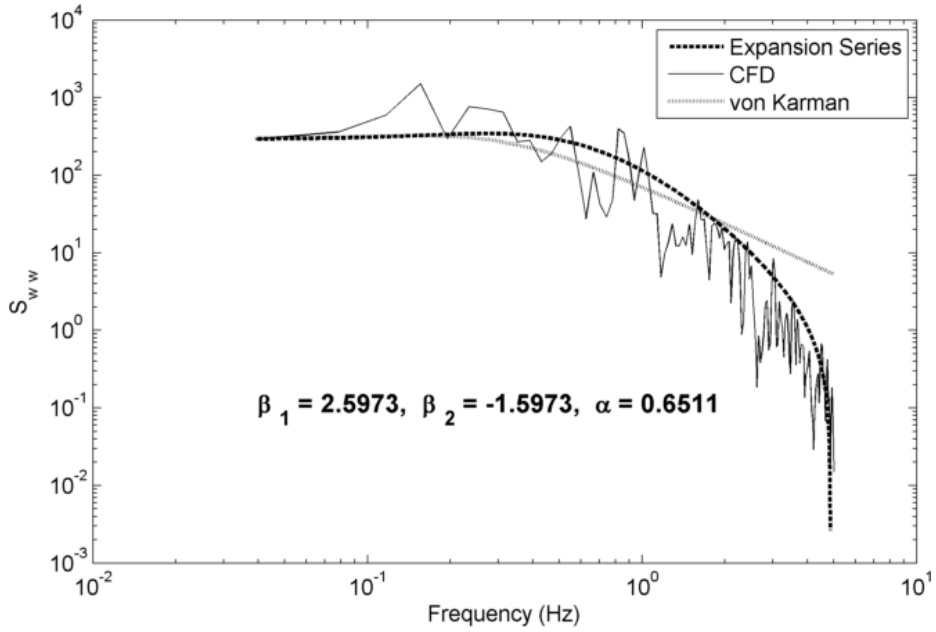

Figure 6.12: Vertical turbulence from ship airwake coupled with helicopter downwash with a two term expansion series ignoring the 'A' constraint

Further figures can be found in Appendix G.

CHAPTER 7: SUMMARY AND CONCLUSIONS

This thesis presents a comprehensive method of developing turbulence models, in closed form, from a database of flow velocity measurements from experimental and CFD investigations. The model development is motivated by the original work of Harris, who proposed that for nonlinearly transformed ABL turbulence, its autocorrelation (equivalently autospectrum) can be expanded into a perturbation type series. The treatment of Harris is restricted to the longitudinal components of homogeneous, isotropic turbulence, without any applications. Specifically, the longitudinal autocorrelation is expanded into a perturbation type series, in which the first term or the basis function is represented by the von Kármán longitudinal autocorrelation function. By comparison, the present approach incorporates all three orthogonal directions (longitudinal, lateral, and vertical) separately, without the assumption of homogeneous, isotropic turbulence. This approach to representing the frequency spectrum can be applied to any turbulent flow field that could benefit from simple, closed form models of the frequency domain. The most promising use for these models is for simulation purposes. If key points within a flow field are accurately modeled by an expansion series, filters can be designed based on these models to output random, simulated, turbulence that meets the characteristics of the measured data; see Appendix H.

Furthermore, this thesis provides guides to the treatment of raw data (Chapter 2) as well as numerical aspects of fitting the data (Appendix D). Furthermore, closed form

expressions for all three velocity components (Chapters 3 and 4) have been provided. These expressions for the lateral and vertical components are essentially identical with only minor differences. These are identified here as three separate expressions for simplicity of presentation. Derivations of these expressions can be seen in Appendix C. Lastly, the method is tested against some of the most complicated flow fields in wind engineering: wind farm wakes, and ship airwakes with helicopter downwash (Chapter 6). The purpose of these applications is to demonstrate that the method is remarkably robust and to gain further insight into the capabilities of the expansion models for simulation and such applications.

A major conclusion is that the method provides models in closed form for all three velocity components, and these models represent a significant improvement over the original von Kármán models, even when the von Kármán model is a decent representation as shown in Figure 6.1 on page 64. Furthermore, these models have the ability to drastically alter the shape of the von Kármán model to fit spectra that are not adequately modeled by the von Kármán model as seen in Figure 6.9 on page 72. The strength of this expansion approach to modeling is that the series has the capability of relocation of the peak of the non-dimensional spectrum, and matching the elevation of the spectrum at high frequencies. If a spectrum has the same general shape as the original von Kármán model, with some minor deviations, the expansion series can provide an excellent fit to the data. Issues arise when the spectrum to be modeled is no longer proportional to the von Kármán model. The problems brought up in Sections 5.2 and 5.3 yield the spectrum unable to provide an adequate fit. These situations are almost always accompanied by a better fit than the von Kármán, however, “better than the von Kármán”

is not a sufficient goal for any practical purposes. This situation is exemplified in Figure 6.3 on page 66. It may be possible to achieve an order of magnitude estimate, but not of acceptable accuracy for most engineering purposes. Coinciding with this limitation of the expansion series, are issues of the spectral data that are to be fit. These issues are detailed in Chapter 2, and some examples are given in Section 5.2. Stable, accurate, raw spectral data, especially in the low frequency range, are paramount to the success of the model, the reason is that the evaluation of the time scale is directly related to the first value of the spectrum due to the α parameter.

The most effective alteration that can be made if a fit is not acceptable is to eliminate the 'A' constraint entirely from the fitting process. This trade off opens up many more fitting shapes and configurations to the expansion series, but, can render the model unstable. That is, in extreme cases, fairly wild and unacceptable shapes can be achieved that are acceptable to the fitting algorithm if only a least squares approach is used.

The preceding method based on a series expansion is tested against a comprehensive database of wake turbulence inside a wind farm, helicopter downwash and ship airwake coupled with helicopter downwash, and this database represents three demanding cases of turbulence. This testing leads to the following specific findings:

1) Generally, no more than a three-term series is necessary to develop a model; in fact, in most cases, a two-term series is found to be adequate for wind engineering applications;

2) These developed models lend themselves well to design of shaping filters driven by white noise (Appendix H); that is, the filter design is as routine as the currently used procedure for the von Kármán models.

CHAPTER 8: FUTURE WORK

Based on the research completed thus far, the following is a listing of future areas of research of considerable promise:

1) Extend the expansion series approach to developing the interpretive models of two-point statistics of cross-spectrum (magnitude and phase) and coherence from the corresponding data points. To aid this research, programic means of calculating the cross-spectrum, coherence, and phase in MATLAB have been included in Appendix D. It should be noted that, similar to what was discussed in Chapter 2, there are several ways of calculating two-point statistics discretely. The means provided in Appendix D have been found to produce the highest quality, most reliable, results. Again, all processes follow Bendat and Piersol (2010).
    a. Study the strengths and weaknesses of the interpretive models of two-point statistics against a comprehensive database inside wind farms and over ship decks with and without downwash coupling.
2) Investigate the simulations of the two point-statistics with respect to the database and the interpretive models through multiple-input and multiple-output shaping filter systems driven by white noise.

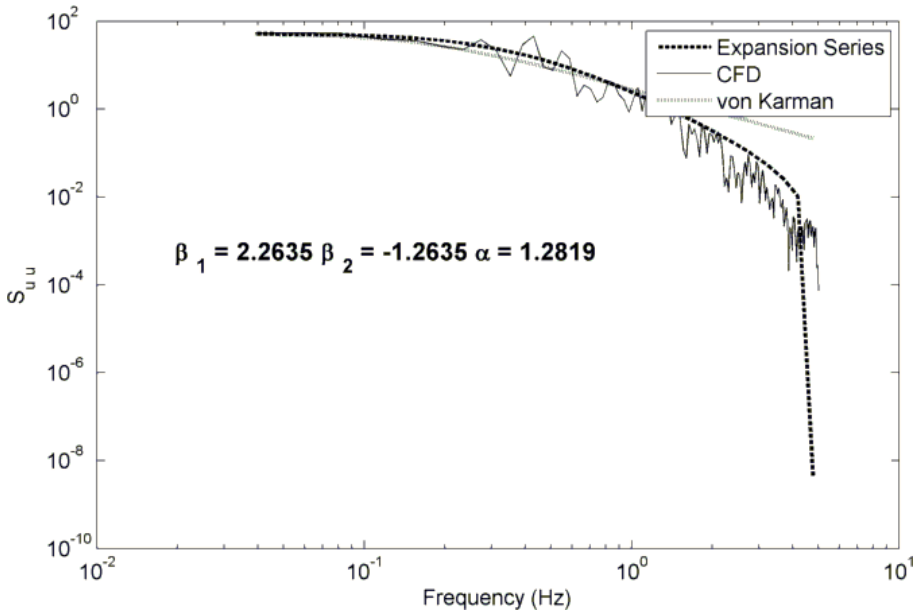

Figure 8.1: Example of an erratic fit that can be attained if the '*A*' constraint is ignored.

3) Explore the feasibility of devising measures that can be taken if fits like the one in Figure 8.1 are undesirable. These measures may sacrifice some of the fitting in a least squares sense, but will eliminate some of the instability that makes Figure 8.1 an unacceptable model for $f > 3$ Hz
4) Consider a comprehensive investigation of efficient numerical methods for fitting highly demanding cases of autospectrum, like those depicted in Sections 6.2 and 6.3. Currently, each individual model, if unsatisfactory, must be fit by manipulating the error to be minimized until an acceptable fit is reached. A complete program that can accept raw turbulence data and output an acceptable model, whether the '*A*' constraint is included or not, should require no 'toying' with the fitting algorithm to compensate for cases like Figure 8.1.

5) As mentioned in Section 6.1, there still exist unexplored means of ignoring intermediate terms in order to achieve a better fit of the measured spectra. A minimization program that could generate a multi-term series that ignores some of the intermediate terms completely could significantly improve the modeling capabilities even further.

APPENDIX A: REQUIRED IDENTITIES FOR DERIVATION

This section provides all the identities that are necessary to yield the closed form expressions that have been detailed in Chapters 3 and 4. The text in which each identity can be found is specified, and each is assigned a tag for simple reference in the derivations to follow in Appendix B and C (i.e. G-1, E-1, etc.).

From:

L.S. Gradshteyn, I.M Ryzhik, 2000. *Table of Integrals, Series, and Products, 6th Ed*. Special Functions, page 724, eq. 6.699 (12)

$$\int_0^\infty x^\mu K_\mu(ax)\cos(bx)\,dx = \frac{1}{2}\sqrt{\pi}\,(2a)^\mu\,\Gamma\left(\mu+\frac{1}{2}\right)(b^2+a^2)^{-\mu-\frac{1}{2}} \tag{G-1}$$

$$Re\ a > 0\,, \qquad b > 0, \qquad Re\ \mu > -\frac{1}{2}$$

From:

A. Erdelyi, 1954. *Table of Integral Transforms, vol. II*. page 371, eq. 19.5 (12)

$$\int_0^\infty x^{\rho-1}K_\mu(x)K_v(x)\cos(2ax)\,dx$$

$$= \frac{2^{\rho-3}}{\Gamma(\rho)}\,\Gamma\left(\frac{\rho+\mu+v}{2}\right)\Gamma\left(\frac{\rho+\mu-v}{2}\right)\Gamma\left(\frac{\rho-\mu+v}{2}\right)\Gamma\left(\frac{\rho-\mu-v}{2}\right) \tag{E-1}$$

$$\times\ {}_4F_3\left(\frac{\rho+\mu+v}{2},\frac{\rho+\mu-v}{2},\frac{\rho-\mu+v}{2},\frac{\rho-\mu-v}{2};\frac{1}{2},\frac{\rho}{2},\frac{\rho+1}{2};-a^2\right)$$

$$Re\ |a| < 1\,, \qquad Re\ \rho > |Re\ \mu| + |Re\ v|$$

From:

L.S. Gradshteyn, I.M Ryzhik, 2000. *Table of Integrals, Series, and Products, 6th Ed*. A generalized Hypergeometric Series, page 1000, eq. 9.14 (1)

$$ {}_pF_q\left(\alpha_1, \alpha_2, \dots, \alpha_p;\ \beta_1, \beta_2, \dots, \beta_q;\ z\right) = \sum_{k=0}^{\infty} \frac{(\alpha_1)_k (\alpha_2)_k \dots \left(\alpha_p\right)_k}{(\beta_1)_k (\beta_2)_k \dots \left(\beta_q\right)_k} \frac{z^k}{k!} \qquad \text{(G-2)} $$

$$ (a)_k = \frac{\Gamma(a-k)}{\Gamma(a)} $$

From:

L.S. Gradshteyn, I.M Ryzhik, 2000. *Table of Integrals, Series, and Products, 6th Ed*. Special Functions, page 887, eq. 8.331

$$ \Gamma(x+1) = x\Gamma(x) \qquad \text{(G-3)} $$

From:

L.S. Gradshteyn, I.M Ryzhik, 2000. *Table of Integrals, Series, and Products, 6th Ed*. Special Functions, page 887, eq. 8.334(2)

$$ \Gamma\left(\frac{1}{2}+x\right)\Gamma\left(\frac{1}{2}-x\right) = \frac{\pi}{\cos(\pi x)} \qquad \text{(G-4)} $$

From:

L.S. Gradshteyn, I.M Ryzhik, 2000. *Table of Integrals, Series, and Products, 6th Ed*. Hypergeometric Functions, page 998, eq.9.131 (1b)

$$ {}_2F_1(\alpha, \beta; \gamma; z) = (1-z)^{-\beta}\, {}_2F_1\left(\beta, \gamma-\alpha; \gamma; \frac{z}{z-1}\right) \qquad \text{(G-5)} $$

From:

L.S. Gradshteyn, I.M Ryzhik, 2000. *Table of Integrals, Series, and Products, 6th Ed*. Hypergeometric Functions, page 998, eq.9.122 (1)

$$ {}_2F_1(\alpha,\beta;\gamma;1) = \frac{\Gamma(\gamma)\Gamma(\gamma-\alpha-\beta)}{\Gamma(\gamma-\alpha)\Gamma(\gamma-\beta)} \tag{G-6} $$

From:

L.S. Gradshteyn, I.M Ryzhik, 2000. *Table of Integrals, Series, and Products, 6th Ed*. Special Functions, page 887, eq.8.335 (1)

$$ \Gamma(2x) = \frac{2^{2x-1}}{\sqrt{\pi}}\Gamma(x)\Gamma\left(x+\frac{1}{2}\right) \tag{G-7} $$

From:

L.S. Gradshteyn, I.M Ryzhik, 2000. *Table of Integrals, Series, and Products, 6th Ed*. Special Functions, page 887, eq.8.334 (3)

$$ \Gamma(1-x)\Gamma(x) = \frac{\pi}{\sin(\pi x)} \tag{G -8} $$

From:

L.S. Gradshteyn, I.M Ryzhik, 2000. *Table of Integrals, Series, and Products, 6th Ed*. Special Functions, page 724, eq. 6.699 (4)

$$ \int_0^\infty x^\lambda K_\mu(ax)\cos(bx)\,dx $$

$$ = 2^{\lambda-1}\mathrm{a}^{-\lambda-1}\,\Gamma\left(\frac{\mu+\lambda+1}{2}\right)\Gamma\left(\frac{1+\lambda-\mu}{2}\right) \tag{G-9} $$

$$ \times\ {}_2F_1\left(\frac{\mu+\lambda+1}{2},\frac{1+\lambda-\mu}{2};\frac{1}{2};-\frac{b^2}{a^2}\right) $$

$$ Re\ a > 0\,, \qquad b > 0, \qquad Re\,(-\lambda \pm \mu) < 1 $$

From:

L.S. Gradshteyn, I.M Ryzhik, 2000. *Table of Integrals, Series, and Products, 6th Ed*. Hypergeometric Functions, page 998, eq. 9.131 (1c)

$$ {}_2F_1(\alpha,\beta;\gamma;z) = (1-z)^{\gamma-\alpha-\beta}\,{}_2F_1(\gamma-\alpha,\gamma-\beta;\gamma;z) \tag{G-10} $$

From:

L.S. Gradshteyn, I.M Ryzhik, 2000. *Table of Integrals, Series, and Products, 6th Ed*. Hypergeometric Functions, page 1000, eq. 9.137 (4)

$$ \begin{aligned} &\gamma\,{}_2F_1(\alpha,\beta-1;\gamma;z) - \gamma\,{}_2F_1(\alpha-1,\beta;\gamma;z) + \\ &(\alpha-\beta)\,(z)\,{}_2F_1(\alpha,\beta;\gamma+1;z) = 0 \end{aligned} \tag{G-11} $$

APPENDIX B: LONGITUDINAL CLOSED FORM DERIVATION

This section provides a guide through the derivation of the closed form solutions found in Chapter 3.

First Term $\xi_u(\tau)$

$$\xi_u(\tau) = \frac{2^{2/3}}{\Gamma\left(\frac{1}{3}\right)}\left(\frac{\alpha_u\tau}{T_u}\right)^{1/3} \times \left[K_{1/3}\left(\frac{\alpha_u\tau}{T_u}\right)\right]$$

$$\chi_{1u}(f) = 4\int_0^\infty \frac{2^{2/3}}{\Gamma\left(\frac{1}{3}\right)}\left(\frac{\alpha_u\tau}{T_u}\right)^{1/3} \times \left[K_{1/3}\left(\frac{\alpha_u\tau}{T_u}\right)\right]\cos(2\pi f\tau)\,d\tau$$

Let: $= 1/3$, $\tau = x$, $a = \alpha_u/T_u$, $b = 2\pi f$

Utilizing (G-1) from Appendix B and simple manipulation, equation (3.12) from page 26 can be derived:

$$\chi_{1u}(f) = 4T_u\frac{\sqrt{\pi}\,\Gamma\left(\frac{5}{6}\right)}{\Gamma\left(\frac{1}{3}\right)}\,\alpha_u^{2/3}\,\frac{1}{(\alpha^2 + 4\pi^2 f^2 T_u^2)^{5/6}}$$

Second Term $\xi_u^2(\tau)$

$$\xi_u^2(\tau) = \frac{2^{4/3}}{\Gamma\left(\frac{1}{3}\right)^2}\left(\frac{\alpha_u\tau}{T_u}\right)^{2/3} \times \left[K_{1/3}\left(\frac{\alpha_u\tau}{T_u}\right)\right]^2$$

$$\chi_{2u}(f) = 4\int_0^\infty \frac{2^{4/3}}{\Gamma\left(\frac{1}{3}\right)^2}\left(\frac{\alpha_u\tau}{T_u}\right)^{2/3} \times \left[K_{1/3}\left(\frac{\alpha_u\tau}{T_u}\right)\right]^2\cos(2\pi f\tau)\,d\tau$$

Let: $\frac{\alpha_u \tau}{T_u} = x$, $a = \frac{f \pi T_u}{\alpha_u}$, and from (E-1) the integral can be evaluated. The definition of the Hypergeometric function from (G-2) will show that for

$$ {}_4F_3(a, b, c, d; e, f, g; z) $$

if $b = f$ and $d = e$, this form will reduce to

$$ {}_4F_3(a, b, c, d; e, f, g; z) = {}_2F_1(a, c; g; z) $$

Furthermore, manipulations utilizing (G-3), (G-4) and (G-5) will lead to the result in (3.20) on page 28.

$$ \chi_{2u}(f) = 4T_u \frac{\sqrt{\pi}\,\Gamma\left(\frac{5}{6}\right)}{\Gamma\left(\frac{1}{3}\right)} \alpha_u^{2/3} \frac{1}{(\alpha_u^2 + \pi^2 f^2 T_u^2)^{5/6}} \left[{}_2F_1\left(\frac{5}{6}, \frac{1}{6}; \frac{4}{3}; \frac{\pi^2 f^2 T_u^2}{\alpha_u^2 + \pi^2 f^2 T_u^2}\right)\right] $$

In the calculation of (3.21) on page 28:

$$ f\chi_{2u}(f_{h.f.}) \approx \frac{\sqrt{\pi}\Gamma\left(\frac{5}{6}\right)}{\Gamma\left(\frac{1}{3}\right)} \frac{8}{(2\pi)^{5/3}} \alpha_u^{2/3} (f_{h.f.} T_u)^{-2/3} $$

(G-6), (G-3) and (G-7) are used.

APPENDIX C: LATERAL CLOSED FORM DERIVATION

This section will provide a guide through the derivation of the closed form solutions found in Chapter 4.

First Term $\xi_v(\tau)$

$$\xi_v(\tau) = \frac{2^{2/3}}{\Gamma\left(\frac{1}{3}\right)}\left(\frac{\alpha_v\tau}{T_v}\right)^{1/3} \times \left[K_{1/3}\left(\frac{\alpha_v\tau}{T_v}\right) - \frac{1}{2}\left(\frac{\alpha_v\tau}{T_v}\right)K_{2/3}\left(\frac{\alpha_v\tau}{T_v}\right)\right]$$

$$\chi_{1v}(f) = 4\int_0^\infty \left(\frac{2^{2/3}}{\Gamma\left(\frac{1}{3}\right)}\left(\frac{\alpha_v\tau}{T_v}\right)^{1/3} \times \left[K_{1/3}\left(\frac{\alpha_v\tau}{T_v}\right) - \frac{1}{2}\left(\frac{\alpha_v\tau}{T_v}\right)K_{2/3}\left(\frac{\alpha_v\tau}{T_v}\right)\right]\right)\cos(2\pi f\tau)\, d\tau$$

Let: $\frac{\alpha_v\tau}{T_v} = x$, $b = \frac{f\pi T_v}{\alpha_v}$. Expansion into two infinite integrals is required of this term. The integral involving $K_{1/3}\left(\frac{\alpha_v\tau}{T_v}\right)$ requires (G -1). The integral involving $K_{2/3}\left(\frac{\alpha_v\tau}{T_v}\right)$ requires (G -9), (G-5), and (G -11). Combining the two results will yield (4.12) on page 39.

$$\chi_{1v}(f) = 4T_v\frac{\sqrt{\pi}\,\Gamma\left(\frac{5}{6}\right)}{6\,\Gamma\left(\frac{1}{3}\right)}\,\alpha_v^{2/3}\left[\frac{3\alpha_v^2 + 32f^2T_v^2\pi^2}{(\alpha_v^2 + 4f^2T_v^2\pi^2)^{11/6}}\right]$$

Second Term $\xi_v^2(\tau)$

$$\xi_v^2(\tau) = \frac{2^{4/3}}{\Gamma\left(\frac{1}{3}\right)^2}\left(\frac{\alpha_v\tau}{T_v}\right)^{2/3} \times \left[K_{1/3}\left(\frac{\alpha_v\tau}{T_v}\right) - \frac{1}{2}\left(\frac{\alpha_v\tau}{T_v}\right)K_{2/3}\left(\frac{\alpha_v\tau}{T_v}\right)\right]^2$$

$$\chi_{2v}(f) = 4\int_0^\infty \left(\frac{2^{4/3}}{\Gamma\left(\frac{1}{3}\right)^2}\left(\frac{\alpha_v\tau}{T_v}\right)^{2/3} \right.$$

$$\left. \times \left[K_{1/3}\left(\frac{\alpha_v\tau}{T_v}\right) - \frac{1}{2}\left(\frac{\alpha_v\tau}{T_v}\right)K_{2/3}\left(\frac{\alpha_v\tau}{T_v}\right)\right]^2 \right)\cos(2\pi f\tau)\, d\tau$$

Let: $\frac{\alpha_v\tau}{T_v} = x$, $a = \frac{f\pi T_v}{\alpha_v}$. Similar to the first term of the lateral series, this integral must be separated into three infinite integrals, evaluated separately, and then combined and refined.

The integral involving $K_{1/3}^2(x)$ requires (E-1) to evaluate. Simplification of the gamma functions and constants should be left until the three infinite integrals are all evaluated and combined. It should be seen that the ${}_4F_3$ hypergeometric function that results can be reduced to a ${}_2F_1$ hypergeometric function.

Both the integral involving $K_{1/3}(x)K_{2/3}(x)$ and $K_{2/3}^2(x)$ require (E-1) to evaluate. Again, gamma functions and constants should be simplified at the end. The ${}_4F_3$ that results can only be reduced to a ${}_3F_2$ in both cases. This is problematic in that at high frequencies, the ${}_3F_2$ will not approach zero fast enough to be neglected. An example of how to treat this ${}_3F_2$ is as follows: From (G-2):

$${}_3F_2\left(\frac{5}{6},\frac{7}{6},\frac{3}{2};\frac{1}{2},\frac{4}{3};z\right) = \sum_{k=0}^{\infty}\frac{\left(\frac{5}{6}\right)_k\left(\frac{7}{6}\right)_k\left(\frac{3}{2}\right)_k}{\left(\frac{1}{2}\right)_k\left(\frac{4}{3}\right)_k}\frac{z^k}{k!}$$

Moreover,

$$\frac{\left(\frac{3}{2}\right)_k}{\left(\frac{1}{2}\right)_k} = \frac{\Gamma\left(\frac{1}{2}\right)}{\Gamma\left(\frac{3}{2}\right)} \frac{\Gamma\left(\frac{3}{2}+k\right)}{\Gamma\left(\frac{1}{2}+k\right)}$$

Using (G-3), it can be shown that

$$\frac{\Gamma\left(\frac{1}{2}\right)}{\Gamma\left(\frac{3}{2}\right)} \frac{\Gamma\left(\frac{3}{2}+k\right)}{\Gamma\left(\frac{1}{2}+k\right)} = \frac{\Gamma\left(\frac{1}{2}\right)}{\Gamma\left(\frac{3}{2}\right)} \frac{\Gamma\left(\frac{1}{2}+k\right)\left(\frac{1}{2}+k\right)}{\Gamma\left(\frac{1}{2}+k\right)} = \frac{\Gamma\left(\frac{1}{2}\right)}{\Gamma\left(\frac{3}{2}\right)}\left(\frac{1}{2}+k\right)$$

Resulting in,

$${}_3F_2\left(\frac{5}{6},\frac{7}{6},\frac{3}{2};\frac{1}{2},\frac{4}{3};z\right) = \frac{\Gamma\left(\frac{1}{2}\right)}{\Gamma\left(\frac{3}{2}\right)} \sum_{k=0}^{\infty} \left(\frac{1}{2}+k\right) \frac{\left(\frac{5}{6}\right)_k \left(\frac{7}{6}\right)_k}{\left(\frac{1}{2}\right)_k} \frac{z^k}{k!}$$

By distributing the quantities within the summation,

$$\frac{\Gamma\left(\frac{1}{2}\right)}{\Gamma\left(\frac{3}{2}\right)} \sum_{k=0}^{\infty} \left(\frac{1}{2}+k\right) \frac{\left(\frac{5}{6}\right)_k \left(\frac{7}{6}\right)_k}{\left(\frac{1}{2}\right)_k} \frac{z^k}{k!} = \frac{\Gamma\left(\frac{1}{2}\right)}{\Gamma\left(\frac{3}{2}\right)} \left[\frac{1}{2} \sum_{k=0}^{\infty} \frac{\left(\frac{5}{6}\right)_k \left(\frac{7}{6}\right)_k}{\left(\frac{1}{2}\right)_k} \frac{z^k}{k!} + \sum_{k=0}^{\infty} k \frac{\left(\frac{5}{6}\right)_k \left(\frac{7}{6}\right)_k}{\left(\frac{1}{2}\right)_k} \frac{z^k}{k!}\right]$$

$$= {}_2F_1\left(\frac{5}{6},\frac{7}{6};\frac{4}{3};z\right) + 2 \sum_{k=0}^{\infty} \frac{\left(\frac{5}{6}\right)_k \left(\frac{7}{6}\right)_k}{\left(\frac{1}{2}\right)_k} \frac{z^k}{(k-1)!}$$

Now considering the summation

$$\sum_{k=0}^{\infty} \frac{\left(\frac{5}{6}\right)_k \left(\frac{7}{6}\right)_k}{\left(\frac{1}{2}\right)_k} \frac{z^k}{(k-1)!}$$

If $k = y + 1$, the above yields

$$\sum_{k=0}^{\infty} \frac{\left(\frac{5}{6}\right)_k \left(\frac{7}{6}\right)_k}{\left(\frac{1}{2}\right)_k} \frac{z^k}{(k-1)!} = \frac{\Gamma\left(\frac{4}{3}\right)\Gamma\left(\frac{11}{6}\right)\Gamma\left(\frac{13}{6}\right)}{\Gamma\left(\frac{5}{6}\right)\Gamma\left(\frac{7}{6}\right)\Gamma\left(\frac{7}{3}\right)}(z) \sum_{y=-1}^{\infty} \frac{\left(\frac{11}{6}\right)_y \left(\frac{13}{6}\right)_y}{\left(\frac{7}{3}\right)_y} \frac{z^y}{(y)!}$$

because

$$\frac{\left(\frac{11}{6}\right)_y \left(\frac{13}{6}\right)_y}{\left(\frac{7}{3}\right)_y} \frac{z^y}{(y)!} \Bigg|_{y=-1} = 0$$

Therefore,

$$\sum_{y=-1}^{\infty} \frac{\left(\frac{11}{6}\right)_y \left(\frac{13}{6}\right)_y}{\left(\frac{7}{3}\right)_y} \frac{z^y}{(y)!} \equiv \sum_{y=0}^{\infty} \frac{\left(\frac{11}{6}\right)_y \left(\frac{13}{6}\right)_y}{\left(\frac{7}{3}\right)_y} \frac{z^y}{(y)!} = {}_2F_1\left(\frac{11}{6}, \frac{13}{6}; \frac{7}{3}; z\right)$$

The result of this expansion of the ${}_3F_2$, along with manipulation using (G-3), (G-4), (G-7), and (G-8) will yield:

$${}_3F_2\left(\frac{5}{6}, \frac{7}{6}, \frac{3}{2}; \frac{1}{2}, \frac{4}{3}; z\right) = {}_2F_1\left(\frac{5}{6}, \frac{7}{6}; \frac{4}{3}; z\right) + \frac{35}{24} z \, {}_2F_1\left(\frac{11}{6}, \frac{13}{6}; \frac{7}{3}; z\right)$$

This procedure must be done a second time so that only ${}_2F_1$ functions remain.

Combining the $K_{1/3}(x)K_{2/3}(x)$, the $K_{2/3}^2(x)$, and the $K_{1/3}^2(x)$ integrals together, and with heavy manipulation using (G-3), (G-4), (G-7), and (G-8), as well as changing the form of two of the ${}_2F_1$ terms using (G-5), will yield (4.20) on page 41:

$$\chi_{2v}(f)$$

$$= \left(4T_v \frac{\sqrt{\pi}\,\Gamma\left(\frac{5}{6}\right)}{6\,\Gamma\left(\frac{1}{3}\right)} \alpha^{-1} \right)$$

$$\times \left[\frac{3\sqrt{3}}{4} \frac{\alpha_v^{5/3}}{(\alpha_v^2 + f^2 T_v^2 \pi^2)^{5/6}}\ {}_2F_1\left(\frac{5}{6}, \frac{1}{6}; \frac{4}{3}; \frac{\pi^2 f^2 T_v^2}{\alpha_v^2 + f^2 T_v^2 \pi^2} \right) \right.$$

$$+ \frac{35\sqrt{3}}{32} \left(\frac{\pi^2 f^2 T_v^2}{\alpha_v^2 + f^2 T_v^2 \pi^2} \right) \frac{\alpha_v^{5/3}}{(\alpha_v^2 + f^2 T_v^2 \pi^2)^{5/6}}\ {}_2F_1\left(\frac{11}{6}, \frac{1}{6}; \frac{7}{3}; \frac{\pi^2 f^2 T_v^2}{\alpha_v^2 + f^2 T_v^2 \pi^2} \right)$$

$$+ \frac{45\sqrt{3}}{256}\ {}_2F_1\left(\frac{11}{6}, \frac{7}{6}; \frac{7}{3}; -\frac{\pi^2 f^2 T_v^2}{\alpha_v^2} \right) - \frac{165\sqrt{3}}{256} \left(\frac{\pi^2 f^2 T_v^2}{\alpha_v^2} \right) {}_2F_1\left(\frac{13}{6}, \frac{17}{6}; \frac{10}{3}; -\frac{\pi^2 f^2 T_v^2}{\alpha_v^2} \right)$$

$$\left. + \frac{2431\sqrt{3}}{6144} \left(\frac{\pi^2 f^2 T_v^2}{\alpha_v^2} \right)^2\ {}_2F_1\left(\frac{19}{6}, \frac{23}{6}; \frac{13}{3}; -\frac{\pi^2 f^2 T_v^2}{\alpha_v^2} \right) \right]$$

where only the first two terms in the bracket contribute to the high frequency limit and all others reduce to zero.

APPENDIX D: NUMERICAL ASPECTS

This section will provide a combination of MATLAB and pseudo code to guide a user in the creation of their own modeling program, beginning with raw wind data.

Numerical Calculation of the PSD

Beginning with a raw turbulence wind data array (meaning that it has a zero mean) that is titled DATA, call the following function in MATLAB®

```
function [PSDRAW,freqRAW]=PSDofRAW(DATA,POINTS,delt,UPPERfLIM)

%PSDRAW=Output PSD
%freqRAW=Corresponding PSD frequencies

%DATA=Input raw wind data array
%POINTS=Number of frequencies to calculate the PSD at between 0 Hz and
the
    %Nyquist Frequency. For speed, will be trimmed to the nearest value
that
    %satisfies POINTS=2^p where p=integer. Generally, 128, 256, and 512
are
    %adequate values of POITNS
%delt=Time between samples of DATA
% UPPERfLIM=Highest limit at which to calculate the PSD, if UPPERfLIM=0
Hz,
% all frequencies will be calculated from 0 Hz to the Nyquist Frequency

%% Orient Raw Data Arrays
if size(DATA,2) > 1
    DATA=DATA';
end
%% Break Data Into Segments
N=2^nextpow2(POINTS); %Transfer POINTS to POINTS=n^p where p=Integer
nd=floor(length(DATA)/N);%Determine number of segments within DATA
array

WINDDATA=DATA(1:nd*N);%Remove excess data points that cannot make up a
full segment

WINDOW=(1-cos(pi*(0:N-1)/N).^2)'; %Create Hanning Window
```

```
SEGMENTS=zeros(nd,POINTS);%Initialize Segment vector

%% Separate Segments into a 2D matrix of (nd x N) dimensions while also
applying the window to the segments
for j1=1:nd
    CHUNK=(WINDDATA(1+N*(j1-1):j1*N));
    SEGMENTS(j1,:)=CHUNK.*WINDOW;
end
%% Create frequency vector

k=0:N/2;
n=0:N-1;

freqRAW=k/(N*delt); %frequency values to calculate the PSD

FFT=zeros(1,length(n));
power=zeros(1,length(k));
POWTOT=zeros(nd,length(k));  %Initialize Vectors
PSDRAW=zeros(1,length(k));

%% Calculate the PSD of each Segment
for f=1:nd
    for kk=1:length(k)
        for nn=1:length(n)
            FFT(nn)=SEGMENTS(f,nn)*exp(-1i*2*pi*k(kk)*n(nn)/N);
        end
        FFT(kk)=sqrt(8/3)*sum(FFT)*delt;
        power(kk)=abs(FFT(kk))^2;
    end

    POWTOT(f,:)=power;
end
%% Average all Segments Together
for h=1:length(k)
    PSDRAW(h)=2/(nd*N*delt)*sum(POWTOT(:,h));
end
%% Reorient Arrays
freqRAW=freqRAW';
PSDRAW=PSDRAW';

if isnan(UPPERfLIM) == 0
    PSDRAW(freqRAW>UPPERfLIM)=[];
    freqRAW(freqRAW>UPPERfLIM)=[];
end
```

Calculate T_i and A

With a quality PSD function generated from the turbulence data, the time scale as well as the high frequency limit should be determined. Both of these tasks are simple using the sub-routines available in MATLAB®. T_i should be calculated, based on the user's discretion, according to (5.1) on page 54. The PSD that was calculated in the previous section, begins at a frequency of zero Hz. In light of this, the first value of the PSD that is not the zero frequency, would be the second value in the `PSDRAW` array from the previous section.

```
VAR=var(DATA);  % Calculate the variance of the DATA array

Tu=PSDRAW(2)/(4*VAR); % Tu is the time scale to be used in future
calculations
```

In calculating the value of A, the user must identify when, if at all, the PSD calculated in the previous section, begins to approach the high frequency limit from quality (iii) from (1.11) from page 8. This is a subjective task, and one that can be complicated especially if high frequency data is not available. Figure D.1 shows the frequency at which a particular PSD decays at the proper rate.

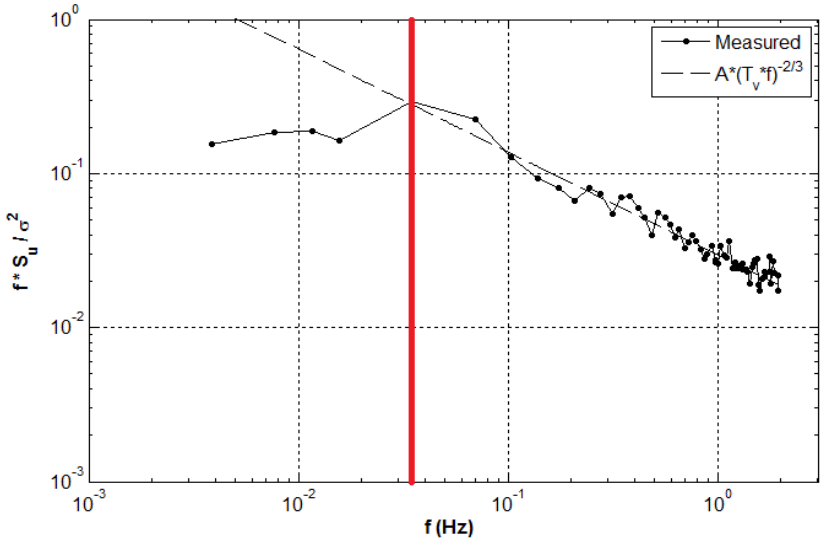

Figure D.1: Sample PSD. It can be seen that the spectrum decays at the proper rate after $f = 0.035\ Hz$

If this 'roll-off' frequency is determined, arrays can be created that consist of only the frequencies and their corresponding spectral magnitude above this 'roll-off' frequency.

```
PSD2COMP=(PSDRAW(freqRAW>freqmin); % Only PSD values above the roll off
frequency (called freqmin)
freq2COMP=freqRAW(freqRAW>freqmin); % Corresponding frequency

%% Search for value of A
% A least squares fit can be utilized to find an approximation of A

Ao=[0.05]; %Initial guess for A
A = fminsearch(@(A) findA(A,freq2COMP,PSD2COMP,Tu,VAR),Ao); % Call
Matlab's fminsearh function
```

```
function [Squares] = findA(A,freq2COMP,PSD2COMP,Tu,VAR)

Squares=sum((VAR*A*Tu^(-2/3)*freq2COMP.^(-5/3)-PSD2COMP).^2);

end
```

A note about the calculation of 'A', is that qualification (iii) from (1.11) from page 8 has been changed to:

$$S_i(f_{h.f.}) = \left(\sigma_i^2 A\, T_i^{-2/3}\right) f^{-5/3}$$

Determination of β Coefficients

With the value of A calculated, a search can be performed to vary the values of β coefficients in an attempt fit the data. This example will use the longitudinal series to create the fit.

```
constants_alpha=[0.746834201056  0.323388695258  0.194117929829...
           0.133860978362  0.099798309222   0.078244974866];

%% Set Limits of Search, as well as Beta and Alpha Constraints

lb=-Inf.*ones(1,N); % Lower bound for Betas
ub=-lb; % Upper bound for Betas
Betas=[1 zeros(1,N-1)]; %Initial guess of Beta coefficients
Aineq=[-constants_alpha(1:N)]; % Constrain alpha to positive values
bineq=[-1e-7];
Aeq=[ones(1,N)]; % Apply Sum(Beta)=1 constraint
beq=[1];

options= optimset('Algorithm','sqp','TolCon',1e-10,...
        'TolFun',1e-8,'TolX',1e-8,'Diagnostics','off');

problem=createOptimProblem('fmincon','x0',Betas,'objective',@(Betas)
FINDTERMS(Betas,PSDRAW,freqRAW,A,VAR),...
'lb',lb,'ub',ub,'Aineq',Aineq,'bineq',bineq,'Aeq',Aeq,'beq',beq,'option
s',options);
```

```
function [Squares] = FINDTERMS(Betas,PSDRAW,freqRAW,A,VAR)

%% Find the Longitudinal Expansion from supplied Beta values

[RuuAPP,~]=Get_RuuVON(Betas);

constants_alpha=[0.746834201056  0.323388695258  0.194117929829...
        0.133860978362717  0.099798309222461   0.078244974866071];

constants_A=[0.1396318231 0.2792636462 0.4188954693 0.5585272923...
        0.6981591154 0.8377909385 0.9774227616];

alpha=dot(Betas,constants_alpha(1:N));

% Calculate the PSD of the longitudinal expansion series generated
[SnPETURB, freqPETURB]=PSDatFREQ(RuuAPP,freqRAW,VAR);
```

```
% Find the least squared error of the model and the data
R=sum(((PSDRAW - SnPETURB)./ PSDRAW).^2);

% Find the error between the models A value and the true A value
AError=abs(A-dot(Betas,constants_A(1:N))*alpha^(2/3))/A*100;

% Combine the two errors
Squares=sum(R+AError);

end
```

```
% Find Longitudinal Expansion Model of Autocorrelation
function [RuuAPP,alpha] = Get_RuuVON(Betas,Tu)

N=length(Betas);

Time=(0:0.001:100)';

constants=[0.746834201056597  0.323388695258742  0.194117929829485...
    0.133860978362717  0.099798309222461   0.078244974866071
0.063551213297927];

alpha=dot(Betas,constants(1:N));
BesselARG=Time.*alpha/Tu;
RuuVON=2^(2/3)/gamma(1/3).*((BesselARG).^(1/3)).*besselk(1/3,BesselARG)
;
RuuVON(1)=1;
RuuAPP=zeros(length(RuuVON),1);

for i=1:length(Betas)
    RuuAPP=RuuAPP+(RuuVON.^i)*Betas(i);
end

end
```

```
% Find PSD of Expansion series from Longitudinal Expansion Model

function [PSDAUTO,freqAUTO]=PSDatFREQ(Rxx,freqAUTO,VAR)

Time=(0:0.001:100)';

PSDAUTO=zeros(length(freqAUTO),1);

for kk=1:length(freqAUTO)
    FFT=Rxx.*cos(2*pi*freqAUTO(kk).*Time);
    PSDAUTO(kk)=4*trapz(Time,FFT)*VAR;
end
```

The above code is an example of utilizing the second method of enforcing the A constraint from page 61. This method does not actually 'enforce' the A constraint, but suggests that it be as close as possible, and still provides a reasonable fit. Lastly, because the entire point of this thesis is to replace the von Kármán model with a better one, the initial estimate of the minimization algorithm should be the von Kármán model itself, i.e. $\beta_1 = 1$. If this is the case, any result from the minimization algorithm in which $\beta_1 \neq 1$ will, by definition, be a better fit than the von Kármán.

Selecting Points to Fit

If ensemble averaging (from Chapter 2) is either not possible, or does not produce a stable enough fit, one method of producing quality fits of turbulence PSD data is to smooth the PSD or alter the number of points to fit. Smoothing of the data is self-explanatory. Moving averaging is generally the best method, however, any elimination of widely varied PSD data will result in a more stable fit of the data, in that a least squares fit will pull the fit to the smoothed line. A more significant method is to evenly space the data, on a log-log plot. It is obvious that a PSD data set calculated at evenly spaced frequencies will contain points on a log-log plot that will be closer and closer together at higher and higher frequencies. This can be seen in any of the figures in Chapter 6. Due to the clustering of data at the higher end of the spectrum, a greater emphasis is on fitting the model to this end of the spectrum, resulting in a less accurate fit at the lower frequency range. The remedy for this is to select points that are evenly spaced on a log-log plot as detailed below. Assume the frequency and PSD data sets are represented by `freqRAW` and `PSDRAW` respectively.

```
function [freq2COMP, PSD2COMP] = EvenlyLogSpaced(freqRAW, PSDRAW,
Length)

%freqRAW- is the input frequency array
%PSDRAW- is the input PSD array
%Length- is the number of evenly spaced points desired for the output
%freq2COMP- and PSD2COMP- are the output evenly spaced frequency and
PSD data

GAP=[0.1:0.1:1 1:100 100:10:1000 1000:100:10000];
for j=1:length(GAP)
    INT=NaN(length(PSDRAW),1);
    PSD2COMP=INT;
    freq2COMP=INT;
    INT(1)=1;
    PSD2COMP(1)=PSDRAW(1);
    freq2COMP(1)=freqRAW(1);
    for i=2:length(PSDRAW)
        SKIP=floor(10^(freqRAW(i) GAP(j)));
        INT(i)=INT(i-1)+SKIP;
        if max(INT) < numel(freqRAW)
            PSD2COMP(length(PSD2COMP)+1,1)=PSDRAW(INT(i));
            freq2COMP(length(freq2COMP)+1,1)=freqRAW(INT(i));
        else
            INT=[];
            PSD2COMP(isnan(PSD2COMP))=[];
            freq2COMP(isnan(freq2COMP))=[];
            break
        end
    end
    if length(PSD2COMP) < Length
        break
    end
end
```

Figure D.2 shows the result of the previous algorithm with an input PSD comprised of 128 points, with an output of 24 evenly spaced points.

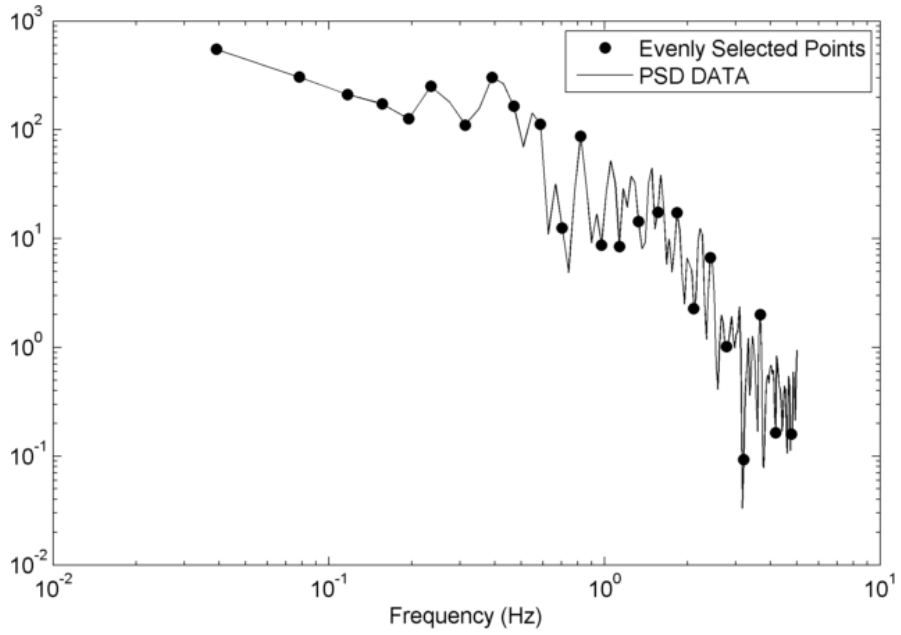

Figure D.2: Comparison of a PSD with evenly spaced values and PSD data that is evenly spaced in a log-log plot

Least Squares Fitting

Similar to the issue of data clustering at high frequencies is the fact that low frequency data is generally three or more order of magnitude greater than high frequency data (when plotting the dimensional spectrum). When performing a least squares fit, the high magnitude data can dominate the fit, while greatly sacrificing the fit at the high frequency (low magnitude) region. A solution to this is to perform a 'Normalized Least Squares Fit'. This normalization reduces the magnitude or the error from each data point to carry the same weight. This fitting was used in the function `FINDTERMS` on page 98, and is given by (D.1).

$$LS_{Error} = \frac{Data\ Value - Modeled\ Value}{Data\ Value} \tag{D.1}$$

This method of performing the least squares fit will greatly improve the model by allowing each point in the measured data to have the same fitting weight.

Cross-Spectrum

The following function can be used to calculate the cross-spectrum (magnitude and phase) of two series of turbulence data, X and Y. The POINTS variable determines the number of frequencies to show, 'delt' is the time between velocity samples, and 'UPPERfLIM' is used if a cut off is required at a frequency below the Nyquist frequency.

```
function [CROSS,freqCROSS] = CROSS_SPECTRA(x,y,POINTS,delt,UPPERfLIM)

if size(x,2) > 1
    x=x';
end
if size(y,2) > 1
    y=y';
end

%% Break Data Into Segments
N=2^nextpow2(POINTS); %Transfer POINTS to POINTS=n^p where p=Integer
while numel(x) < N
    N=2^(nextpow2(N)-1);
end

nd=floor(numel(x)/N); %Determine number of segments within DATA array

if nd == 0
    nd=1;
end

WINDDATAx=x(1:nd*N);
WINDDATAy=y(1:nd*N);

WINDOW=(1-cos(pi*(0:N-1)/N).^2)'; %Create Hanning Window

SEGMENTSx=zeros(nd,N); %Initialize Segment vector
SEGMENTSy=zeros(nd,N);

%% Seperate Segments into a 2D matrix of (nd x N) dimensions and apply
window
for j1=1:nd
    CHUNKx=WINDDATAx(1+N*(j1-1):j1*N);
    CHUNKy=WINDDATAy(1+N*(j1-1):j1*N);
    SEGMENTSx(j1,:)=CHUNKx.*WINDOW;
```

```
    SEGMENTSy(j1,:)=CHUNKy.*WINDOW;
end

%% Create frequency vector
k=0:N/2;
n=0:N-1;

freqCROSS=k/(N*delt); %frequency values to calculate the PSD

FFTxfirst=zeros(1,length(n));
FFTyfirst=zeros(1,length(n));
FFTx=zeros(1,length(k));
FFTy=zeros(1,length(k));
power=zeros(1,length(k));
POWTOT=zeros(nd,length(k));  %Initialize Vectors
CROSS=zeros(1,length(k));

%% Calculate the PSD of each Segment
for f=1:nd
    for kk=1:length(k)
        for nn=1:length(n)
            FFTxfirst(nn)=SEGMENTSx(f,nn)*exp(-1i*2*pi*k(kk)*n(nn)/N);
            FFTyfirst(nn)=SEGMENTSy(f,nn)*exp(-1i*2*pi*k(kk)*n(nn)/N);
        end
        FFTx(kk)=trapz(FFTxfirst)*delt*sqrt(8/3);
        FFTy(kk)=trapz(FFTyfirst)*delt*sqrt(8/3);
        power(kk)=conj(FFTx(kk))*FFTy(kk);
    end
    POWTOT(f,:)=power;
end

%% Average all Segments Together
for h=1:length(k)
    CROSS(h)=2/(nd*N*delt)*sum(POWTOT(:,h));
end

%% Reorient Arrays
freqCROSS=freqCROSS';
CROSS=CROSS';

CROSS (1)= CROSS (1)/2;
CROSS (end)= CROSS (end)/2;

if isnan(UPPERfLIM) == 0
    CROSS (freqCROSS>UPPERfLIM)=[];
    freqCROSS(freqCROSS>UPPERfLIM)=[];
end
```

The following function calculates the coherence of two turbulence velocity arrays X and Y. Note that previous function such as CROSS_SPECTRUM.m are used.

```
function [Cxy,freq] = Coherence(x,y,POINTS,delt,UPPERfLIM)

[PSDxx,freq]=PSDofRAW(x,POINTS,delt,UPPERfLIM);
[PSDyy,~]=PSDofRAW(y,POINTS,delt,UPPERfLIM);
[PSDxy,~]=CROSS_SPECTRA(x,y,POINTS,delt,UPPERfLIM);

Cxy=abs(PSDxy).^2./(PSDxx.*PSDyy);

end
```

The following function calculates the phase of a two turbulence velocities X and Y.

```
function [PHASE,freq] = PHASE(x,y,POINTS,delt,UPPERfLIM)

 [PSDxy,freq]=CROSS_SPECTRA(x,y,POINTS,delt,UPPERfLIM);

 PHASE=atan2d(imag(PSDxy),real(PSDxy));

end
```

Figure D.3-Figure D.11show samples of the cross-spectrum between two points, one 10 feet below the rotor of a hovering helicopter, the other 15 feet below the rotor, along with the phase and coherence between these two points.

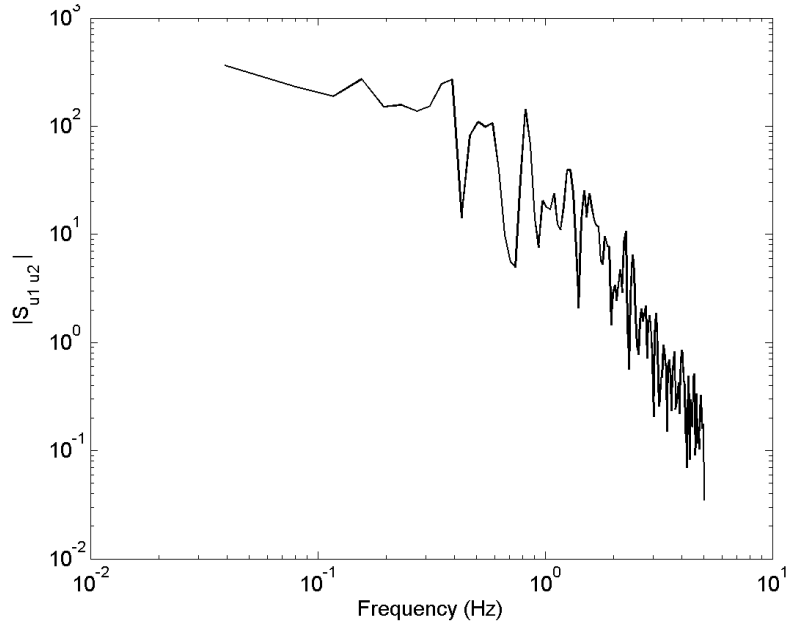

Figure D.3: Cross-spectrum of longitudinal turbulence between two points located 10 feet and 15 feet below a hovering helicopter rotor

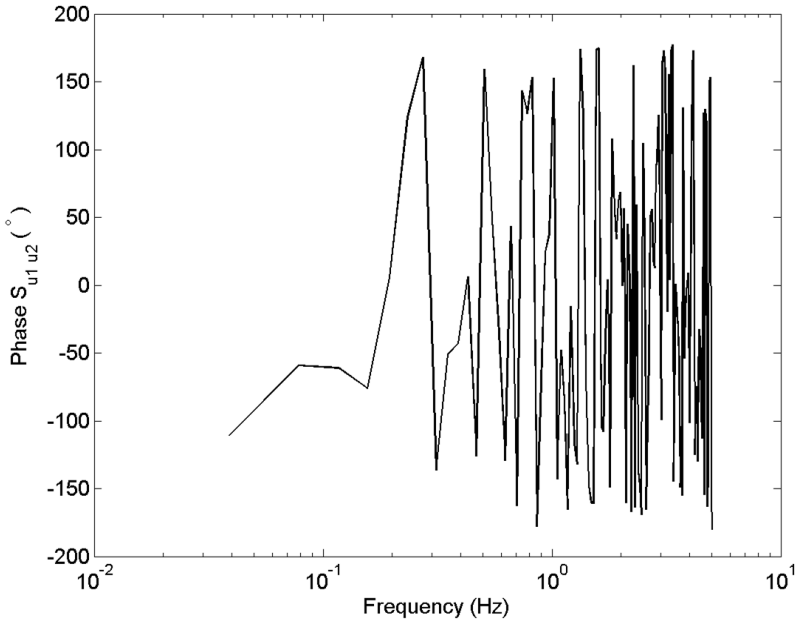

Figure D.4: Phase of cross-spectrum of longitudinal turbulence between two points located 10 feet and 15 feet below a hovering helicopter rotor

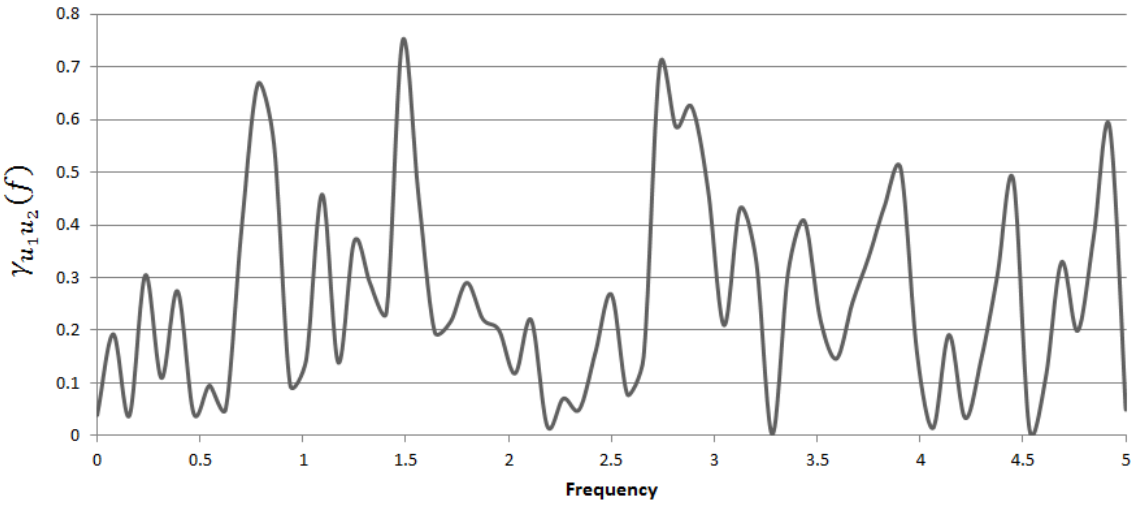

Figure D.5: Coherence of longitudinal turbulence between two points located 10 feet and 15 feet below a hovering helicopter rotor

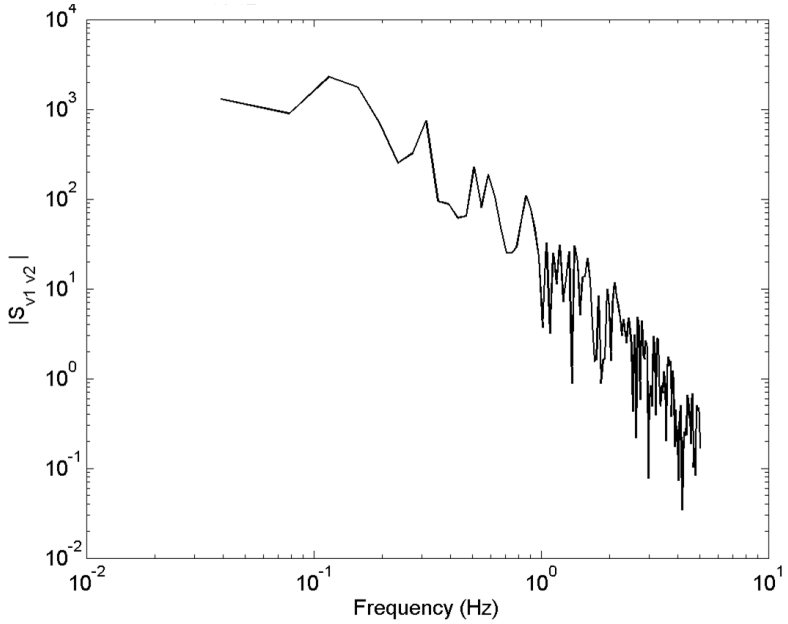

Figure D.6: Cross-spectrum of lateral turbulence between two points located 10 feet and 15 feet below a hovering helicopter rotor

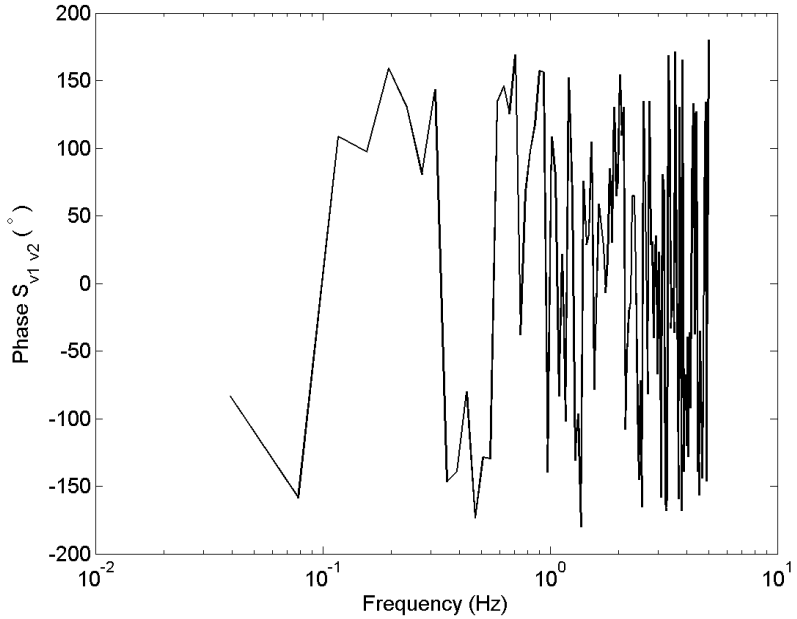

Figure D.7: Phase of cross-spectrum of lateral turbulence between two points located 10 feet and 15 feet below a hovering helicopter rotor

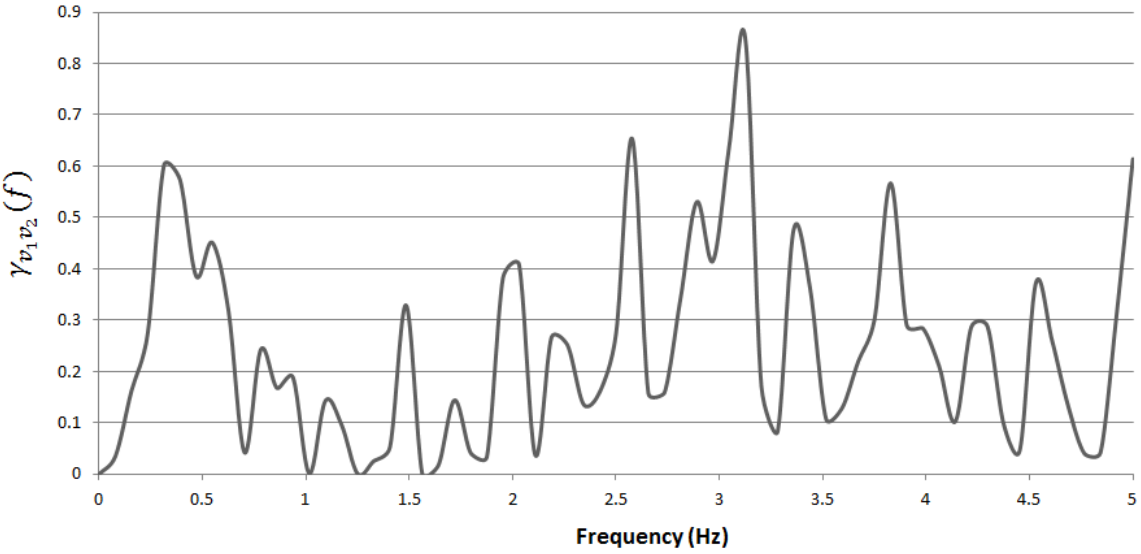

Figure D.8: Coherence of lateral turbulence between two points located 10 feet and 15 feet below a hovering helicopter rotor

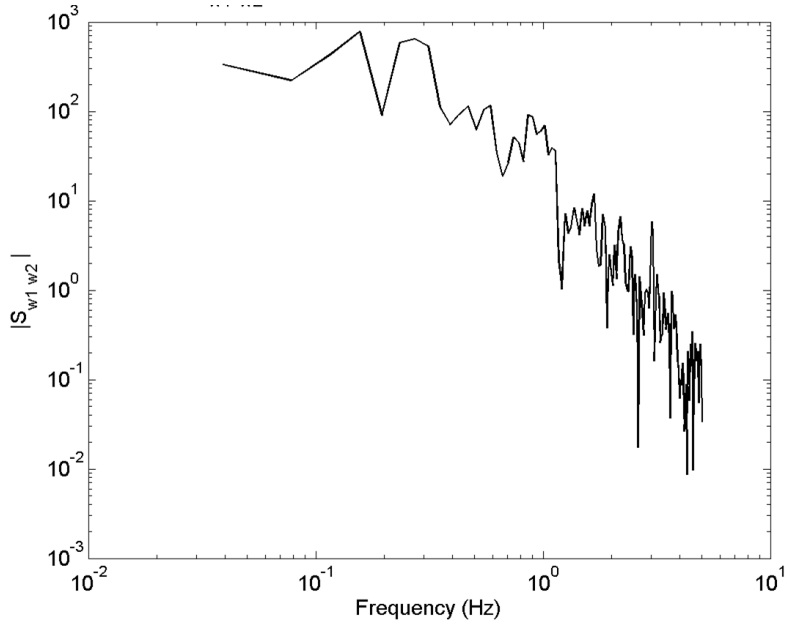

Figure D.9: Cross-spectrum of vertical turbulence between two points located 10 feet and 15 feet below a hovering helicopter rotor

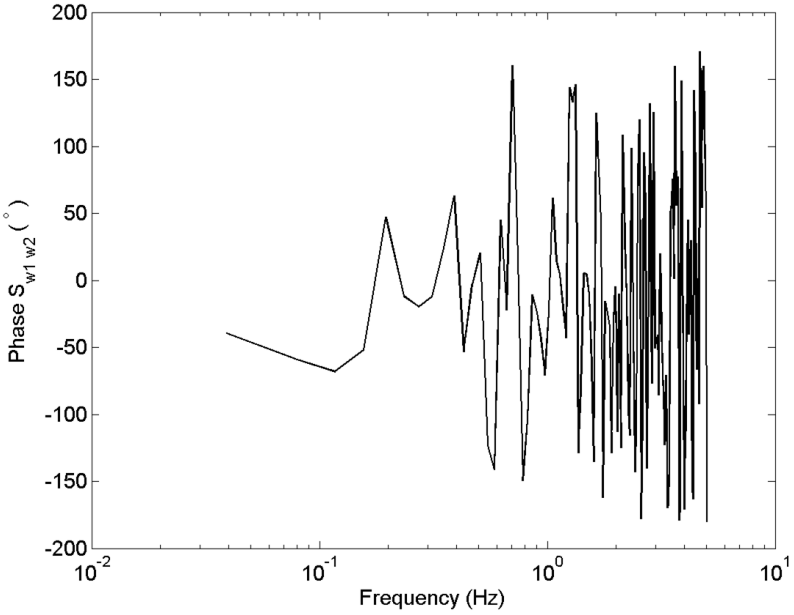

Figure D.10: Phase of cross-spectrum of vertical turbulence between two points located 10 feet and 15 feet below a hovering helicopter rotor

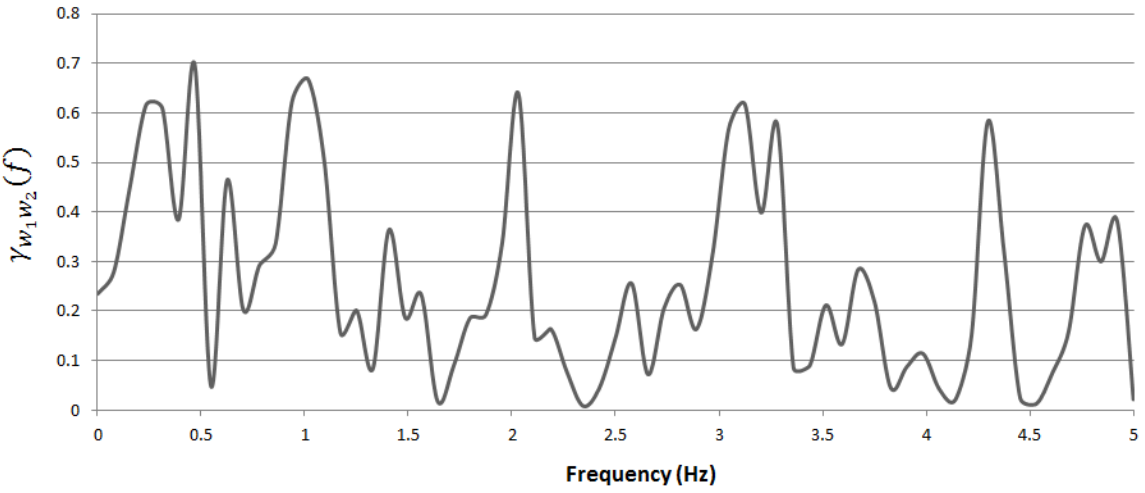

Figure D.11: Coherence of vertical turbulence between two points located 10 feet and 15 feet below a hovering helicopter rotor

APPENDIX E: FURTHER WIND FARM RESULTS

Figure E.1-Figure E.7 show several other cases of developed models in closed form from the autospectral database for a wind farm over a complex terrain. Included are two and three term series expansions, both including, and excluding the 'A' constraint. These results should serve as a reference point for future research.

Two Term Series without 'A' Constraint

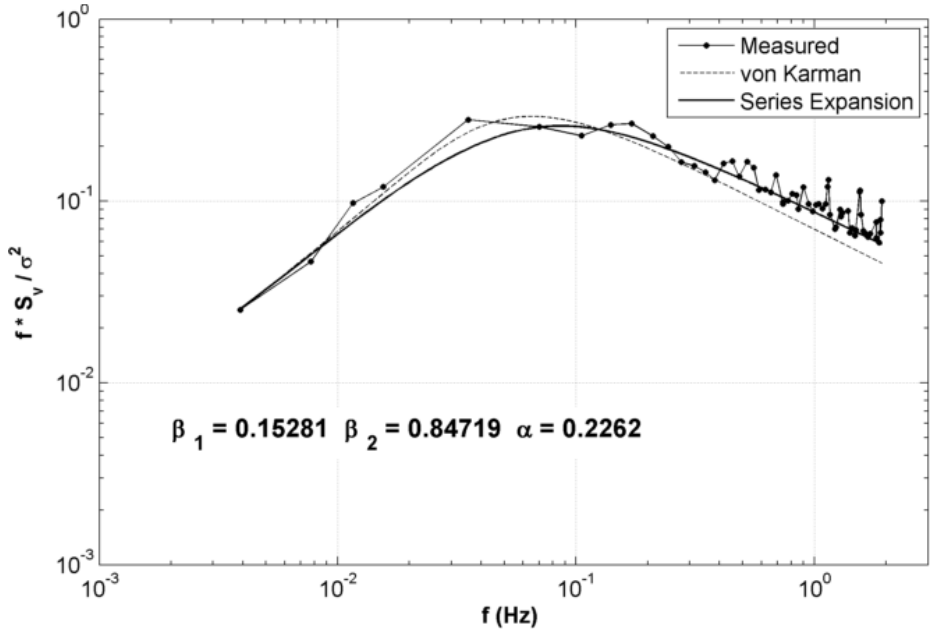

Figure E.1: Two term series expansion of lateral turbulence without constraining the fit to the 'A' constraint

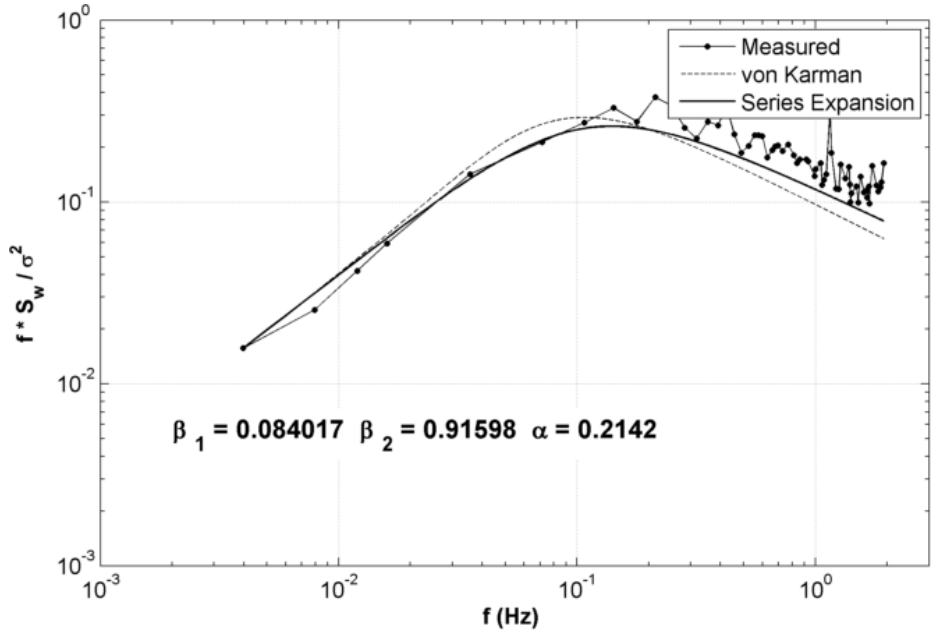

Figure E.2: Two term series expansion of vertical turbulence without constraining the fit to the 'A' constraint

Three Term Series with 'A' Constraint

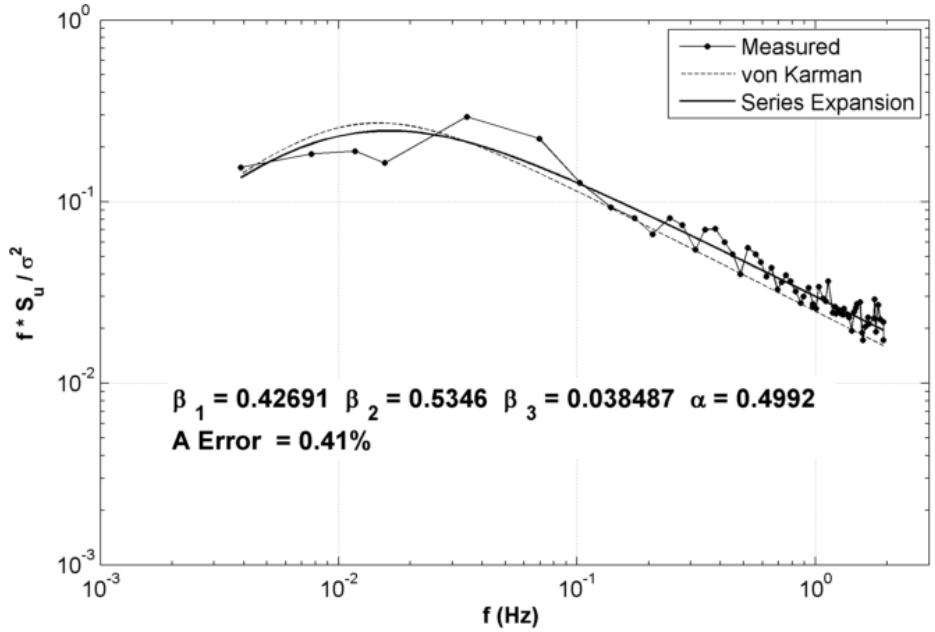

Figure E.3: Three term series expansion of longitudinal turbulence while constraining the fit to the 'A' constraint

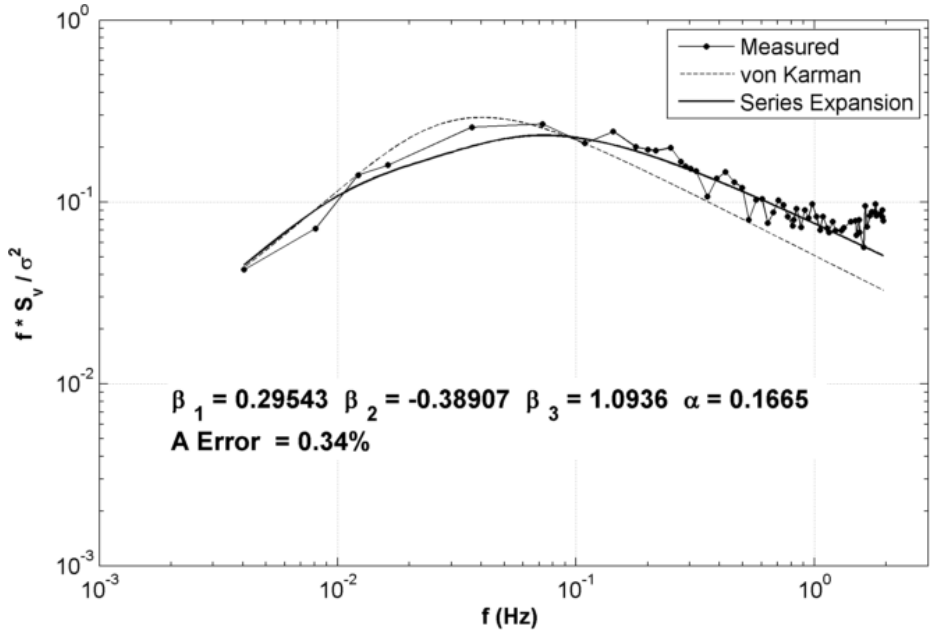

Figure E.4: Three term series expansion of lateral turbulence while constraining the fit to the ‘A’ constraint

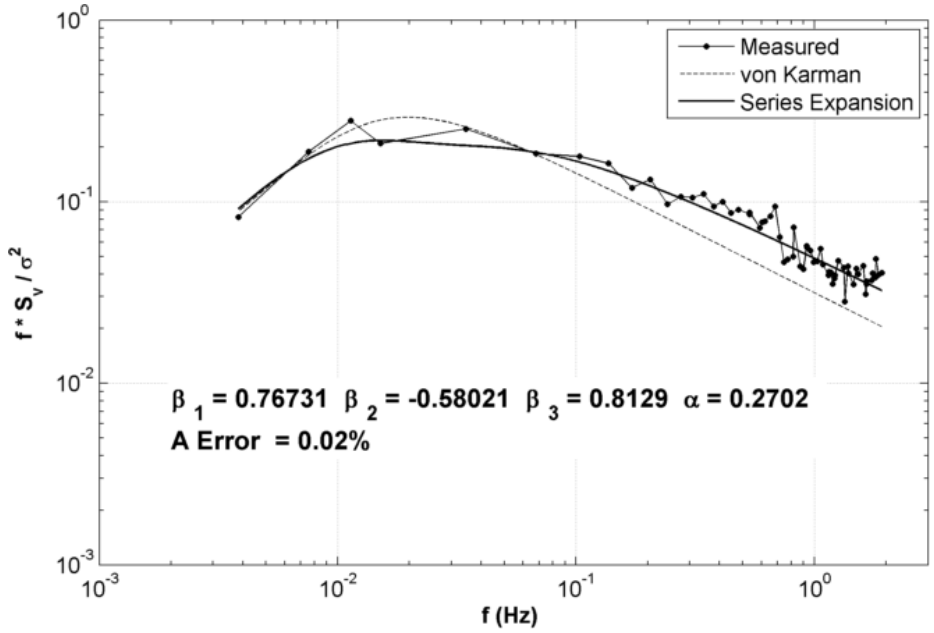

Figure E.5: Three term series expansion of lateral turbulence while constraining the fit to the ‘A’ constraint

Three Term Series without 'A' Constraint

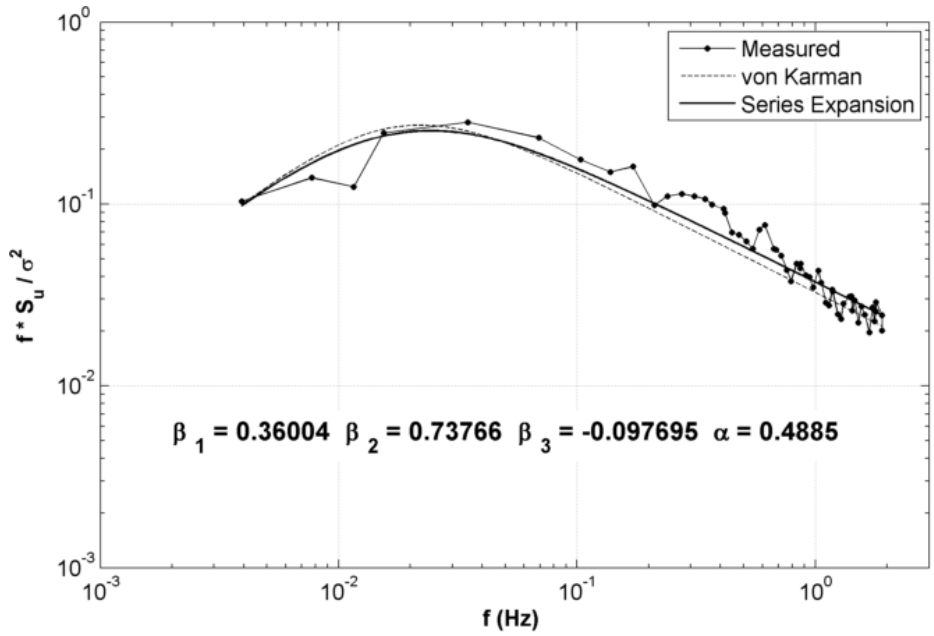

Figure E.6: Three term series expansion of longitudinal turbulence without the 'A' constraint

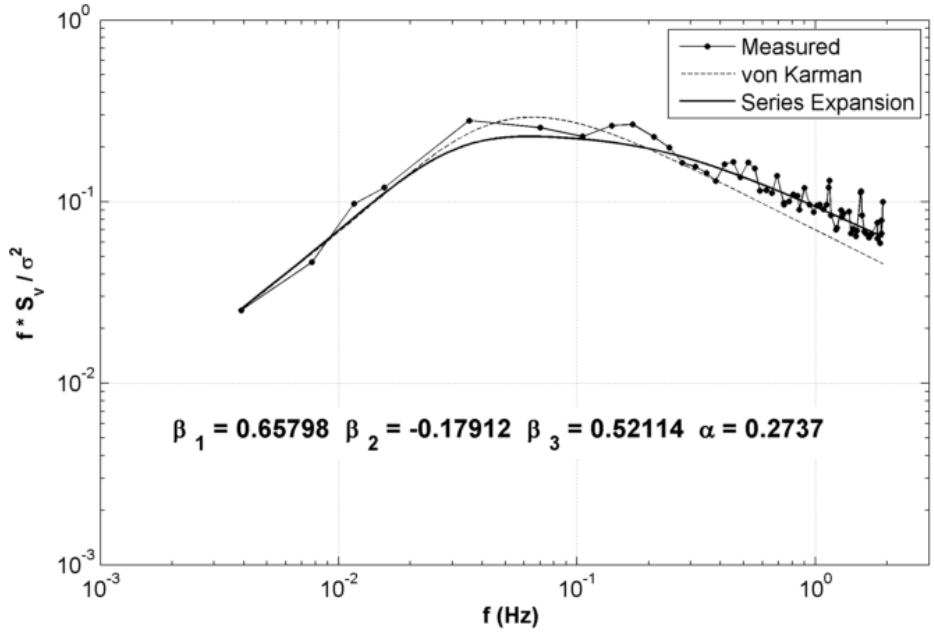

Figure E.7: Three term series expansion of lateral turbulence without the 'A' constraint

APPENDIX F: FURTHER HELICOPTER DOWNWASH RESULTS

Figure F.1-Figure F.5 show other results for downwash turbulence below the rotor of a hovering helicopter, including two and three term series, both enforcing and not enforcing the ‘A’ constraint. Here as well, these results should serve as a reference point for future research.

Two Term Series without ‘A’ Constraint

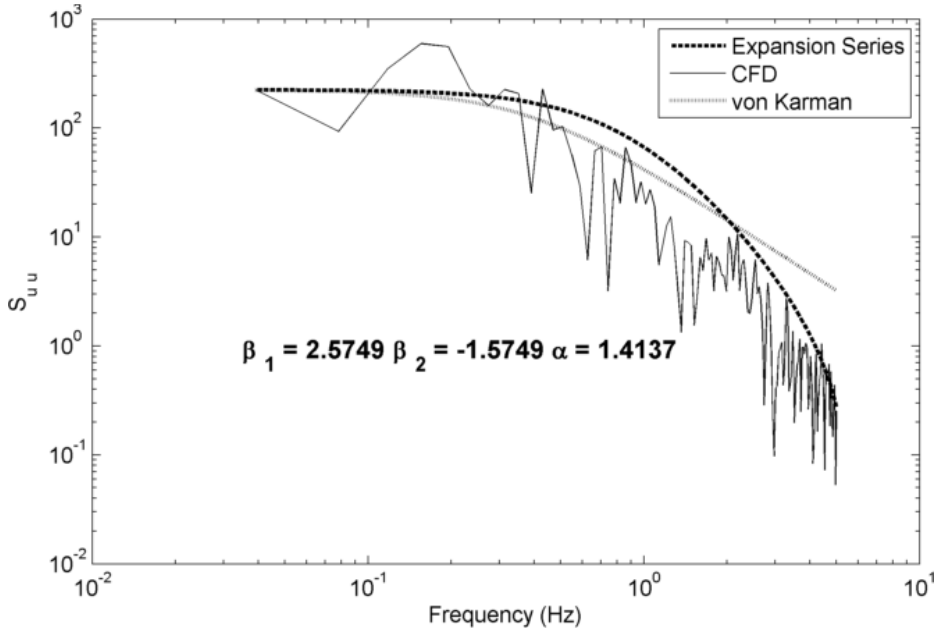

Figure F.1: Two term expansion series of longitudinal turbulence under a hovering helicopter rotor, without the ‘A’ constraint

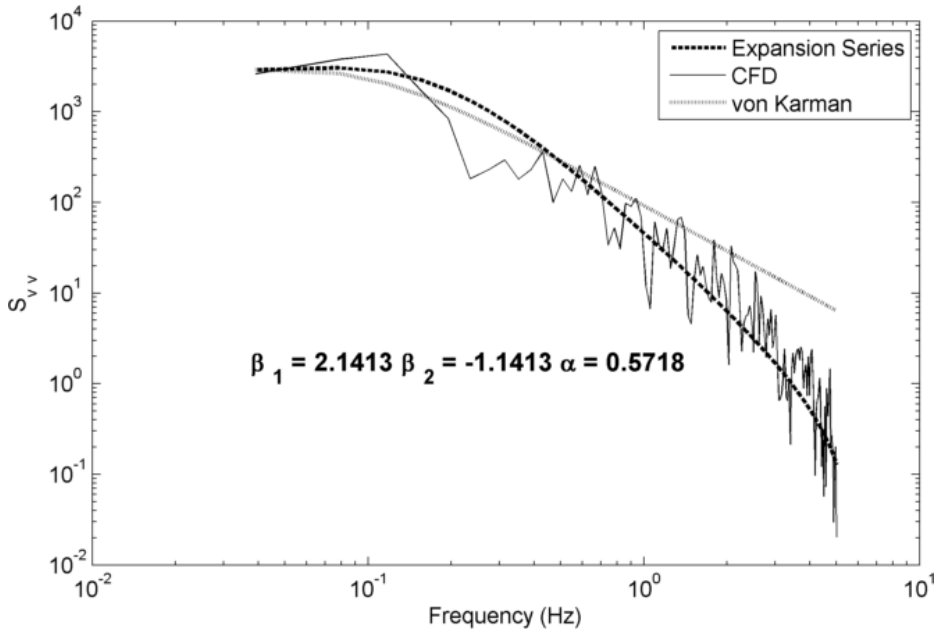

Figure F.2: Two term expansion series of lateral turbulence under a hovering helicopter rotor, without the 'A' constraint

Three Term Series with 'A' Constraint

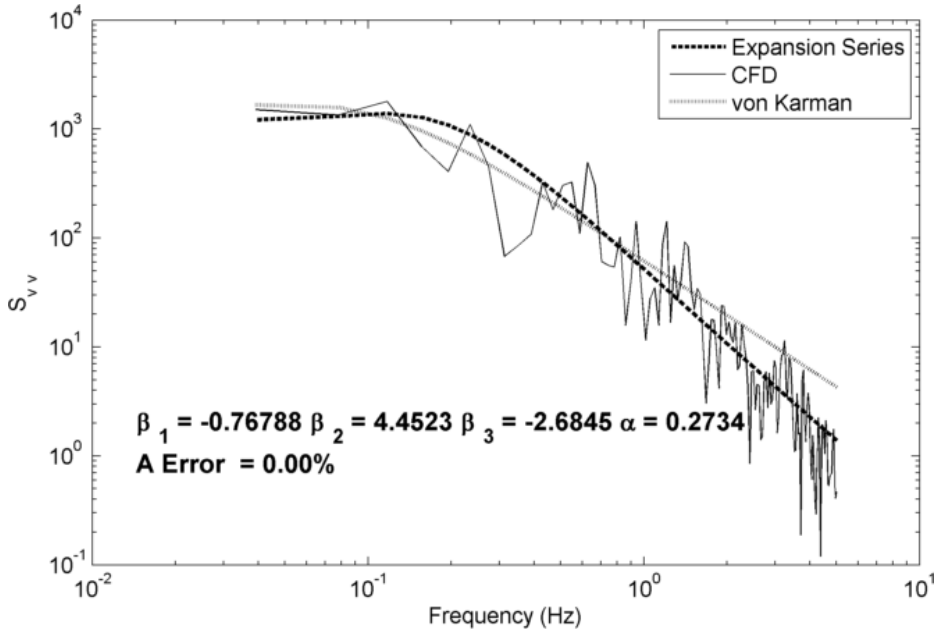

Figure F.3: Three term expansion series of lateral turbulence under a hovering helicopter rotor, with the 'A' constraint

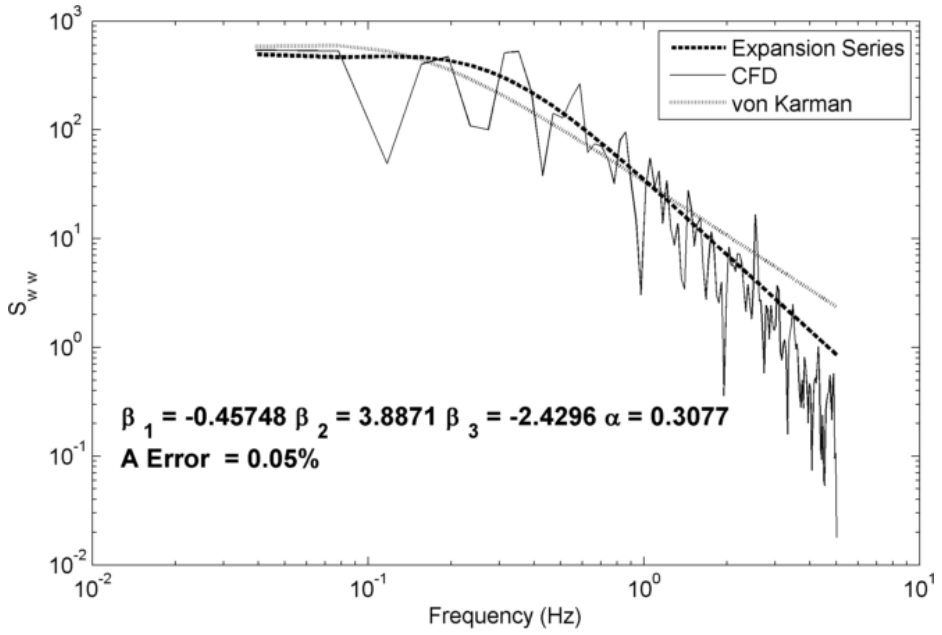

Figure F.4: Three term expansion series of vertical turbulence under a hovering helicopter rotor, with the 'A' constraint

Three Term Series without 'A' Constraint

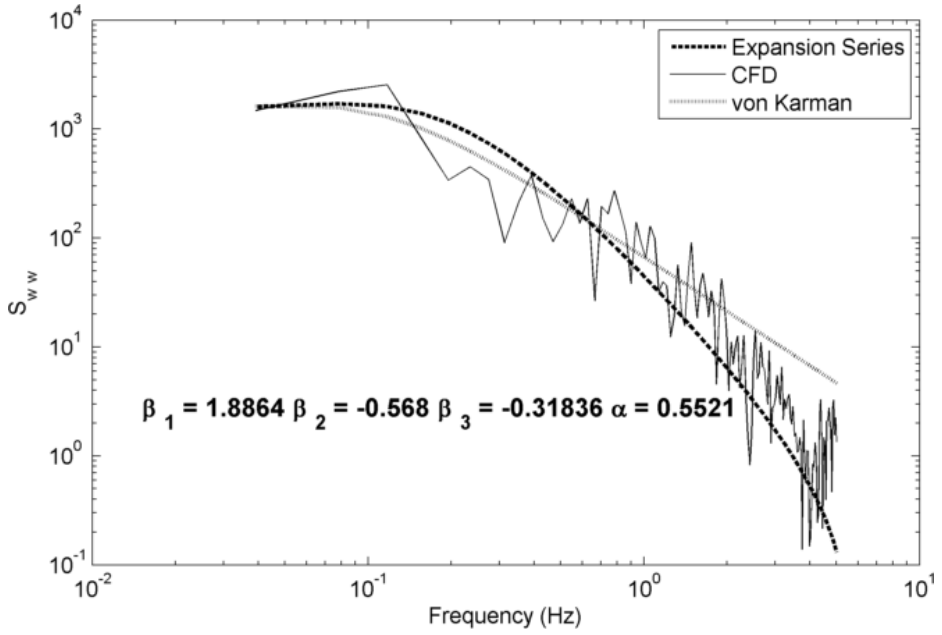

Figure F.5: Three term expansion series of vertical turbulence under a hovering helicopter rotor, without the 'A' constraint

APPENDIX G: FURTHER DOWNWASH AND AIRWAKE RESULTS

Figure G.1-Figure G.7 show other results for downwash turbulence (below the rotor of a hovering helicopter) coupled with airwake turbulence shed from the ship superstructure, including two and three term series, both enforcing and not enforcing the 'A' constraint. These results should serve as a reference point for future research.

Two Term Series with 'A' Constraint

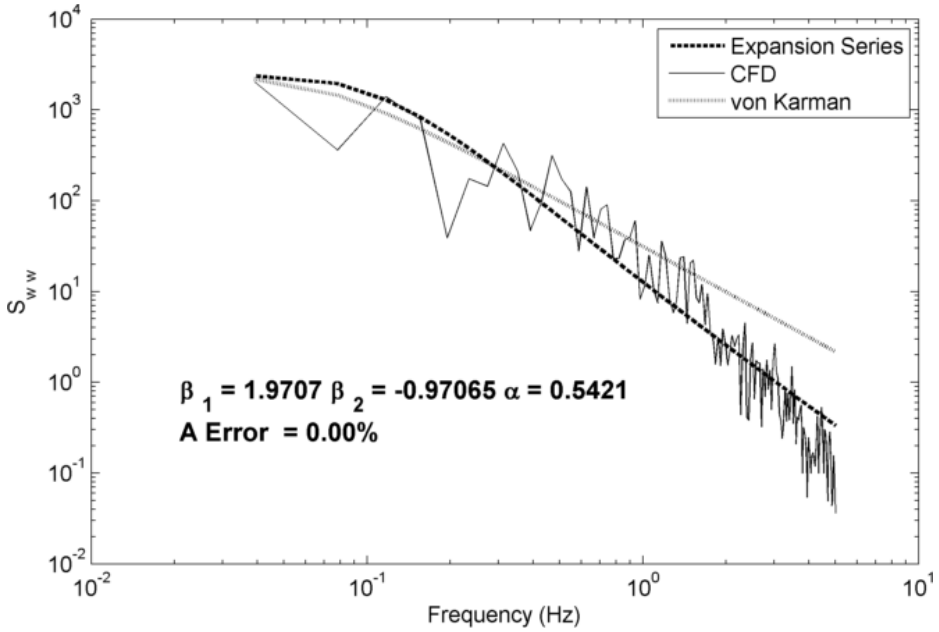

Figure G.1: Two term expansion series of vertical turbulence under a hovering helicopter rotor coupled with ship airwake, with the 'A' constraint

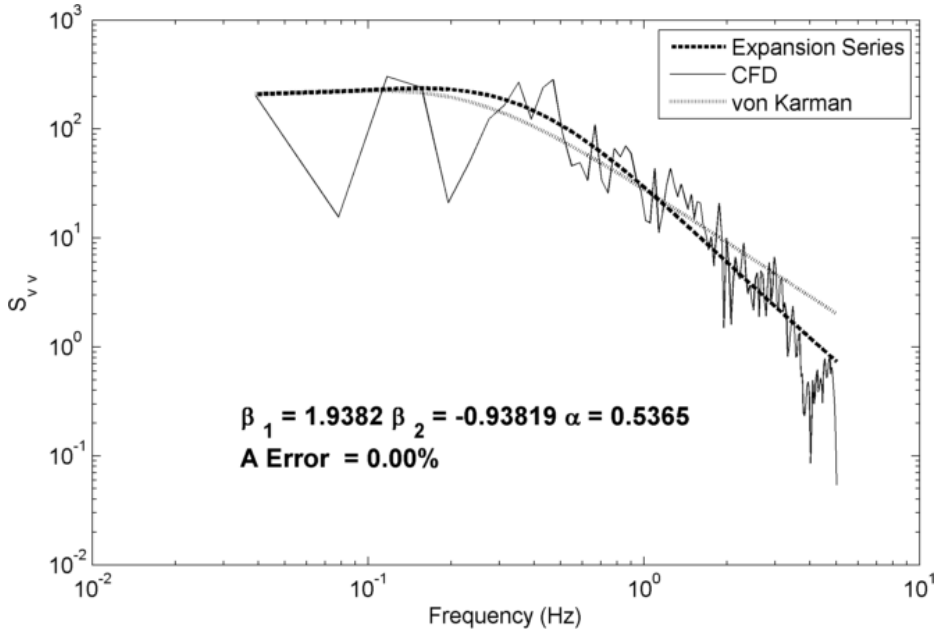

Figure G.2: Two term expansion series of lateral turbulence under a hovering helicopter rotor coupled with ship airwake, with the 'A' constraint

Two Term Series without 'A' Constraint

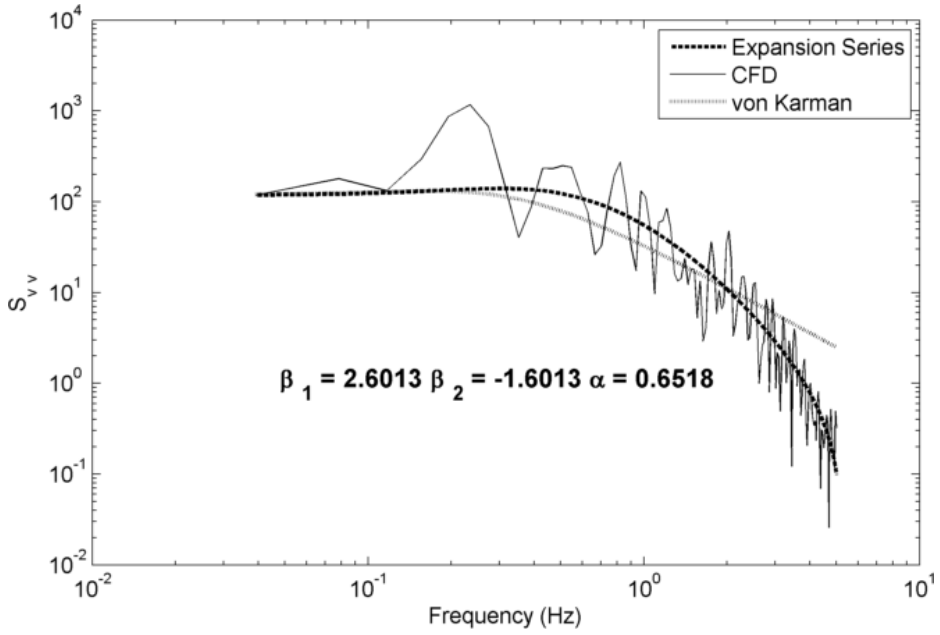

Figure G.3: Two term expansion series of lateral turbulence under a hovering helicopter rotor coupled with ship airwake, without the 'A' constraint

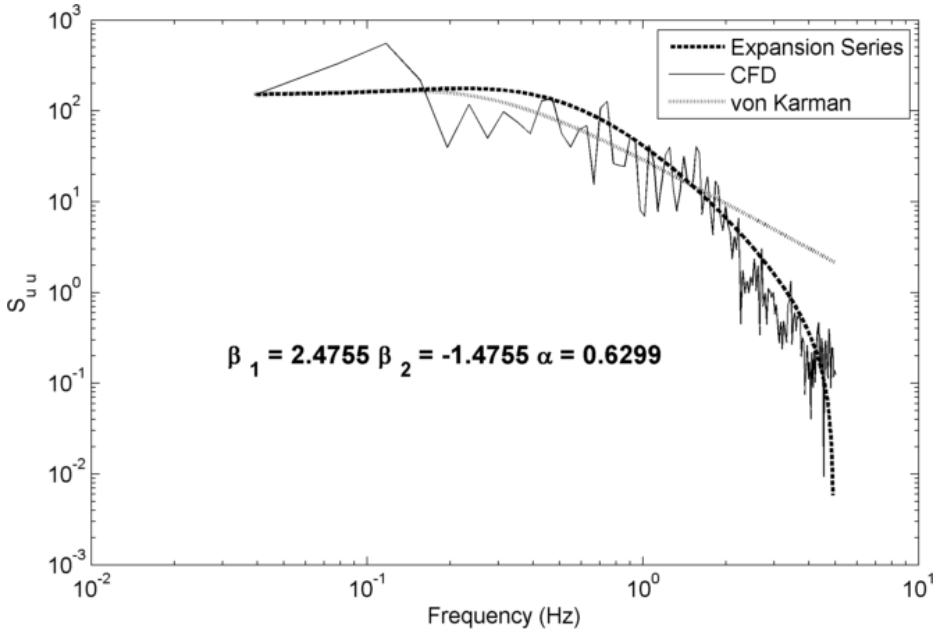

Figure G.4: Two term expansion series of longitudinal turbulence under a hovering helicopter rotor coupled with ship airwake, without the 'A' constraint

Three Term Series with 'A' Constraint

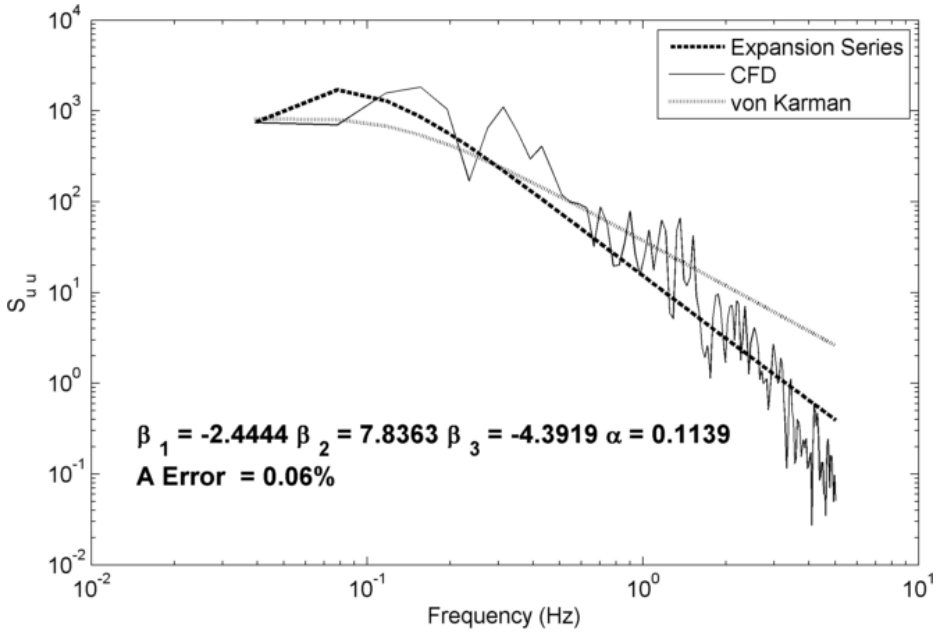

Figure G.5: Three term expansion series of longitudinal turbulence under a hovering helicopter rotor coupled with ship airwake, with the 'A' constraint

Three Term Series without 'A' Constraint

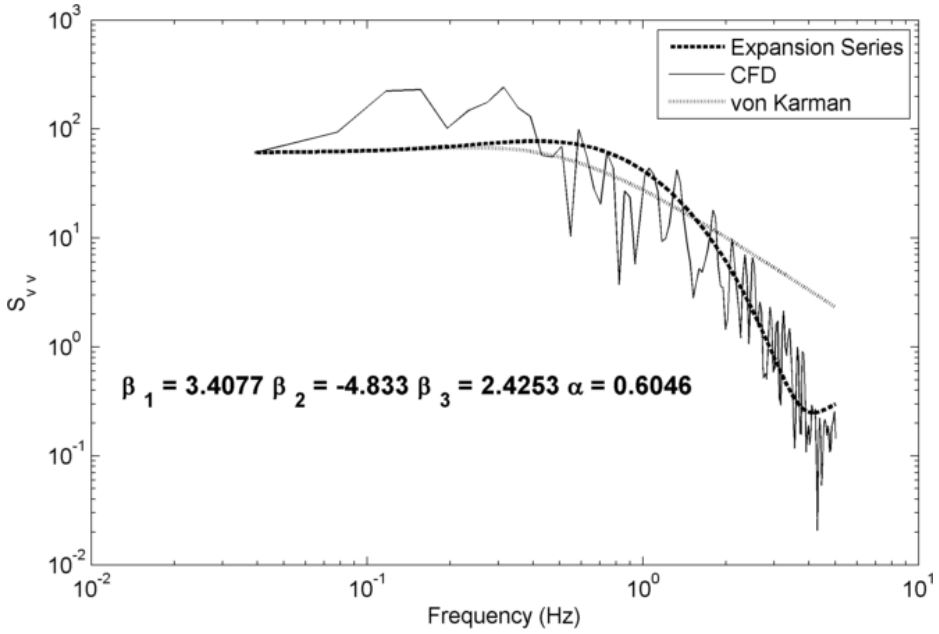

Figure G.6: Three term expansion series of lateral turbulence under a hovering helicopter rotor coupled with ship airwake, without the 'A' constraint

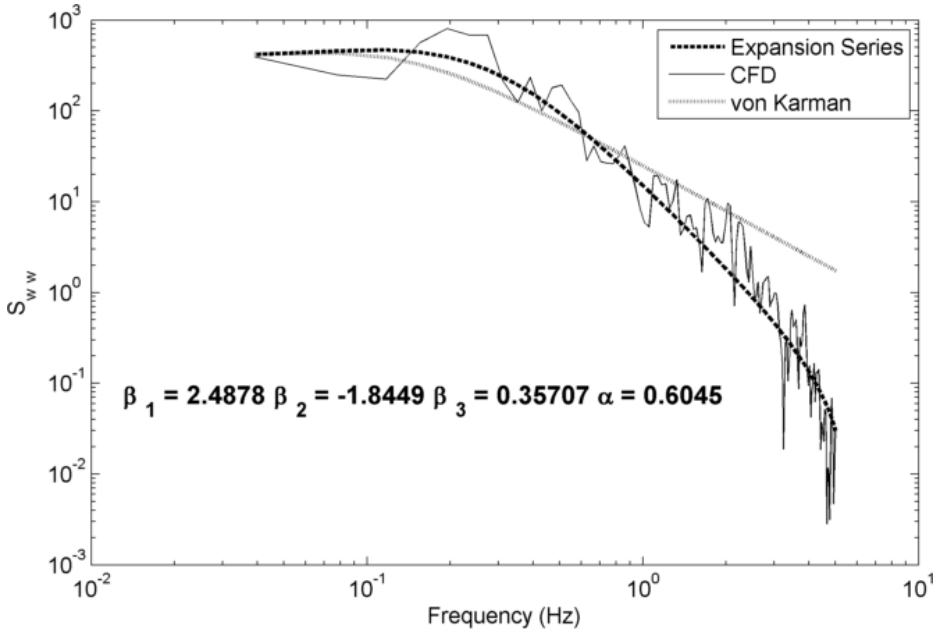

Figure G.7: Three term expansion series of vertical turbulence under a hovering helicopter rotor coupled with ship airwake, without the 'A' constraint

APPENDIX H: FILTER DESIGN

The developed models of autospectrum are found to be extremely suitable for simulation through shaping filters driven by white noise. In fact, such an approach has been widely used in conjunction with the von Kármán models. Given the autospectrum, say $S_i(f)$, the simulation or reconstruction of the time histories simplifies to designing a shaping filter with system function $H(f)$ and is passing white noise with an autospectrum of unity. Now, the output autospectrum is $H(f)^2$ and it is equal to $S_i(f)$. Shown in (H.1) is the standard filter model used to fit a spectral model.

$$H_i(f) = 2\sqrt{T_i}\sigma_i \left(\frac{1 + b_1(2\pi j T_i f) + b_2(2\pi j T_i f)^2}{1 + a_1(2\pi j T_i f) + a_2(2\pi j T_i f)^2 + a_3(2\pi j T_i f)^3} \right) \qquad \text{(H.1)}$$

In this equation, T_i and σ_i represent the time constant and rms value of the i^{th} component, respectively. The remaining five constant (a_1, a_2, a_3, b_1, and b_2) are computed by a least squares fitting to the target autospectum $S_i(f)$.

The following MATLAB function should be minimized in a similar manner to previous functions to determine the coefficients in (H.1) that yield the optimal shaping filter to represent the modeled spectra. The variables ‘coeff0’ are the initial guesses of the coefficients from (H.1); ‘freq_model’ are a frequency array of the model generated; ‘PSD_model’ is an equally sized array of PSD values that were generated from the model at the frequencies of ‘freq_model’; ‘T_i’ is the time scale of the turbulence that is modeled; and ‘VAR’ is the variance of the turbulence to be modeled.

```
function [Squares] = Get_Filter(coeff0,freq_model,PSDS_MODEL,Ti, VAR)

a1=coeff0(1);
a2=coeff0(2);
a3=coeff0(3);
b1=coeff0(4);
b2=coeff0(5);

omega=2*pi*freq_model;

Hs=2*sqrt(VAR)*sqrt(Ti)*(1+b1*(Ti*1i*omega)+b2*(Ti*1i*omega).^2)./...
    (1+a1*(Ti*1i*omega)+a2*(Ti*1i*omega).^2+a3*(Ti*1i*omega).^3);

filt=abs(Hs).^2;

figure(1)
loglog(freq_model,PSDS_MODEL,'x',freq_model,filt)

Squares=sum(((PSDS_MODEL-filt)./PSDS_MODEL).^2);

end
```

As can be seen in (H.1), the number of varying parameters in this shaping filter is five. Given this fact, filters with extreme accuracy can be fit to the models produced from the database. The results from the spectra generated from the helicopter downwash database are shown in Figure H.1-Figure H.3. Similarly, filter design results from turbulence inside a wind farm are shown in Figure H.4-Figure H.6.

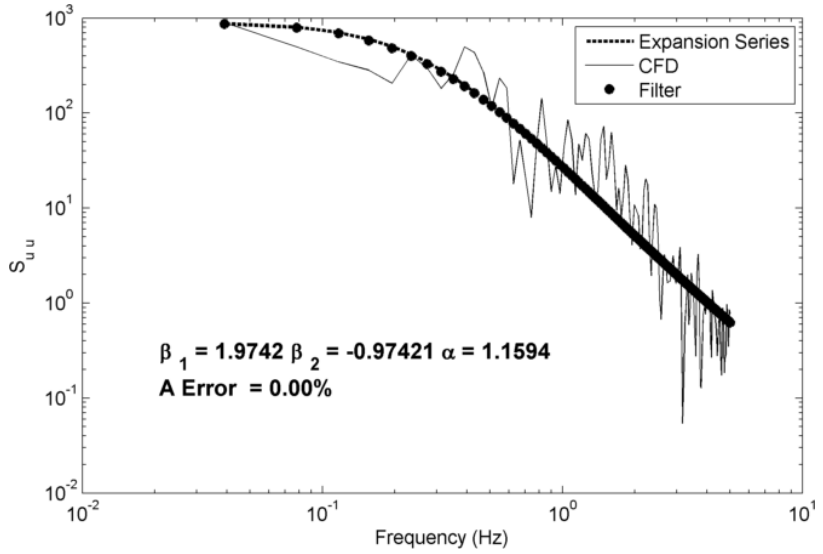

Figure H.1: Filter generated using longitudinal turbulence model with coefficients: $a_1 = 0.7476\ a_2 = -0.1473\ a_3 = -0.0128\ b_1 = 0.0868\ and\ b_2 = -0.082$

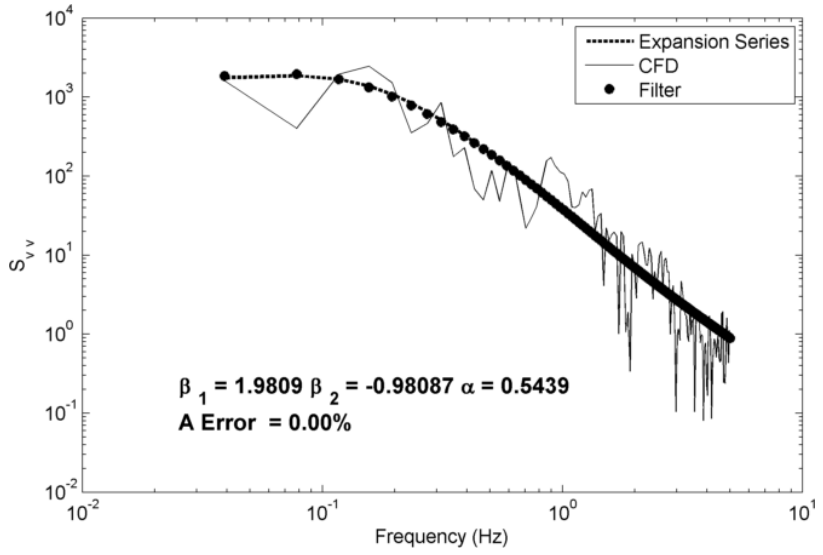

Figure H.2: Filter generated using lateral turbulence model with coefficients: $a_1 = -0.2302\ a_2 = -4.2251\ a_3 = 0.9728\ b_1 = 4.0106\ b_2 = 0.5849$

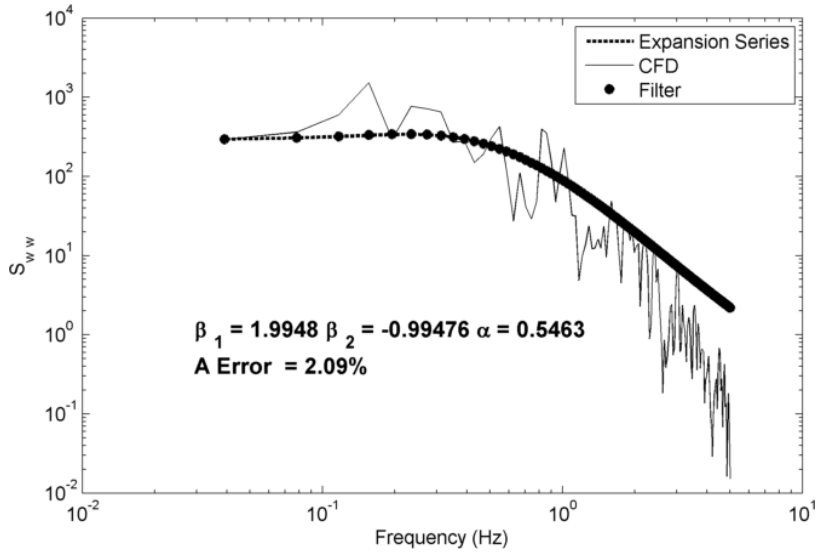

Figure H.3: Filter generated using vertical turbulence model with coefficients: $a_1 = 0.3027\ a_2 = -3.6158\ a_3 = 1.2774\ b_1 = 3.6520\ b_2 = 0.7622$

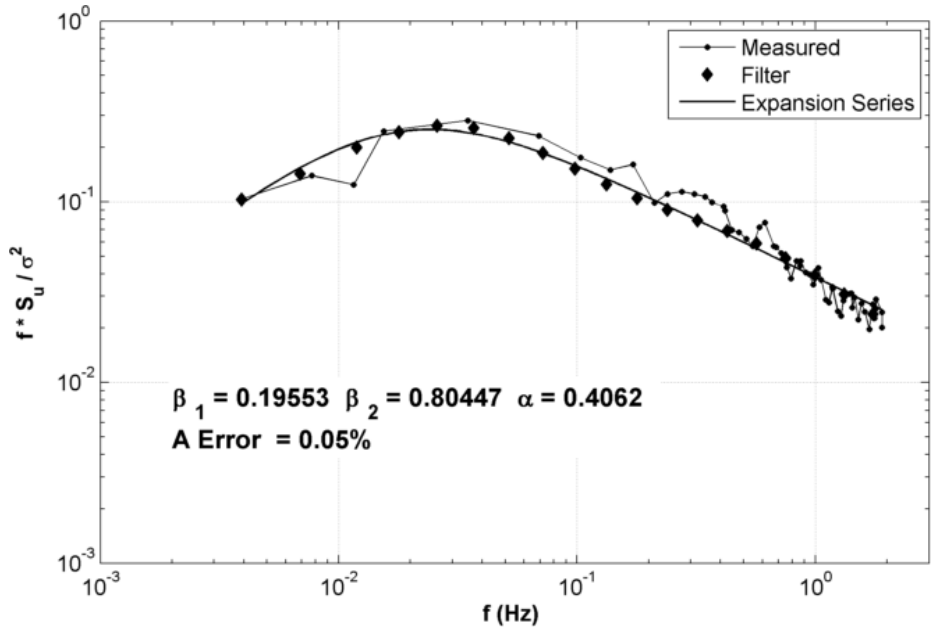

Figure H.4: Filter generated using longitudinal turbulence model with coefficients: $a_1 = 8.858025\ a_2 = -6.36053\ a_3 = -0.40565\ b_1 = -5.49938\ b_2 = 0.547604$

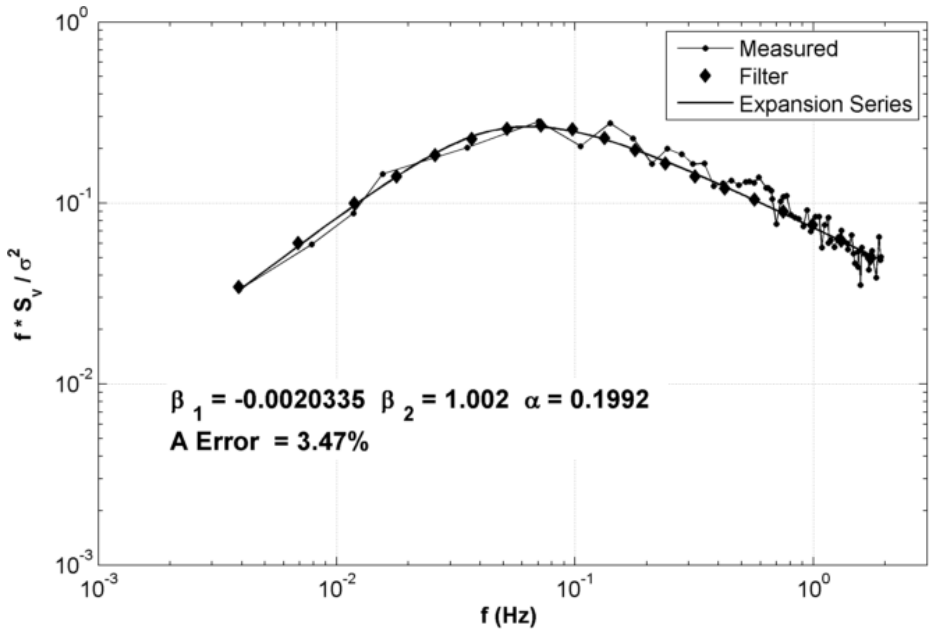

Figure H.5: Filter generated using lateral turbulence model with coefficients: $a_1 = 1.6827\ a_2 = -3.13357\ a_3 = 0.3243\ b_1 = 2.6955\ b_2 = 0.4431$

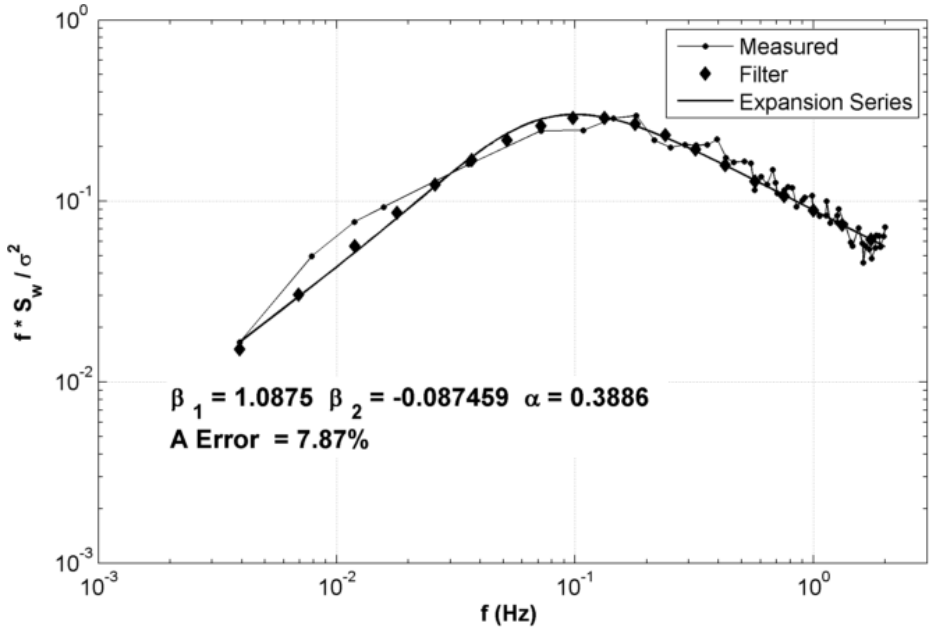

Figure H.6: Filter generated using vertical turbulence model with coefficients: $a_1 = -31.1245\ a_2 = 35.8645\ a_3 = 4.5433\ b_1 = 37.9825\ b_2 = 6.1338$

REFERENCES

Barthelmie, R. J., Frandsen, S. T., Hanse, K., Schepers, J. G., Radon, K., Schlez, W., Neubert, A., Jensen, L.E., Neckelmann, S. 2009, "Modeling the impact of wakes on power output at Nysted and Horns Rev", European Wind Energy Conference.

Bendat, J. S., Piersol, A. G., 2010. Random data: Analysis and measurement procedures, 4th Ed. New York: Wiley.

Fay, J. 1994, Introduction to Fluid Mechanics, MIT Press, Cambridge, MA.

Gaonkar, G. H., 2013, "On Modeling and Simulation of Airwake and Airwake-Downwash Turbulence for Helicopter Shipboard Operations", American Helicopter Society 69th Annual Forum Proceedings, Phoenix, AZ, May 21-23.

Gaonkar, G. H., Mohan, R. 2012, "Extracting Stochastic Airwake Models of from a Database for Engineering Analysis and Simulation", Journal of the American Helicopter Society. April, vol. 57, pp 022004-45. pp. 022004(1-15)

Harris, R. 1990, "Some Further Thoughts On The Spectrum Of Gustiness In Strong Winds", Journal Of Wind Engineering And Industrial *Aerodynamics*, vol. 33, no. 3, pp. 461-477.

Manwell, J.F., McGowan, J.G. & Rogers, A.L. 2009, *Wind energy explained: theory, design and application,* Wiley. Chichester, U.K.

Mathieu, J., Julian, S. 2000, *An Introduction to Turbulent Flow*, Campridge University Press, Chapter 7.

MATLAB and Optimization Toolbox Release 2013b, The MathWorks, Inc., Natick, Massachusetts, United States.

Morfiadakis, E.E., Glinou, G.L. & Koulouvari, M.J. 1996, "The Suitability of the von Kármán Spectrum for the Structure of Turbulence in a Complex Terrain Wind Farm", *Journal of Wind Engineering & Industrial Aerodynamics*, vol. 62, no. 2, pp. 237-257.

Tamura, Y., Karrem, A., Solari, G., Kwok, K. C. S. & Holmes, J. D. *Report from IAWE Working Group WGE-Dynamic Response*, 2003.

U.S. Military Handbook MIL-HDBK-1797, 19 December 1997.

U.S. Military Specification MIL-F-8785C, 5 November 1980.

Taylor, G.I. 1935, "Statistical Theory of Turbulence", Proceedings of the Royal Society of London. Series A, Mathematical and Physical Sciences, vol. 151, no. 873, pp. 421-444.

Vermeer, L.J., Sørensen, J.N. & Crespo, A. 2003, "Wind Turbine Wake Aerodynamics", Progress in Aerospace Sciences, vol. 39, no. 6, pp. 467-510.

Von Kármán, T. 1948, "Progress in the Statistical Theory of Turbulence", *Proceedings of the National Academy of Sciences of the United States of America*, vol. 34, no. 11, pp. 530-539.

Weiner, N., 1949. Extrapolation, Interpolation, and Smoothing of Stationary Time Series, with Engineering Applications, Whiley, New York.

Wilkinson, C H, Zan, S J, Gilbert, N E, Funk,J D. 1999, "Modelling and Simulation of Ship Airwakes for Helicopter Operations: A Collaborative Venture," STAR. vol. 37.